INFORMATION TO USERS

This manuscript has been reproduced from the microfilm master. UMI films the text directly from the original or copy submitted. Thus, some thesis and dissertation copies are in typewriter face, while others may be from any type of computer printer.

The quality of this reproduction is dependent upon the quality of the copy submitted. Broken or indistinct print, colored or poor quality illustrations and photographs, print bleedthrough, substandard margins, and improper alignment can adversely affect reproduction.

In the unlikely event that the author did not send UMI a complete manuscript and there are missing pages, these will be noted. Also, if unauthorized copyright material had to be removed, a note will indicate the deletion.

Oversize materials (e.g., maps, drawings, charts) are reproduced by sectioning the original, beginning at the upper left-hand corner and continuing from left to right in equal sections with small overlaps.

Photographs included in the original manuscript have been reproduced xerographically in this copy. Higher quality 6" x 9" black and white photographic prints are available for any photographs or illustrations appearing in this copy for an additional charge. Contact UMI directly to order.

ProQuest Information and Learning
300 North Zeeb Road, Ann Arbor, MI 48106-1346 USA
800-521-0600

Random Vibration and Fracture of Tapered Composite Laminates

Chen Hai

A Thesis

In

The Department

Of

Mechanical and Industrial Engineering

Presented in Partial Fulfillment of the Requirement

For the Degree of Master of Applied Science at

Concordia University

Montreal, Quebec, Canada

January 2002

Abstract

Random Vibration and Fracture of Tapered Composite Laminates

Chen Hai

Polymer-matrix tapered composite laminates with internal taper are considered in the present thesis. Appropriate finite element models for the tapered laminates are developed using quadratic isoparametric elements. Both the rectangular and triangular isoparametric elements are employed in the model in order to obtain accurate solutions. Singularity elements are used to model the vicinity of the crack tip in the laminate. Appropriate computational methods including the displacement extrapolation method and virtual crack extension method are employed for the determination of the following fracture parameters: stress intensity factor, energy release rate, and J-integral. In order to determine the response to random excitation, the normal mode method is employed in conjunction with the finite element method. The associated computer programs are developed using FORTRAN® and MATLAB® programming languages.

The fracture behavior and the dynamic response to stationary random excitation of different types of internally tapered laminate are investigated based on the finite element model. The locations of delamination initiation are predicted based on the stress analysis results and the Von Mises failure criterion. The energy release rates and J-integral values corresponding to the delamination at the critical location of the laminate are computed. The effects of taper angle and the laminate configuration on the fracture behavior

and the random vibration of the laminate are determined. The probability of failure is then calculated and the use of this information in determining the location of failure initiation is demonstrated.

Acknowledgments

The author wishes to express his indebtedness to his thesis supervisor Dr. Rajamohan Ganesan for his invaluable guidance and encouragement throughout the development of this thesis.

I would like to thank my wife, Mrs. Yun Zhu very much for her encouragement and financial support during the period of the present study.

Table of Contents

List of Figures

List of Tables

Nomenclature

Mathematical

$[\,]$	A rectangular or square matrix
$\{\,\}$	A column matrix
$[\,]^T$	Matrix transpose
$[\,]^{-1}$	Matrix inverse
$[\,]^{-T}$	Inverse transpose

Latin symbols

A	Area
A_1, A_2, A_3	Three sub-areas of the triangle
a	Crack length
[B]	Strain-displacement matrix
[C]	Matrix of damping coefficients
[D]	Matrix of elastic constants
D	Dissipation function
E_1	Longitudinal modulus (GPa)
E_2	Transverse modulus (GPa)
E	Elastic modulus (GPa)
E(f)	Mean
$E(f^2)$	Mean square value
F_6	In-plane shear strength (MPa)
F_0	Magnitude of loading
F	Tensile strength (GPa)
$\{f\}$	Structure force vector (N)
f_i	Frequency(Hz)
$\{f^e\}$	Element force vector (N)

G_I,G_{II}	Energy release rates
G	Shear modulus (GPa)
G_{12}	In-plane shear modulus (GPa)
$G_f(\omega)$	One-sided power spectral density function
$H(\omega)$	Transformation function (Frequency response function)
I_{33}	Gaussian numerical integration
J	Jacobian matrix
[K]	Structure stiffness matrix (Global)
$[K_i^e]$	Element stiffness matrix
K_I	Stress intensity factor
$[k_i]$	Elemental stiffness matrices containing changed stiffness coefficients
$[K]_L^e$	Element stiffness matrix in the local coordinate
$[K]_g^e$	Element stiffness matrix in the global coordinate
[L]	Matrix of differential operators
L	Side length of element
[M]	Structure mass matrix (Global)
$[M^e]$	Element mass matrix
θ	Angle between material coordinate and element coordinate
N_e	The number of elements
N_i	Shape function
n	Integration points
p	Surface forces per unit area
P(f)	Probability distribution function
p(f)	Probability density function
q	Column matrix of system displacements
Q_j	Generalized force
R_0	Magnitude of random excitation
$S_f(\omega)$	Power spectral density function
h	Plane element thickness

t	Time
$[T]_{CL}$	Transformation matrix between Cartesian and material coordinates for two-dimension
$[T]$	Transformation matrix between Cartesian and material coordinates for three-dimension
$[T]_0$	Transformation matrix between global and element coordinates for two-dimension
$[T]_6$	Transformation matrix between global and element coordinates for triangle element
$[T]_8$	Transformation matrix between global and element coordinates for rectangle element
T	Kinetic energy
u ,v	Components of displacement
$\{u\}$	Column matrix of nodal displacements
U_0	Strain energy density
U	Strain energy
$\{U\}$	Magnitude of displacement vector
w_j	Weighting factor
x, y, z	Cartesian coordinates

Greek symbols

α, β, γ	Natural coordinates used in triangle shape functions N_i
α_1, β_1	Proportional damping constants
$\{\varepsilon\}$	Strain components
$[\phi]$	Eigenvector
ρ	Material density (Kg/m^3)
$\{\sigma\}$	Stress components
$\sigma=[\ E(f^2)]^{1/2}$	Standard deviation
$\sigma_1, \sigma_2, \sigma_{12}$	Stresses in the 1-2 plane

σ_f	Standard deviation of excitation
σ_f^2	Variance
ξ_j , η_i	i^{th} Gauss points
φ	Angle between global coordinate and element coordinate
ω_i	Circular frequency (radians per second)
ν	Poisson's ratio
$\upsilon(u)$	Rate of the response process crossing the value s upward.
Γ_0 , Γ_1	Two contours used to calculate J integral
Π	Potential energy

Chapter 1

Introduction

1.1 Composite Materials and Structures

The use of composite materials in mechanical components and structures has increased in the past two decades. Phenolic resin reinforced with asbestos fibers was introduced in the beginning of the twentieth century. The first fiberglass boat was made in 1942; reinforced plastics were also used in aircraft and electrical components at this time. Filament winding was invented in 1946 and incorporated into missile applications in 1950s. The first boron and high strength carbon fibers were introduced in the early 1960s, with applications of advanced composites to aircraft components by 1968. Metal matrix composites such as boron/aluminum were introduced in 1970. Dupont developed Kevlar fibers in 1973. Starting in the 1970s applications of composites expanded widely in industries. The 1980s marked a significant increase in the utilization of high modulus fiber.

The composites have unique advantages over monolithic materials: high strength, high stiffness, long fatigue life, low density, and adaptability to the intended function of the structure. Composites afford the unique possibility of designing the material and structure in one unified and concurrent process. The large number of degrees of freedom available enables material optimization under several given constraints simultaneously, such as

minimum weight and maximum dynamic stability. It is usually desirable to tailor the material to match the localized strength and stiffness requirements in order to minimize the weight, when composite materials are used in aircraft components.

1.2 Tapered Composite Structure

Many aircraft structural components made from composite materials incorporate taper in their design. Design using tapered laminate structure has been studied extensively in recent years; most of the works have focused on parameters of the tapered structure. A composite tapered structure of a helicopter yoke is a good example of the application of taper to the design of a composite structure. A helicopter main rotor yoke is a helicopter structural part made of laminated composite material. Delamination failure of the main rotor yoke under loading conditions has been investigated analytically by many researchers. Analysis of tapered structure, many times, is conducted employing the finite element method. The computation is able to accurately predict the failure location, energy release, stress intensity factor, and fatigue life under a random excitation, which mostly correspond to the interlaminar shear stress concentration predicted by the stress analysis. The test for delamination of tapered laminate used random response technique to determine the location of the delamination. The test is limited to transverse loading and is performed on representative specimens cut out of actual yokes.

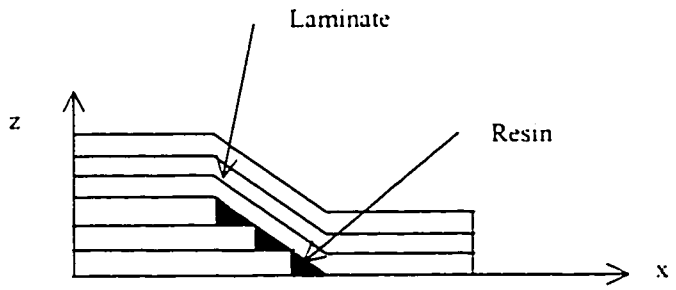

Figure 1.1 A type of tapered laminate

One type of the tapered laminates made of graphite/epoxy composite materials is described in Figure 1.1, which is formed by terminating some plies. This creates geometry and material discontinuities, which are sources for delaminating initiation and propagation. In this thesis, the following research works are conducted on tapered laminates.

1.3 Scope and Objectives of the Thesis

1.3.1 Delamination Prediction for Tapered Laminated Composites

This research work aims at the development of a methodology that may be used to accurately predict delamination location and energy release rate in laminated composite structures. The research consists of three primary tasks:

Determination of the mode-I and mode-II stress intensity factors for the laminate.

The laminate with delaminations at certain locations is used to determine the energy release rates of the laminated composite.

The energy release rate analysis involves the development of a two dimensional analysis that can be used for rapid determination of energy release rates for delamination in practical structural geometry.

1.3.2. Random Vibration of Tapered Laminate

This research work aims at the development of a procedure, that accurately and efficiently predicts delamination growth in composite components. Delamination in this geometry typically initiates at ply drop-off location within the tapered region of the structure. This research consists of two primary tasks:

A crack propagation analysis of the tapered structural geometry involving a two-dimensional crack tip stress analysis.

Random vibration analysis of the tapered laminate with and without delamination.

1.4 Organization of the Thesis

The Chapter 1 provided a brief introduction and described the aim of the research work of the thesis and the scope and objectives of the thesis.

A recent literature survey is provided in Chapter 2. This survey encompasses the detailed studies on the effects of dropping some plies in the tapered composite. The application of the finite element method in this area,

particularly in the computation of fracture parameters and response to random excitation is also investigated.

In Chapter 3, the finite element formulation is given. A fully three-dimensional problem is reduced to a two-dimensional problem. The quadratic iso-parametric and triangular elements are introduced and used. The singularity element, virtual crack extension method and J integral are all described in this Chapter. The equations of motion are obtained using Newton's second law of motion. The equations of motion for the finite element model, proportional damping, eigenvalues and eigenvectors, natural frequencies and normal modes, and transformation function are all described in Chapter 3. The aspects of response to random excitation are described in this Chapter. The numerical results and comparisons with reference results are presented in Chapter 3. The program construction is also described in this Chapter.

In Chapter 4, the parametric study using the finite element model is presented. The interlaminar stress distribution between resin and laminate is obtained and analyzed. The area of stress concentration is determined, and the crack is assumed to initiate in this area. The energy release rates and the stress intensity factors for different loading positions are calculated. The mean values and the standard deviations of the displacements are determined based on the frequencies and modes of free vibration of the tapered structure. The conditional probability of failure that can be used to determine when the tapered laminate would fail is calculated.

Chapter 2

Literature Survey

2.1 Introduction

The delamination in composite laminates has been studied extensively in recent years. This thesis focuses on the kind of tapered composite laminate (see Figure 1.1), for which the three-dimensional stress analysis is reduced to a two-dimensional analysis using the assumption of plane strain.

2.2 Tapered Structure

Detailed studies on the effects of dropping some plies in tapered composite laminate have resulted in many publications. Because of the advantages of a tapered structure in the engineering design, the tapered structure has widely been introduced into manufacturing. Recent works on tapered composite structures were engaged in two major areas:

1) The stress analysis of the vicinity of the generated crack, and crack propagation using energy release rate. The works on tapered composite structures in this area were carried out by Adams *et al* [1], Curry *et al* [2], Fish and Lee [3], Kemp and Johnson [4], Mukherjee and Varughese [5], Murri *et al* [6], Ochoa and Chan [7], Poon *et al* [8], Harrison and johnson [9], Vizzini [10], Rhim and Vizzini [11], Salpekar *et al* [12], Vizzini and Lee [13], and Wisnom *et al* [14].

2) Another set of works focussed on the optimal design of a tapered structure. The parametric studies on tapered composite laminates were conducted by Botting *et al* [15], Cairns *et al* [16], Cui *et al* [17], Fish and Vizzini [18], and Llanos *et al* [19].

The basic types of tapered structure can be separated into three forms: External, Mid-plane, and Internal Longitudinal or Transverse (see Figure 2.1).

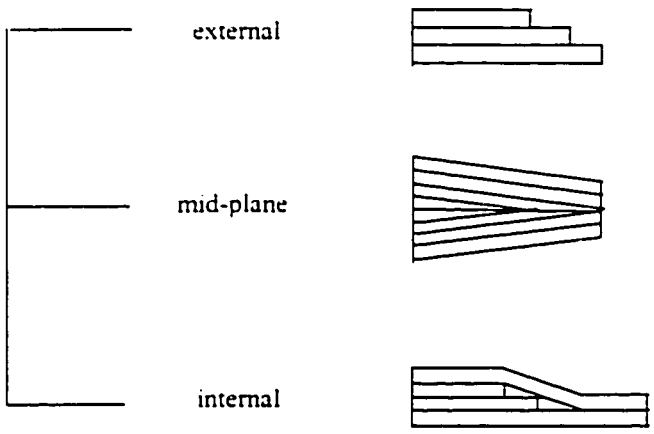

Figure 2.1 Three types of tapered structures

The Internal-ply-drop-off tapers, in which the dropped plies are on a surface of the laminate, were examined by Daoust and Hoa [20], Hoa *et al* [21], Miravete [22], and Wu and Webber[23].

The Mid-plane-ply-drop-off tapers, in which the dropped plies are at the Mid-plane of the laminate, were examined by Hofman and Ochoa [24].

In Internal-transverse-ply-drop-off tapers, the dropped plies are in the interior of the laminate. Usually, the tapered angles are about 2-15 degrees, the tapered structures are symmetric, and the materials used are graphite/epoxy or glass/epoxy.

Reference [3] presented a three-dimensional model of a tapered composite laminate. The size of the model is given in close relationship with the part of tapered laminate. In the model, due to the symmetry of the problem, only one quarter of the tapered section needed to be modeled. The interply resin region surrounding the ply drops was modeled. The dimensions of the model are in terms of the ply thickness H and the resin layer thickness R. The model can be sorted as an internal taper laminate (see Figure 2.2).

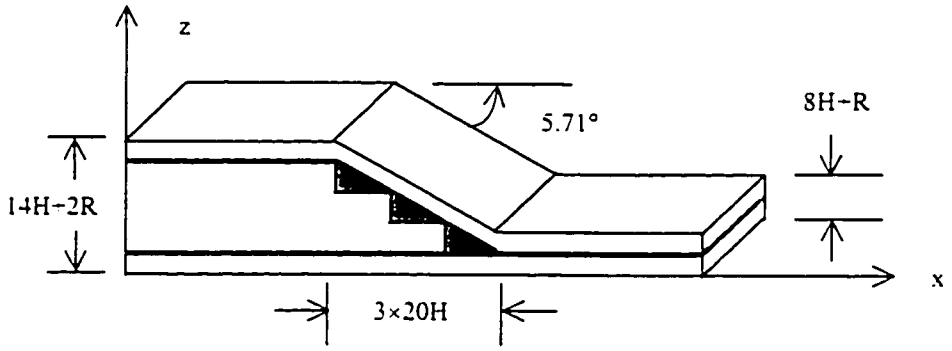

Figure 2.2 Geometry of a type of tapered laminate

The internal forms were separated into three forms in reference [25]. The authors considered that the internal forms could cause a significant weakness from a manufacturing point of view. To avoid dropping a number of plies in a single block, a staircase arrangement may be used where the dropped plies are together, but successive drops are spaced apart, as shown in Figure 2.3(a). A variation of this is to overlap the ends of the dropped plies as in

Figure 2.3(b). Another possibility is to place continuous interleaving plies between the dropped plies, as shown in Figure 2.3(c).

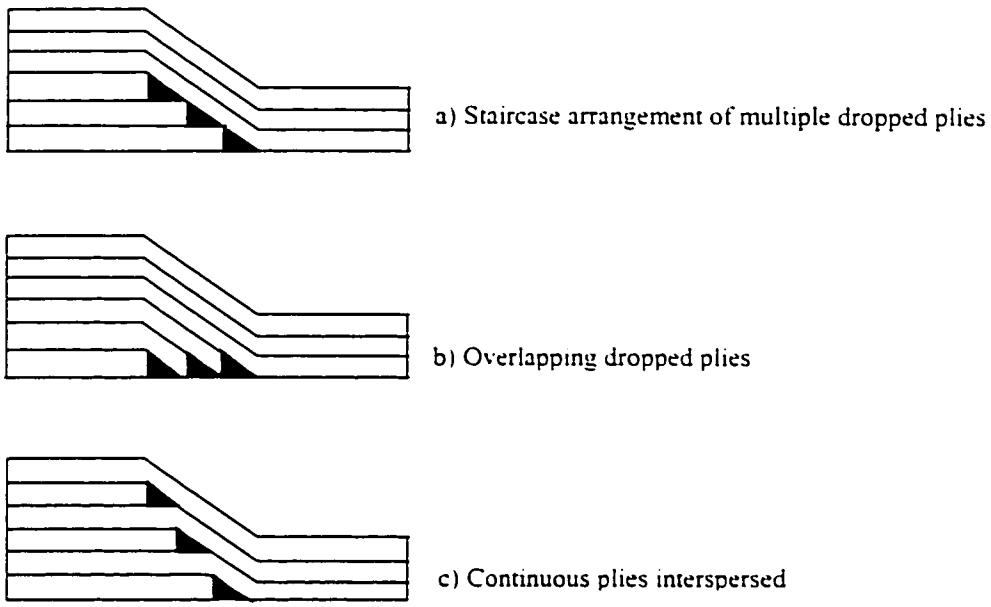

Figure 2.3 Schematic illustration of different taper configurations

2.3 Finite Element Method

The key features of the finite element method can be found in many of the existing works. Clough [26] first used the term "finite element" in 1960. Since then, the literature on finite element applications has grown exponentially.

Fully three-dimensional displacement formulation was used in the analysis by Hoa *et al* [21]. In this paper, the three-dimensional mesh at the ply drop region was obtained by the refinement technique. Some of the

works employed Quasi-3D displacement formulation by reducing the three-dimensional problem into a two-dimensional problem, which is based on the assumption of plane strain. All of the deformations are in the plane. Material properties and stresses are transformed from Quasi-3D into a two-dimensional plane strain problem. These applications of Quasi-3D approaches can be seen in the works of Kemp and Curry [2, 4]. In Curry's paper, sixteen-ply graphite-epoxy laminates, containing four contiguous plies terminated at the mid-plane, were studied. The analysis assumed a state of generalized plane deformation [27] for which the width-direction strain was set to zero, and the finite element method was applied to determine the three-dimensional stress state. A three-dimensional finite element model was used by Fish *et al* [3] to calculate the stress state in the ply drop region of the tapered laminate. The finite element model was reduced since only one-quarter of the tapered section needed to be modeled.

2.4 Computational Fracture Mechanics

Stress intensity factor solutions for literally hundreds of configurations have been published; the majority of which were inferred from numerical models. Elastic-plastic analyses to compute the J integral and crack tip opening displacement are also becoming relatively common. The domain integral approach enables one to generate K and J solutions from finite element models with surprisingly coarse meshes. It is often necessary to determine the distribution of stresses and strains in a body that is subjected to external loads or displacements. In limited cases, it is possible to obtain a closed-form analytical solution for the stresses and strains. William [28] used such an approach to derive solutions for the stresses and strains near the

tip of a sharp crack in an elastic material. A variety of numerical techniques have been applied to problems in solid mechanics, including finite difference [29], finite element [30] and boundary integral equation methods. The vast majority of analyses of cracked bodies utilize the finite elements.

The traditional methods in computational fracture mechanics can be divided into two categories: point matching and energy methods. The point matching technique entails inferring the stress intensity factor from the stress or displacement fields in the body, while energy methods compute the energy release rate in the body and relate energy release rate to stress intensity. One advantage of energy methods is that they can be applied to nonlinear material behavior.

Stress and Displacement Matching considers a cracked body subjected to pure Mode I loading. On the crack plane, the stress intensity factor is related to the stress in the horizontal x direction. The stress intensity factor can be determined by plotting the quantity in the first part of equation (3.42) [see Ref. 31] against the distance from the crack tip, and extrapolating to r=0. Alternatively, the stress intensity factor in the second part of equation (3.42) can be estimated from a similar extrapolation of crack opening displacement. The stress intensity factor obtained using opening displacements tends to give more accurate estimates of stress intensity factor than using stresses. These extrapolation approaches require a high degree of mesh refinement for reasonable accuracy [31].

The energy release rate can be calculated from the rate of change in global potential energy with crack growth. Two separate numerical analyses of a

given geometry are performed, one with crack length a, and another with crack length a+Δa, and the energy release rate is given by (-Δ(potential energy)/Δa). This technique requires minimal post-processing and is more efficient than the point matching methods, and further the computation of global energy estimates does not require refined meshes.

Contour integration, J integral, can be evaluated numerically along a contour surrounding the crack tip. This method can be applied to both linear and nonlinear problems, and the path independence (in elastic materials) enables the user to evaluate J at a remote contour. This method has a good numerical accuracy.

The virtual crack extension method [31] is separated into a stiffness derivative formulation and continuum approach.

In 1974, Parks [32] and Hellen [33] independently proposed the finite element method for inferring energy release rate in elastic bodies. Parks [34] extended this method to nonlinear behavior and large deformation at the crack tip. Under fixed load condition, the energy release rate can be written as:

$$-\left(\frac{\partial \Pi}{\partial a}\right)_{load} = \frac{K_I^2}{E} = -\frac{1}{2}\{u\}^T \frac{\partial [K]}{\partial a}\{u\} \qquad (2.1)$$

where Π is the potential energy, [K] is the stiffness matrix, and K_I is the stress intensity factor. Sometimes, it would not be necessary to change all of the elements in the mesh; moving an element near the crack tip and leaving the rest of the mesh intact could accommodate the crack growth. The energy release rate is related to this change in element stiffness:

$$-\left(\frac{\partial \Pi}{\partial a}\right)_{load} = -\frac{1}{2}\{u\}^T\left(\sum_{i=1}^{N_c}\frac{\partial\left[k_i^e\right]}{\partial a}\right)\{u\} \tag{2.2}$$

where $[k_i^e]$ are the elemental stiffness matrices and N_c is the number of elements. If the elemental stiffness matrices of changed stiffness are between two contours Γ_0 and Γ_1, Parks demonstrated that this quantity is equivalent to the J integral. The value of the energy release rate and J integral are independent of the choice of the inner and outer contours.

DeLorenzi [35, 36] improved the virtual crack extension method by considering the energy release rate of a continuum. The main advantages of the continuum approach are; the methodology is not restricted to the finite element method, and the approach does not require large numerical calculations.

Shih, *et al* [37, 38] have formulated the energy domain integral methodology, which is a general framework for numerical analysis of the J integral. This approach is extremely versatile, as it can be applied to both

quasi-static and dynamic problems with elastic, plastic, or viscoplastic material response, as well as thermal loading. This approach is very similar to the virtual crack extension method.

The Griffith's criterion states that the strain energy is released when a crack grows. The amount of released energy depends on the size of the crack extension and the material constants. Irwin's crack closure integral, energy release rate G, can be written as

$$G = \lim_{\Delta a \to 0} \frac{1}{2\Delta a} \int_0^{\Delta a} p \cdot \Delta u da \tag{2.3}$$

where p, a vector, represents the surface forces per unit area that are required to close the crack, and u, a vector, represents the displacements of the crack surface. One can evaluate Irwin's crack closure integral numerically for finite crack extensions using the finite element method. In reference [12], the Rybicki's method was used to obtain the strain energy release rate components. The total strain energy release rate was the sum of the strain energy release rate components.

2.5 Response to Random Excitation

The response of a deterministic structure to stationary random excitation will be described in this section. It has been assumed that parameters of the structure are known constants, and power spectral density is calculated as a

function of the external excitation. The treatment of a linear MDOF system subjected to stationary random excitations is based on the differential equations of the structure, and the stationary random excitation is a vector of random forces; usually the power spectral density matrix defines these forces. For lightly damped systems, $|H(\omega)|$ is a function whose values are very small over most of the frequency axis, with large values only in the vicinity of the resonance frequency. In solving the problem, the main interest has been the determination of the mean square value $E(f^2)$ of the response at each point and its standard deviation. The mean square of the response is obtained by integrating over the frequency range. When the excitation has zero mean, the mean square value $E(f^2)$ is equal to the variance of f, and the standard deviation of response is given by $\sigma = [E(f^2)]^{1/2}$.

2.6 Discussion

A three-dimensional state of a tapered laminate is reduced to a two-dimensional state using the assumption of plane strain. All of the deformations are in the plane. Material properties and stresses are transformed from Quasi-3D into a two-dimensional plane strain problem.

Recent works on tapered composite structures were engaged in two major areas: the stress analysis of the vicinity of the generated crack and the optimal design of a tapered structure. The basic types of tapered structure can be separated into three forms: External, Mid-plane, and Internal Longitudinal or Transverse. The internal forms were separated into three forms: staircase arrangement of multiple dropped plies, overlapping dropped plies, and continuous plies interspersed. The interply resin region

surrounding the ply drops was modeled. The dimensions of model are in terms of the ply thickness H and the resin layer thickness R.

The traditional methods in computational fracture mechanics can be divided into two categories: point matching and energy methods. The point matching technique entails inferring the stress intensity factor from the stress or displacement fields in the body, while energy methods compute the energy release rate in the body and relate energy release rate to stress intensity.

In the response of a deterministic structure to stationary random excitation, the mean square value $E(f^2)$ of the response at each point and its standard deviation are of interest to designers and engineers.

Chapter 3

Formulation and Solution Methodology

3.1 Introduction

The finite element formulation for the static fracture and the random vibration analyses of tapered laminates is provided in this chapter. The fully three-dimensional problem is reduced to a two-dimensional problem using plane strain theory. The quadratic and triangular shape functions are introduced, and the three-dimensional stress-strain relationships are modified into two-dimensional relationships. Numerical results are then obtained and comparisons with the results given in reference works are made.

3.2 Finite Element Formulation

3.2.1 Finite Element for Plane Strain

A fully three-dimensional problem reduces to a two-dimensional problem if all quantities are independent of one of the coordinate directions, which is assumed here to be the y-axis. The normal strain in the y direction (thickness direction), ε_y, is zero and shear strains γ_{xy} and γ_{zy} are zero. Then a plane strain condition is said to exist. The element stiffness matrix is then correspondingly determined.

$$[K^e] = \int_{v^e} [B]^T [D][B] dV \tag{3.1}$$

In fact, a typical sub-matrix of $[K^e]$ corresponding to nodes i and j can be evaluated from the expression

$$K_{ij}^e = \int_{-1}^{1} \int_{-1}^{1} B_i^T [D] B_j h \det[J] d\xi d\eta \tag{3.2}$$

where h is the element thickness, [J] is the Jacobian matrix and [D] is the matrix of elastic constants. Further

$$dxdz = \det[J]\, d\xi d\eta \tag{3.3}$$

3.2.2 Strain Displacement Matrix B

The use of the natural coordinate system (ξ,η) allows us to use elements with curvilinear shapes. The coordinate values $x(\xi,\eta)$ and $z(\xi,\eta)$ at any point (ξ,η) within the element are defined by the expressions

$$x(\xi,\eta) = \sum_{i=1}^{n} N_i(\xi,\eta) \cdot x_i$$

$$z(\xi,\eta) = \sum_{i=1}^{n} N_i(\xi,\eta) \cdot z_i \tag{3.4}$$

The displacements u(ξ,η) and v(ξ,η) at any point are given by

$$u(\xi,\eta) = \sum_{i=1}^{n} N_i(\xi,\eta)\cdot u_i$$

$$v(\xi,\eta) = \sum_{i=1}^{n} N_i(\xi,\eta)\cdot v_i \qquad (3.5)$$

Let f be some function of x and y, then the chain rule yields

$$\frac{\partial f}{\partial \xi} = \frac{\partial f}{\partial x}\frac{\partial x}{\partial \xi} + \frac{\partial f}{\partial z}\frac{\partial z}{\partial \xi}$$

$$\frac{\partial f}{\partial \eta} = \frac{\partial f}{\partial x}\frac{\partial x}{\partial \eta} + \frac{\partial f}{\partial z}\frac{\partial z}{\partial \eta} \qquad (3.6)$$

so that the derivatives of f (ξ,η) can be written as

$$\begin{Bmatrix} \frac{\partial f}{\partial \xi} \\ \frac{\partial f}{\partial \eta} \end{Bmatrix} = \begin{bmatrix} \frac{\partial x}{\partial \xi} & \frac{\partial z}{\partial \xi} \\ \frac{\partial x}{\partial \eta} & \frac{\partial z}{\partial \eta} \end{bmatrix} \begin{Bmatrix} \frac{\partial f}{\partial x} \\ \frac{\partial f}{\partial z} \end{Bmatrix} \qquad (3.7)$$

where the Jacobian matrix [J] is written according to the equation (3.4) as

$$[J] = \sum_{i=1}^{n} \begin{bmatrix} \frac{\partial N_i}{\partial \xi} \cdot x_i & \frac{\partial N_i}{\partial \xi} \cdot z_i \\ \frac{\partial N_i}{\partial \eta} \cdot x_i & \frac{\partial N_i}{\partial \eta} \cdot z_i \end{bmatrix}$$

(3.8)

and inverse Jacobian matrix is

$$[J]^{-1} = \frac{1}{\det J} \begin{bmatrix} \frac{\partial z}{\partial \eta} & -\frac{\partial z}{\partial \xi} \\ -\frac{\partial x}{\partial \eta} & \frac{\partial x}{\partial \xi} \end{bmatrix}$$

(3.9)

The strain-displacement relationship for most problems can be written in the form

$$\{\varepsilon\}=[L]\{u\}$$

(3.10)

where $\{\varepsilon\}$ is the strain vector, $\{u\}$ is the displacement vector, and [L] is the matrix of displacement differential operators. $\{\varepsilon\}$ can be written as

$$\{\varepsilon\} = \sum_{i=1}^{n} \begin{bmatrix} \frac{\partial N_i}{\partial x} & 0 \\ 0 & \frac{\partial N_i}{\partial z} \\ \frac{\partial N_i}{\partial z} & \frac{\partial N_i}{\partial x} \end{bmatrix} \begin{Bmatrix} u_i \\ v_i \end{Bmatrix}$$

$$= \sum_{i=1}^{n} B_i \delta_i$$

$$= [B_1, B_2, \ldots, B_n] \begin{Bmatrix} u_1 \\ v_1 \\ \vdots \\ v_n \end{Bmatrix} \qquad (3.11)$$

The stress-strain relationship for an elastic material, in the absence of initial stresses and strains, may be written in the form

$$\{\sigma\}=[D]\{\varepsilon\} \qquad (3.12)$$

where [D] is the matrix of elastic constants. For plane stress situation

$$[D] = \frac{E}{1-\nu^2} \begin{bmatrix} 1 & \nu & 0 \\ \nu & 1 & 0 \\ 0 & 0 & \frac{1-\nu}{2} \end{bmatrix} \qquad (3.13)$$

and for plane strain situation

$$[D] = \frac{E(1-\nu)}{(1+\nu)(1-\nu)} \begin{bmatrix} 1 & \frac{\nu}{1-\nu} & 0 \\ \frac{\nu}{1-\nu} & 1 & 0 \\ 0 & 0 & \frac{1-2\nu}{2(1-\nu)} \end{bmatrix} \tag{3.14}$$

3.2.3 Quadratic Iso-Parametric Element

The quadratic shape functions are given in reference [39]. The equation (3.2) can be evaluated using Gaussian numerical integration.

$$I_{3,3} = \int_{-1}^{1}\int_{-1}^{1} f(\xi,\eta)d\xi d\eta = \sum_{j=1}^{3}\sum_{i=1}^{3} w_j\, w_i f(\xi_j,\eta_i) \tag{3.15}$$

where w_j and w_i are the weighting factors, ξ_j and η_i are the i^{th} Gauss points. They are given in Table 3.1.

Table 3.1 Gauss points and weights for the quadratic elements

i or j	Location ξ_j or η_i	Weight w_j or w_i
1	-0.774596669241483	0.5555555555555556
2	0.0000000000000000	0.8888888888888889
3	+0.774596669241483	0.5555555555555556

3.2.4 Triangular Element

Consider a triangle that is divided into three sub-areas A_1, A_2, and A_3. Let A be the total area of the triangle, $A=A_1+A_2+A_3$. Then,

$$\alpha = \frac{A_1}{A}, \quad \beta = \frac{A_2}{A}, \quad \gamma = \frac{A_3}{A} \tag{3.16}$$

Consequently,

$$\alpha + \beta + \gamma = 1 \tag{3.17}$$

where α, β, and γ are natural coordinates used to define the shape functions N_i for the triangular element as in the following.

$$\begin{aligned} N_1&=\alpha\,(2\alpha-1)\\ N_2&=4\alpha\beta\\ N_3&=\beta(2\beta-1)\\ N_4&=4\beta\gamma\\ N_5&=\gamma(2\gamma-1)\\ N_6&=4\gamma\alpha \end{aligned} \tag{3.18}$$

In evaluating K^e and det J, one may directly use the expressions given in equations (3.7), (3.8) and (3.9). Denoting that $\alpha=\xi$, $\beta=\eta$, $\gamma=1-\xi-\eta$

$$\frac{\partial f}{\partial \xi} = \frac{\partial f}{\partial x}\frac{\partial x}{\partial \xi} + \frac{\partial f}{\partial z}\frac{\partial z}{\partial \xi}$$
$$= \frac{\partial f}{\partial x}\frac{\partial x}{\partial \alpha} - \frac{\partial f}{\partial x}\frac{\partial x}{\partial \gamma} + \frac{\partial f}{\partial z}\frac{\partial z}{\partial \alpha} - \frac{\partial f}{\partial z}\frac{\partial z}{\partial \gamma} \tag{3.19a}$$

and

$$\frac{\partial f}{\partial \eta} = \frac{\partial f}{\partial x}\frac{\partial x}{\partial \eta} + \frac{\partial f}{\partial z}\frac{\partial z}{\partial \eta}$$
$$= \frac{\partial f}{\partial x}\frac{\partial x}{\partial \beta} - \frac{\partial f}{\partial x}\frac{\partial x}{\partial \gamma} + \frac{\partial f}{\partial z}\frac{\partial z}{\partial \beta} - \frac{\partial f}{\partial z}\frac{\partial z}{\partial \gamma} \tag{3.19b}$$

Now the equation (3.2) can be evaluated using the Gaussian numerical integration as

$$I_{3,3} = \iint_A f(\alpha, \beta, \gamma)\, d\alpha d\beta$$
$$= \frac{1}{2}\sum_{i=1}^{n} w_i f(\alpha_i, \beta_i, \gamma_i) \tag{3.20}$$

where n=7. The Gauss quadrature points and weights corresponding to the triangular elements are given in Table 3.2.

Table 3.2 Gauss points and weights for the triangular elements

Integration points	Location α_i	Location β_i	Location γ_i	Weight w_i
1	0.33333333333333	0.33333333333333	0.33333333333333	0.22500000000000
2	0.79742698535309	0.10128650732346	0.10128650732346	0.12593918054483
3	0.10128650732346	0.79742698535309	0.10128650732346	0.12593918054483
4	0.10128650732346	0.10128650732346	0.79742698535309	0.12593918054483
5	0.05971587178977	0.47014206410512	0.47014206410512	0.13239415278851
6	0.47014206410512	0.05971587178977	0.47014206410512	0.13239415278851
7	0.47014206410512	0.47014206410512	0.05971587178977	0.13239415278851

3.2.5 Properties of Composite Laminate

Consider a small element of a lamina of constant thickness t, wherein the principal material axes are labeled as 1 and 2, that is direction 1 is parallel to the fibers, the direction 2 is normal to them. The lamina geometric axes are x and y as depicted in Figure 3.1. The equations relating σ_x, σ_y and σ_{xy} to σ_1, σ_2, and σ_{12}, are given below in matrix form.

$$\begin{bmatrix} \sigma_1 \\ \sigma_2 \\ \sigma_{12} \end{bmatrix} = [T]_{CL} \begin{bmatrix} \sigma_x \\ \sigma_y \\ \sigma_{xy} \end{bmatrix} \tag{3.21}$$

where

$$[T]_{CL} = \begin{bmatrix} m^2 & n^2 & 2mn \\ n^2 & m^2 & -2mn \\ -mn & mn & m^2 - n^2 \end{bmatrix} \tag{3.22}$$

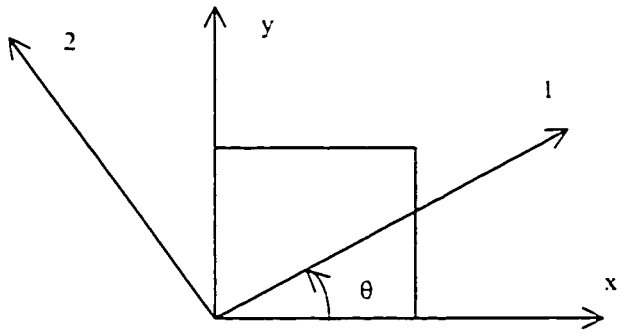

Figure 3.1 Lamina coordinate systems

where m =cosθ, n=sinθ, and θ is defined positive as shown in Figure 3.1. The subscripts CL refer to the classical two-dimensional case only, that is, in the 1-2 plane or the x-y plane only. Analogously, a strain relationship also follows for the classical isothermal case:

$$\begin{bmatrix} \varepsilon_1 \\ \varepsilon_2 \\ \varepsilon_{12} \end{bmatrix} = [T]_{CL} \begin{bmatrix} \varepsilon_x \\ \varepsilon_y \\ \varepsilon_{xy} \end{bmatrix} \tag{3.23}$$

The two-dimensional relationships can be modified into the following three-dimensional transformation equation.

$$\begin{Bmatrix}\sigma_1\\ \sigma_2\\ \sigma_3\\ \sigma_4\\ \sigma_5\\ \sigma_6\end{Bmatrix}=[T]\begin{Bmatrix}\sigma_x\\ \sigma_y\\ \sigma_z\\ \sigma_{yz}\\ \sigma_{xz}\\ \sigma_{xy}\end{Bmatrix} \quad and \quad \begin{Bmatrix}\varepsilon_1\\ \varepsilon_2\\ \varepsilon_3\\ \varepsilon_4\\ \varepsilon_5\\ \varepsilon_6\end{Bmatrix}=[T]\begin{Bmatrix}\varepsilon_x\\ \varepsilon_y\\ \varepsilon_z\\ \varepsilon_{yz}\\ \varepsilon_{xz}\\ \varepsilon_{xy}\end{Bmatrix} \tag{3.24}$$

wherein

$$[T]=\begin{bmatrix} m^2 & n^2 & 0 & 0 & 0 & 2mn \\ n^2 & m^2 & 0 & 0 & 0 & -2mn \\ 0 & 0 & 1 & 0 & 0 & 0 \\ 0 & 0 & 0 & m & -n & 0 \\ 0 & 0 & 0 & n & m & 0 \\ -mn & mn & 0 & 0 & 0 & (m^2-n^2) \end{bmatrix} \tag{3.25}$$

If one systematically uses these expressions, and utilizes Hooke's Law relating stress and strain, the general equations for a lamina made of a fiber reinforced composite material in terms of the principal material directions (1,2,3) can be obtained:

$$\begin{Bmatrix}\sigma_1\\ \sigma_2\\ \sigma_3\\ \sigma_4\\ \sigma_5\\ \sigma_6\end{Bmatrix}=\begin{bmatrix} Q_{11} & Q_{12} & Q_{13} & 0 & 0 & 0 \\ Q_{12} & Q_{22} & Q_{23} & 0 & 0 & 0 \\ Q_{13} & Q_{23} & Q_{33} & 0 & 0 & 0 \\ 0 & 0 & 0 & 2Q_{44} & 0 & 0 \\ 0 & 0 & 0 & 0 & 2Q_{55} & 0 \\ 0 & 0 & 0 & 0 & 0 & 2Q_{66} \end{bmatrix}\begin{Bmatrix}\varepsilon_1\\ \varepsilon_2\\ \varepsilon_3\\ \varepsilon_4\\ \varepsilon_5\\ \varepsilon_6\end{Bmatrix} \tag{3.26}$$

To transform these relationships to the x-y-z coordinate system, equation (3.24) has been used and the result is given below.

$$\begin{Bmatrix} \sigma_x \\ \sigma_y \\ \sigma_z \\ \sigma_{yz} \\ \sigma_{xz} \\ \sigma_{xy} \end{Bmatrix} = \begin{bmatrix} \overline{Q}_{11} & \overline{Q}_{12} & \overline{Q}_{13} & 0 & 0 & 2\overline{Q}_{16} \\ \overline{Q}_{12} & \overline{Q}_{22} & \overline{Q}_{23} & 0 & 0 & 2\overline{Q}_{26} \\ \overline{Q}_{13} & \overline{Q}_{23} & \overline{Q}_{33} & 0 & 0 & 2\overline{Q}_{36} \\ 0 & 0 & 0 & 2\overline{Q}_{44} & 2\overline{Q}_{45} & 0 \\ 0 & 0 & 0 & 2\overline{Q}_{45} & 2\overline{Q}_{55} & 0 \\ \overline{Q}_{16} & \overline{Q}_{26} & \overline{Q}_{36} & 0 & 0 & 2\overline{Q}_{66} \end{bmatrix} \begin{Bmatrix} \varepsilon_x \\ \varepsilon_y \\ \varepsilon_z \\ \varepsilon_{yz} \\ \varepsilon_{xz} \\ \varepsilon_{xy} \end{Bmatrix} \tag{3.27}$$

When we only consider the plane strain case (see Figure 3.2), the strains ε_y, ε_{yz}, ε_{xy} are equal to zero.

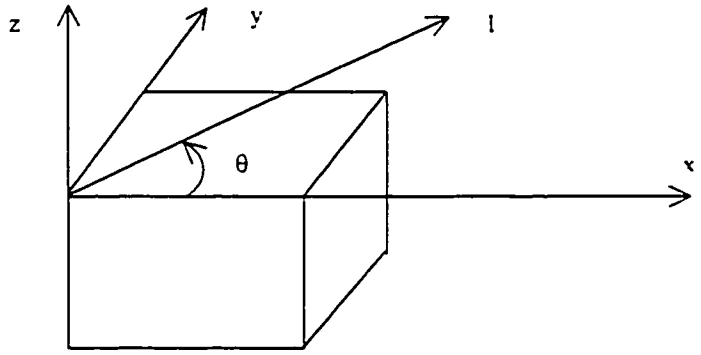

Figure 3.2 Plane strain case

Correspondingly, the three-dimensional stress-strain relationships can be reduced to the two-dimensional form:

$$\begin{Bmatrix} \sigma_{x} \\ \sigma_{z} \\ \sigma_{xz} \end{Bmatrix} = \begin{bmatrix} \overline{Q}_{11} & \overline{Q}_{13} & 0 \\ \overline{Q}_{13} & \overline{Q}_{33} & 0 \\ 0 & 0 & 2\overline{Q}_{55} \end{bmatrix} \begin{Bmatrix} \varepsilon_{x} \\ \varepsilon_{z} \\ \varepsilon_{xz} \end{Bmatrix} \tag{3.28}$$

In addition, one can write the equation:

$$\begin{Bmatrix} \sigma_{y} \\ \sigma_{yz} \\ \sigma_{xy} \end{Bmatrix} = \begin{bmatrix} \overline{Q}_{12} & \overline{Q}_{23} & 0 \\ 0 & 0 & 2\overline{Q}_{45} \\ \overline{Q}_{16} & \overline{Q}_{36} & 0 \end{bmatrix} \begin{Bmatrix} \varepsilon_{x} \\ \varepsilon_{z} \\ \varepsilon_{xz} \end{Bmatrix} \tag{3.29}$$

The stiffness coefficients are given by:

$$\begin{aligned}
\overline{Q}_{11} &= Q_{11}m^4 + 2(Q_{12} + 2Q_{66})m^2n^2 + Q_{22}n^4 \\
\overline{Q}_{12} &= (Q_{11} + Q_{22} - 4Q_{66})m^2n^2 + Q_{12}(m^4 + n^4) \\
\overline{Q}_{13} &= Q_{13}m^2 + Q_{23}n^2 \\
\overline{Q}_{16} &= -mn^3Q_{22} + m^3nQ_{11} - mn(m^2 - n^2)(Q_{12} + 2Q_{66}) \\
\overline{Q}_{23} &= Q_{13}n^2 + Q_{23}m^2 \\
\overline{Q}_{33} &= Q_{33} \\
\overline{Q}_{36} &= (Q_{13} - Q_{23})mn \\
\overline{Q}_{45} &= (Q_{55} - Q_{44})mn \\
\overline{Q}_{55} &= Q_{55}m^2 + Q_{44}n^2
\end{aligned} \tag{3.30}$$

Consider that the lamina is transversely isotropic, that is to have the same properties in both the 2 and 3 directions, then $\nu_{12}=\nu_{13}=\nu_{23}=\nu_{32}$, $\nu_{21}=\nu_{31}$, $G_{12}=G_{13}=G_{23}=G_{32}$, $G_{21}= G_{31}$, $E_{22}=E_{33}$ with resulting simplification:

$Q_{11}= E_{11}(1-\nu_{23}\nu_{32})/\Delta \quad =E_{11}(1-\nu_{12}\nu_{12})/\Delta$

$Q_{12}= E_{11}(\nu_{21}+\nu_{31}\nu_{23})/\Delta \quad =E_{11}(\nu_{21}+\nu_{21}\nu_{12})/\Delta$

$Q_{13}= E_{11}(\nu_{31}+\nu_{21}\nu_{32})/\Delta \quad =E_{11}(\nu_{21}+\nu_{21}\nu_{12})/\Delta$

$Q_{22}= E_{22}(1-\nu_{31}\nu_{13})/\Delta \quad =E_{22}(1-\nu_{21}\nu_{12})/\Delta$

$Q_{23}= E_{22}(\nu_{32}+\nu_{12}\nu_{31})/\Delta \quad =E_{22}(\nu_{12}+\nu_{12}\nu_{21})/\Delta$

$Q_{33}=E_{33}(1-\nu_{12}\nu_{12})/\Delta \quad =E_{22}(1-\nu_{12}\nu_{12})/\Delta$

$Q_{44}=G_{23}=G_{12}$

$Q_{55}=G_{13}=G_{12}$

$Q_{66}=G_{12}$

$\Delta=1-\nu_{12}\nu_{21}-\nu_{23}\nu_{32}-\nu_{31}\nu_{13}-2\nu_{21}\nu_{32}\nu_{13}=1-\nu_{12}\nu_{21}-\nu_{12}\nu_{12}-\nu_{21}\nu_{12}-2\nu_{21}\nu_{12}\nu_{12}$

(3.31)

The shear strains in all the equations refer to the tonsorial (on mathematical) shear strains.

3.2.6 Coordinate Transformation Matrix

Consider the global coordinate and element coordinate (local coordinate) systems. Further, φ denotes the angle between the global coordinate and the element coordinate. So we can obtain the transformation matrix as

$$[T]_0 = \begin{bmatrix} \cos\varphi & \sin\varphi \\ -\sin\varphi & \cos\varphi \end{bmatrix}$$

(3.32)

and

$$[T]_6 = \lceil T_0\ T_0\ T_0\ T_0\ T_0\ T_0 \rfloor_{diag} \quad \text{for triangle element}$$
$$[T]_8 = \lceil T_0\ T_0\ T_0\ T_0\ T_0\ T_0\ T_0\ T_0 \rfloor_{diag} \quad \text{for rectangle element} \tag{3.33}$$

The element stiffness matrix in the local coordinate system can be transformed into the global coordinate system:

$$[K]_g^e = [T]^T [K]_L^e [T] \tag{3.34}$$

where $[K]_L^e$ is the element stiffness matrix in the local coordinate, $[K]_g^e$ is the element stiffness matrix in the global coordinate, and further [T] is $[T_6]$or $[T_8]$.

3.2.7 Singularity Element

The nature of the singularity at the crack tip is known to be of type (stress σ)~ $r^{-1/2}$ for stresses, and (displacements u,v) ~ $r^{-1/2}$ for the displacements, where r is the distance from the crack tip. If the cracks correspond to Mode I and Mode II, and the material is linearly elastic and isotropic, the stresses and displacement are as given in Ref. [31, pp. 54]. Stress intensity factors K_I and K_{II} depend on the geometry of the structure, and the distribution and magnitude of random excitation. A crack propagates when the stress

intensity factor reaches a critical value. The critical value is a material property.

Irwin [31] defined the energy release rate, $d\Pi/da$, which is a measure of the energy available for an increment of crack extension. It can be shown that for the plane strain case with unit thickness in an isotropic material,

$$\frac{d\Pi}{da} = \frac{1-\upsilon^2}{E} K_i^2 \qquad (3.35)$$

The energy release rate is the rate of change in potential energy with crack area, which is also called the crack extension force or the crack driving force.

The six-node plane triangle element can display $r^{-1/2}$ type singularity in its strain field if its side nodes are moved to quarter points near the crack tip. The quarter-point sides should be straight and the side node opposite the crack tip should be at mid-side.

Another effective singularity element can be formed from a four-sided quadratic element by collapsing one side to produce a triangle.

Rectangular Quarter-Point Elements with the quarter points also display singularity only along two sides and the diagonal. They are less accurate than triangular Quarter-Point Elements.

Consider a quadrilateral element with the mid-side nodes at the quarter point. For convenience, let us evaluate the element shape functions along the boundary between nodes 1 and 2, and further node 3 is the quarter point. The shape functions along the line are given in Ref. [31],

$$N_1 = -\frac{1}{2}\xi(1-\xi)$$
$$N_2 = \frac{1}{2}\xi(1-\xi)$$
$$N_3 = (1-\xi^2) \tag{3.36}$$

The x coordinate along the side 1-2 is related to ξ coordinate by

$$x = -\frac{1}{2}\xi(1-\xi)x_1 + \frac{1}{2}\xi(1-\xi)x_2 + (1-\xi^2)x_3 \tag{3.37}$$

Setting $x_1=0$, $x_2=L$, and $x_3=L/4$, and considering the relation

$$\xi = -1 + \sqrt{\frac{x}{L}} \quad , \quad \frac{\partial x}{\partial \xi} = \sqrt{xL} \tag{3.38}$$

one can show that

$$u(x,0) = -\left[2\sqrt{\frac{x}{L}} - 1\right]\left[1 - \sqrt{\frac{x}{L}}\right]u_1 + \left[-1 + 2\sqrt{\frac{x}{L}}\right]\left(2\sqrt{\frac{x}{L}}\right)u_2 - 4\left[\sqrt{\frac{x}{L}} - \frac{x}{L}\right]u_3$$

(3.39)

Solving for the strain in the x coordinate leads to

$$\varepsilon_x = \frac{\partial u(x,0)}{\partial x} = -\frac{1}{\sqrt{xL}}\left\{\frac{1}{2}\left[3 - 4\sqrt{\frac{x}{L}}\right]u_1 + \frac{1}{2}\left[-1 + 4\sqrt{\frac{x}{L}}\right]u_2 + 2\left[1 - 2\sqrt{\frac{x}{L}}\right]u_3\right\}$$

(3.40)

Thus, the strain changes at a rate of $(xL)^{-1/2}$ as $x^{-1/2}$ approaches zero along side 1-2. So we can obtain a $x^{-1/2}$ singularity at node 1. The singularity elements are used in the present work.

Quarter-Point Elements can be made to display a stress or strain singularity by appropriate definition of its geometry. A common approach to calculate stress intensity factors from a finite element analysis is the crack-opening displacement method. From displacements of nodes along the line with $\theta = \pm\pi$, the Mode I and Mode II stress intensity factors are given by, as in Ref. [39].

$$K_I = \frac{2G}{\kappa+1}\left(\frac{\pi}{2L}\right)^{1/2}[(4v_{B2} - v_{C2}) - (4v_{B1} - v_{C1})]$$

$$K_{II} = \frac{2G}{\kappa+1}\left(\frac{\pi}{2L}\right)^{1/2}[(4u_{B2} - u_{C2}) - (4u_{B1} - u_{C1})] \qquad (3.41)$$

where L is the side length of element, B is quarter point, C is the vertex of element. These equations are applicable only for an element obtained by collapsing one side. Many analyses have used a rate of L/a ~ 0.1, where a is the crack length.

In another method, K_I is estimated from a cracked body subjected to pure Mode I loading. On the crack plane, K_I is related to the stress in the crack opening direction. K_I can be obtained following an extrapolation scheme that uses the following equations:

$$K_I = \lim_{r\to 0}\left(\sigma_2\sqrt{2\pi r}\right)^{1/2}$$

$$K_{II} = \frac{2G}{\kappa+1}\lim_{r\to 0}\left[u_2\sqrt{\left(\frac{2\pi}{r}\right)}\right] \qquad (3.42)$$

3.2.8 Virtual Crack Extension Method

Parks and Hellen [31] independently proposed the finite element method for determining the energy release rate in elastic bodies. Consider a two-dimensional cracked body, which is subjected to load. The potential energy of the body, in terms of the finite element solution, is given as

$$\Pi = \frac{1}{2}\{u\}^T [K]\{u\} - \{u\}^T \{f\}$$

(3.43)

where Π is the potential energy, $\{u\}$ is the matrix of displacements, and $[K]$ is the stiffness matrix. The energy release rate is the derivative of Π with respect to crack area, for both fixed load and fixed displacement conditions. Under fixed load condition, the energy release rate is

$$= -\left(\frac{\partial \Pi}{\partial a}\right)_{load}$$
$$= -\frac{\partial \{u\}^T}{\partial a}([K]\{u\} - \{f\}) - \frac{1}{2}\{u\}^T \frac{\partial [K]}{\partial a}\{u\} + \{u\}^T \frac{\partial [f]}{\partial a}$$

(3.44)

The first term must be equal to zero, the third term must also vanish, since loads are held constant. The energy release rate can be written as:

$$-\left(\frac{\partial \Pi}{\partial a}\right)_{load} = -\frac{1}{2}\{u\}^T \frac{\partial [K]}{\partial a}\{u\}$$

(3.45)

It can be shown that for plane stress case and plane strain case, respectively, and for unit thickness:

$$-\left(\frac{\partial \Pi}{\partial a}\right)_{load} = \frac{K_I^2}{E} \quad or \quad \frac{(1-\nu^2)K_I^2}{E}$$

(3.46)

where, K_I is the stress intensity factor. Sometimes, it would not be necessary to change all of the elements in the mesh; one could accommodate the crack growth by moving the element near the crack tip and leaving the rest of the mesh intact. The energy release rate is related to this change in element stiffness:

$$-\left(\frac{\partial \Pi}{\partial a}\right)_{load} = -\frac{1}{2}\{u\}^T\left(\sum_{i=1}^{N_c}\frac{\partial [k^e]}{\partial a}\right)\{u\} \tag{3.47}$$

where $[k_i^e]$ are the elemental stiffness matrices and N_c is the number of elements. If the elemental stiffness matrices of changed stiffness are between two contours Γ_0 and Γ_1, Parks demonstrated that this quantity is equivalent to the J integral. The value of the energy release rate and J integral are independent of the choice of the inner and outer contours.

The equation (3.47) can be expressed as:

$$\frac{d\Pi}{da} = \frac{\Pi_2 - \Pi_1}{h(a+\Delta a - a)} = \frac{\frac{1}{2}\{u_2\}^T[K_2]\{u_2\} - \frac{1}{2}\{u_1\}^T[K_1]\{u_1\}}{h\Delta a} \tag{3.48}$$

where Π_1 is the potential energy corresponding to the crack length a, and Π_2 is the potential energy for the crack length a+Δa, $\Delta\Pi$ is the difference

between the two potential energy quantities, h is the thickness of the finite element model.

3.2.9 J Integral

It can be shown as in Ref. [40] that the J integral is independent of the actual path and is given by the integral below, provided that the initial and end points of the contour Γ are on opposite faces of the crack and that the contour contains the crack tip.

$$J = \int_{\Gamma} (U_0 dz - f_i \frac{\partial u_i}{\partial x} ds)$$

(3.49)

where U_0 is the strain energy density, f_i is the traction vector, u_i is the displacement vector, ds is an element of arc along the integration contour Γ.

For the linear elastic case it can be shown, for each particular mode of deformation, that the energy release rate equals the J integral. The J integral can be written for an individual element as in the following:

$$J = \int_1^1 \left\{ \frac{1}{2} \left(\sigma_{xx} \frac{\partial u}{\partial x} + \sigma_{xy} \left(\frac{\partial u}{\partial y} + \frac{\partial v}{\partial x} \right) + \sigma_{yy} \frac{\partial v}{\partial y} \right) \frac{\partial y}{\partial \eta} - \left[(\sigma_{xx} n_1 + \sigma_{xy} n_2) \frac{\partial u}{\partial x} + (\sigma_{xy} n_1 + \sigma_{yy} n_2) \frac{\partial v}{\partial x} \right] \sqrt{\left(\frac{\partial x}{\partial \eta} \right)^2 + \left(\frac{\partial y}{\partial \eta} \right)^2} \right\} d\eta$$
$$= \int_1^1 I d\eta$$

(3.50)

The above equation (3.50) can be evaluated using Gaussian numerical integration.

3.3 Equations of Motion for a System

The dynamic analysis of any structure starts with the formulation of the equations of motion. The equations of motion of any dynamic system can be written down using Newton's second law of motion. The equations of motion of the system can be derived using Lagrange's equations. These equations are also applicable to tapered composite structures.

3.3.1 Lagrange's Equations

For a system of N masses, which are free to move in three dimensions, the kinetic energy is given by [41]

$$T = \frac{1}{2}\{\dot{q}\}^T[M]\{\dot{q}\} \tag{3.51}$$

where [M] is a matrix of inertia coefficients. Similarly the strain energy of the system can be expressed as

$$U = \frac{1}{2}\{q\}^T[K]\{q\} \tag{3.52}$$

where [K] is a matrix of stiffness coefficients. Defining dissipation function as

$$D = \frac{1}{2}\{\dot{q}\}^T[C]\{\dot{q}\} \tag{3.53}$$

where [C] is a matrix of damping coefficients, the equations of motion of the system are derived using Lagrange's equations as

$$\frac{d}{dt}\left(\frac{\partial T}{\partial \dot{q}_j}\right)+\frac{\partial D}{\partial \dot{q}_j}+\frac{\partial U}{\partial q_j}=Q_j, \quad j=1,2,\cdots,n$$

(3.54)

where q is a column matrix of system displacements and Q_j is a generalized force.

3.3.2 Equations of Motion for Finite Element

The main ideas behind FEM approach to structural modal analysis are employed. The dynamic system will be a plane strain problem based on which a model is built up in discrete system format corresponding to the composite laminate.

Consider a multi degree of freedom system represented by mass, stiffness and damping matrices, [M], [K], and [C] respectively. When it is excited by a deterministic force f (t), the differential equations of motion can be written in the form of a coupled system.

$$[M]\{\ddot{u}\}+[C]\{\dot{u}\}+[K]\{u\}=\{f\}$$

(3.55)

The dynamic system is made up of two dimensional parabolic isoparametric elements. The plane elements have continuously distributed

mass and stiffness properties. A method of solving this equation subject to the relevant boundary conditions is now described.

3.3.3 Proportional Damping

One of the easiest methods for representing damping is that based on the concept of proportional damping. We define a damping matrix as

$$[C] = \alpha_1[M]+\beta_1[K] \tag{3.56}$$

This method is also advantageous because it is often mathematically convenient to have the damping matrix proportional to the mass and stiffness matrices. The values for the two constants are assumed as $\alpha_1 = 0.0001$ and $\beta_1 = 0.00002$. Parameters α_1 and β_1 should be obtained using modal testing and system identification technique. Since this is a complex work, it is not carried out in the present thesis. Therefore, to demonstrate the overall procedure, some representative values of α_1 and β_1 have been estimated in comparison with similar materials and by experience. Therefore, the results have corresponding limitation.

3.3.4 Computation of Eigenvalues and Eigenvectors

The eigenvalues/eigenvectors (modal parameters) are determined for the system based on an analytical technique and free vibration analysis.

3.3.4.1 Natural frequencies and normal modes

Let us assume that displacement vector $\{u\}=\{U\}e^{i\omega t}$, and consider the free vibration of the multi degree of freedom system. Substituting displacement vector $\{u\}=\{U\}e^{i\omega t}$ into equation (3.55), we obtain

$$([K]-\omega^2[M])\{U\}=\{0\} \tag{3.57}$$

Denoting that $\lambda=\omega^2$, the standard form of eigenvalue problem is

$$([A]-\lambda[I])\{U\}=\{0\} \tag{3.58}$$

where $[A]=[M]^{-1}[K]$.

It is possible to compute the eigenvectors using the eigenvalues.

3.3.4.2 Transformation Function

Once the eigenvectors have been obtained, the generalized mass and stiffness matrices and generalized force vector can be obtained. The displacement coordinate will be translated to modal coordinate, so that one can get the equations of motion in modal coordinates and in terms of the generalized mass and the stiffness matrices and the force vector.

$$[\overline{M}] = [\phi]^T [M][\phi]$$

(3.59)

$$[\overline{K}] = [\phi]^T [K][\phi]$$

(3.60)

$$[\overline{C}] = [\phi]^T [C][\phi] = \alpha [\overline{M}] - \beta [\overline{K}]$$

(3.61)

$$\{\overline{f}\} = [\phi]^T \{f\}$$

(3.62)

where [ϕ] is the modal matrix consisting of eigenvectors.

The dynamic behavior of a structure can be characterized in terms of natural frequencies, mode shapes and damping. The response in frequency domain will be calculated using equations (3.57-3.62). The motion equations can be written as

$$\left(-\omega^2[\overline{M}]+\omega[\overline{C}]+[\overline{K}]\right)\{U\}=\{\bar{f}\}$$

(3.63)

The eigenvectors [ϕ] are orthogonal to each other, and we get n number of uncoupled equations. Denoting the j^{th} line of the matrix [ϕ] by a row vector [ϕ_j], one can get the j^{th} response of the dynamic system. The transformation function (the frequency response function) H (ω) is,

$$H(\omega)=\left[-\omega^2[\overline{M}]+\omega[\overline{C}]+[\overline{K}]\right]^{-1}$$

(3.64)

The frequency response function of the coupled system can be written as

$$H(\omega)=\left[-\omega^2[M]+\omega[C]+[K]\right]^{-1}$$

(3.65)

3.4 Response to Random Excitation

The crack propagation depends on the response to the random excitation of the tapered laminate. In the case of random forces, there is no way of predicting an exact value of response at a future instant of time. Such forces and corresponding response can only be described by means of stochastic processes.

3.4.1 Representation of the Excitation

The probability of realizing a value of f(t) that is less than some specified value f_0, which is denoted as $P(f_0)$, is given by

$$P(f_0)=\text{Prob}[f(t)<f_0] \tag{3.66}$$

Now, when the value of f_0 is changed within the range of the random process, one can set P(f). The function P(f) is known as the probability distribution function which increases as f increases. The probability density function is denoted by p(f), according to

$$p(f)=\frac{dP(f)}{df} \tag{3.67}$$

Various parameters are used to describe the shape of a probability density curve. The most important one is the expected value or mean, which is given by

$$E[f] = \int_{-\infty}^{\infty} f p(f)\,df \tag{3.68}$$

The value E[f] is called the first moment of f and is given the notation μ_f. The second central moment is the variance, which is

$$E[(f - \mu_f)^2] = \sigma_f^2 \tag{3.69}$$

where σ_f is the standard deviation of f. It is a measure of the dispersion or spread about the mean.

A particularly important probability distribution is the Gaussian or normal distribution, the probability density of which is given by

$$p(f) = \frac{1}{(2\pi)^{1/2}\sigma_f} \exp\{-(f - \mu_f)^2 / 2\sigma_f^2\} \tag{3.70}$$

The Gaussian distribution is completely defined by its mean μ_f and standard deviation σ_f. It is symmetrical about the mean.

3.4.2 Power Spectral Density Function

A random excitation is essentially a non-periodic function. Such a function can be represented by means of a Fourier integral, namely,

$$f(t) = \int_{-\infty}^{\infty} F(i\omega) e^{i\omega t} d\omega \tag{3.71}$$

where

$$F(i\omega) = \int_{-\infty}^{\infty} f(t) e^{-i\omega t} dt \tag{3.72}$$

where ω denotes the cycle frequency.

A random excitation can not be represented directly by means of Fourier transforms. To have stationary properties a random signal must be assumed to continue over an infinite period of time. There is no difficulty in determining the Fourier transform of the signal $f_T(t)$ which is identical to f(t) within the interval $-T \leq t \leq +T$ and zero at all other times.

$$f_T(t) = \int_{-\infty}^{\infty} F_T(i\omega) e^{i\omega t} d\omega \tag{3.73}$$

and

$$F_T(i\omega) = \int_{-\infty}^{\infty} f_T(t) e^{-i\omega t} dt \tag{3.74}$$

The mean square of f(t) is, therefore

$$\begin{aligned} \overline{f^2(t)} &= \lim_{T\to\infty} \overline{f_T^2(t)} \\ &= \int_{-\infty}^{\infty} \lim_{T\to\infty} \frac{\pi}{T} |F_T(i\omega)|^2 \, d\omega \\ &= \int_{-\infty}^{\infty} S_f(\omega) \, d\omega \end{aligned} \tag{3.75}$$

where

$$S_f(\omega) = \lim_{T\to\infty} \frac{\pi}{T} |F_T(i\omega)| \tag{3.76}$$

This is called as the power spectral density function.

The power spectral density function, $S_f(\omega)$, is an even function which is defined over the range $-\infty \leq \omega \leq +\infty$. When making practical measurements it is more convenient to deal with positive frequencies. In this case a one-sided power spectral density function, $G_f(\omega)$, is introduced such that

$$G_f(\omega) = 2S_f(\omega) \text{ for } \omega > 0 \tag{3.77}$$

and

$$\overline{f^2(t)} = \int_{-\infty}^{\infty} G_f(\omega) d\omega \tag{3.78}$$

3.5 Response of a Multi-degree of Freedom System

In the equation (3.55), {f} is the applied force vector which is assumed to be a weakly stationary, ergodic process having a Gaussian probability density distribution with a zero mean. The probability density function is, therefore

$$p(f) = \frac{1}{(2\pi)^{1/2}\sigma_f} e^{-f^2/2\sigma^2} \tag{3.79}$$

If both the functions u(t) and f(t) in equation (3.55) are truncated so that they are zero outside the interval (-T,T), then they can be expressed in terms of their Fourier transforms, namely,

$$u_T(t) = \int_{-\infty}^{\infty} U_T(iw) e^{i\omega t} d\omega \tag{3.80}$$

$$f_T(t) = \int_{-\infty}^{\infty} F_T(iw) e^{i\omega t} d\omega \tag{3.81}$$

where $U_T(i\omega)$ and $F_T(i\omega)$ are the Fourier transforms of $u_T(t)$ and $f_T(t)$ respectively. The Fourier transform of the response in r-th degree of freedom is therefore

$$U_r(i\omega)=[H(i\omega)]_r F(i\omega) \tag{3.82}$$

where

$$H(i\omega)=[K-\omega^2 M+i\omega C]^{-1} \tag{3.83}$$

is the receptance matrix. Here $[H(i\omega)]_r$ indicates row r of H. Note that degree of freedom r will represent one of the degrees of freedom at a particular node. The power spectral density function of the response in degree of freedom r is

$$S_{u_r}(\omega) = \lim_{T\to\infty} \frac{\pi}{T} |U_r(i\omega)|^2 \tag{3.84}$$

It can be shown that

$$S_{u_r}(\omega) = \{H^*(i\omega)\}_r S_f(i\omega) \{H(i\omega)\}_r^T \tag{3.85}$$

where $S_f(i\omega)$ is the cross-spectral density matrix of excitation. In the case of a multi-degree-of-freedom system equation (3.86) gives

$$S_{u_r}(\omega) = \{H_{11}^*(i\omega) \ldots H_{1r}^*\} S_f(i\omega) \begin{bmatrix} H_{11}(i\omega) \\ \vdots \\ H_{1r}(i\omega) \end{bmatrix} \tag{3.86}$$

$$S_{u_r}(\omega) = \{H_{r1}^*(i\omega) \ldots H_{rr}^*\} S_f(i\omega) \begin{bmatrix} H_{r1}(i\omega) \\ \vdots \\ H_{rr}(i\omega) \end{bmatrix} \tag{3.87}$$

with

$$S_f(i\omega) = \begin{bmatrix} S_{f_1 f_1} & \cdots & S_{f_1 f_r} \\ \vdots & \vdots & \vdots \\ S_{f_r f_1} & \cdots & S_{f_r f_r} \end{bmatrix} \tag{3.88}$$

where

$$S_{f_i f_j} = \lim_{T \to \infty} \frac{\pi}{T} \left[\frac{\int_T f_i(t) e^{-i\omega t} dt}{2\pi} \right] \left[\frac{\int_T f_j(t) e^{i\omega t} dt}{2\pi} \right] \tag{3.89}$$

If the two forces arise from independent sources, then they will be uncorrelated. This means that

$$R_{f_i f_j}(\tau) = 0 = R_{f_j f_i}(\tau) \tag{3.90}$$

The equation for the cross-spectral density is

$$S_{f_1 f_2}(\omega) = \frac{1}{2\pi}\int_{-\infty}^{\infty} R_{f_1 f_2}(\tau) e^{-i\omega\tau} d\tau$$

(3.91)

The inverse relationship is

$$R_{f_1 f_2}(\tau) = \frac{1}{2\pi}\int_{-\infty}^{\infty} S_{f_1 f_2}(\omega) e^{i\omega\tau} d\omega$$

(3.92)

where i≠j and i.j=1.2.3.....r. Substituting equation (3.90) into equation (3.91) gives

$$S_{f_i f_j}(i\omega) = 0 = S_{f_j f_i}(i\omega)$$

(3.93)

Equation (3.87) therefore reduces to

$$S_{u_r}(\omega) = \left|H_{i1}(i\omega)\right|^2 S_{f_1 f_1}(\omega) + \cdots + \left|H_{ir}(i\omega)\right|^2 S_{f_r f_r}(\omega)$$

(3.94)

The power spectral density of the response is, therefore, equal to the sum of the power spectral densities obtained with the forces acting separately.

The mean square response is given by

$$\sigma_u^2 = \int_{-\infty}^{\infty} S_u(\omega) d\omega \tag{3.95}$$

The spectral moments of this system can be calculated using

$$\begin{aligned} \sigma_{0,u}^2 &= \int_{-\infty}^{\infty} S_u(\omega) d\omega \\ \sigma_{1,u}^2 &= \int_{-\infty}^{\infty} \omega S_u(\omega) d\omega \\ \sigma_{2,u}^2 &= \int_{-\infty}^{\infty} \omega^2 S_u(\omega) d\omega \end{aligned} \tag{3.96}$$

The first expression is the mean square of the displacement and the last one is the mean square of the velocity.

The standard deviations of the response are

$$\sigma_{i,u} = \sqrt{\sigma_{i,u}^2} \qquad i = 1,2,3 \tag{3.97}$$

3.6 Numerical Results and Comparison

3.6.1 Comparison for a Two-dimensional Model of a Cylinder

A two-dimensional solid example considered is the case of a thick circular cylinder conforming to plane strain conditions that is also considered in Ref. [42]. In figure 3.3 the geometrical dimensions and the material properties are shown:

Elastic Modulus E = 1000
Poisson Ratio ν = 0.3
Thickness h = 1.0
Normal Pressure p=10

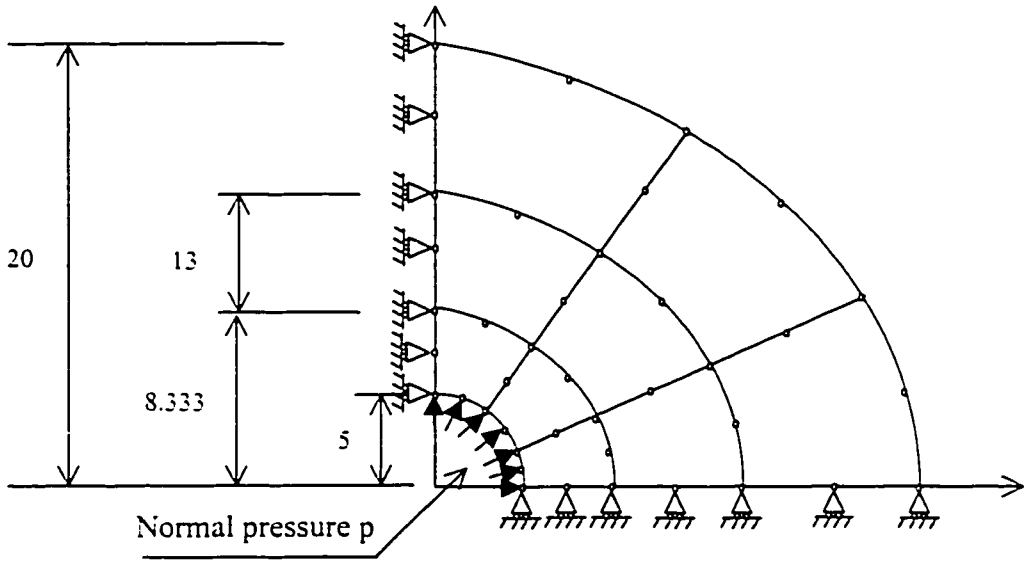

Figure 3.3 Reference model

The material property values and dimensions were given in Ref. [42] and they represent normalized values [42]. The element subdivision employed 9 parabolic isoparametric elements. The loading considered is the application of an internal pressure of 10, with the external boundary being unloaded. Both the displacements and stresses obtained in the present work are

compared with the results given in Ref. [42]. The comparisons are provided in tables 3.3, 3.4, 3.5 and 3.6. Excellent agreement between the results is observed. C-R refers to the present results, and R-R refers to the reference results.

Table 3.3 Comparison between the displacements

node	C-R		R-R	
	x-disp.	y-disp.	x-disp.	y-disp.
1	0.0710	0	0.0710	0
2	0.0542	0	0.0542	0
3	0.0444	0	0.0444	0
4	0.0361	0	0.0361	0
5	0.0311	0	0.0311	0
6	0.0267	0	0.0267	0
7	0.0242	0	0.0242	0
8	0.0685	0.0183	0.0685	0.0183
9	0.0429	0.0115	0.0429	0.0115
10	0.0300	0.0081	0.0300	0.0081
11	0.0234	0.0063	0.0234	0.0063
12	0.0615	0.0355	0.0614	0.0355
13	0.0469	0.0271	0.0469	0.0271
14	0.0385	0.0222	0.0385	0.0222
15	0.0313	0.0181	0.0313	0.0181
16	0.0270	0.0156	0.0270	0.0156
17	0.0231	0.0133	0.0231	0.0133
18	0.0210	0.0121	0.0210	0.0121
19	0.0501	0.0501	0.0501	0.0501
20	0.0314	0.0314	0.0314	0.0314
21	0.0220	0.0220	0.0220	0.0220
22	0.0171	0.0171	0.0171	0.0171
23	0.0355	0.0615	0.0355	0.0614
24	0.0271	0.0469	0.0271	0.0469
25	0.0222	0.0385	0.0222	0.0385
26	0.0181	0.0313	0.0181	0.0313
27	0.0156	0.0270	0.0156	0.0270
28	0.0133	0.0231	0.0133	0.0231
29	0.0121	0.0210	0.0121	0.0210
30	0.0183	0.0685	0.0183	0.0685
31	0.0115	0.0429	0.0115	0.0429
32	0.0081	0.030	0.0081	0.0300
33	0.0063	0.0234	0.0063	0.0234
34	0	0.0710	0	0.0709
35	0	0.0542	0	0.0542
36	0	0.0444	0	0.0444
37	0	0.0361	0	0.0361
38	0	0.0311	0	0.0311
39	0	0.0267	0	0.0267
40	0	0.0242	0	0.0242

Table 3.4 Comparison between total nodal forces

Element no.	Node no.	C-R		R-R	
		X	Y	X	Y
1	1	4.460	.0167	4.460	.0195
	12	3.873	2.217	3.873	2.217
	8	16.67	4.467	16.67	4.467
4	12	3.857	2.243	3.857	2.243
	23	2.243	3.857	2.243	3.857
	19	12.20	12.20	12.20	12.20
7	23	2.217	3.873	2.217	3.873
	34	.0167	4.460	.0195	4.460
	30	4.467	16.67	4.467	16.67

Table 3.5 Comparison between the reactions

node	C-R		R-R	
	x-force	y-force	x-force	y-force
1	0	-6.1267	0	-6.1287
2	0	-15.0690	0	-15.0710
3	0	-5.8100	0	-5.8089
4	0	-9.4652	0	-9.4642
5	0	-4.2696	0	-4.2695
6	0	-7.7360	0	-7.7352
7	0	-1.5235	0	-1.5229
34	-6.1268	0	-6.1287	0
35	-15.0690	0	-15.0710	0
36	-5.8100	0	-5.8089	0
37	-9.4652	0	-9.4642	0
38	-4.2696	0	-4.2696	0
39	-7.7360	0	-7.7352	0
40	-1.5235	0	-1.5223	0

Table 3.6 Comparison between the stresses

Element no.	C-R			R-R		
	x-stress	y-stress	xy-stress	x-stress	y-stress	xy-stress
1	-5.1827	5.5287	-3.0918	-5.1816	5.5287	-3.0918
2	-1.5547	2.5970	-1.1985	-1.5542	2.5970	-1.1983
3	-0.2575	1.4753	-0.5002	-0.2575	1.4751	-0.5002
4	0.1751	0.1751	-6.1835	0.17355	0.1734	-6.1836
5	0.5215	0.5215	-2.3968	0.5214	0.5214	-2.3967
6	0.6089	0.6089	-1.0005	0.6088	0.6088	-1.0003
7	5.5287	-5.1827	-3.0918	5.5287	-5.1820	-3.0918
8	2.5970	-1.5547	-1.1985	2.5970	-1.5540	-1.1983
9	1.4753	-0.2575	-0.5002	1.4751	-0.2570	-0.5002

3.6.2 Comparison of Eigenvalues

3.6.2.1 Comparison Between the 6-node and 8-node Elements

In Figure 3.3, a two-dimensional solid example, the case of a thick circular cylinder conforming to plane strain conditions is considered. Now, the quadratic elements of Figure 3.3 are changed to triangular elements for the comparison of the 6-node and 8-node Elements. The first six eigenfrequencies are obtained and provided in Table 3.7.

Table 3.7 Comparison between different elements

Mode	Eigenvalues 8-node Element	Eigenvalues 6-node Element	% Difference
1	0.0682	0.0678	0.57
2	0.3629	0.3863	6.06
3	0.4203	0.4228	0.59
4	0.8692	0.8664	0.32
5	1.2809	1.2834	0.19
6	1.7219	1.7385	0.95

From this table, it can be observed that the eigenvalues of the 6-node and 8-node elements are in excellent agreement; the differences are less than 6.06 % and the 6-node elements can be used.

3.6.2.2 Comparison Between Finite Element and Analytical Solution

Consider a cantilever shear wall shown in Figure 3.4, which can be treated as a deep beam. The beam is 60.96 m long, 15.24 m wide, and the thickness is 0.2289 m. The material properties are:

Young's modulus $E=34.474\times10^{9}$ N/m^2

Poisson's ratio $\nu=0.11$

Mass per unit volume $\rho=568.2$ kg/m^3

There are two degrees of freedom at each node. In the Ref. [39], 32 linear triangular elements and 27 nodes have been used. The left end of the deep beam was fixed. We only used two elements of 8-node rectangular element and 13 nodes. The results obtained are compared with the analytically derived results that are given in Ref. [39], in Table 3.8.

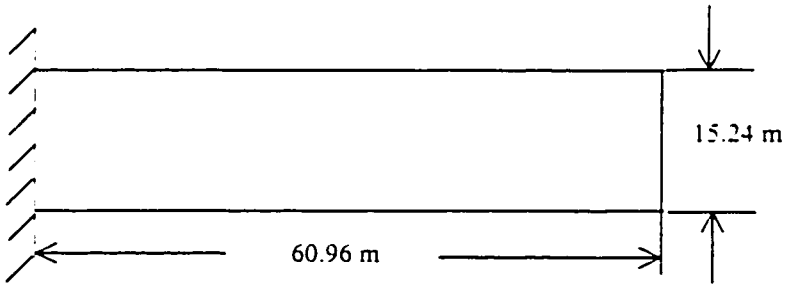

Figure 3.4 A cantilever shear wall

As can be seen from the comparison in Table 3.8, the differences are less than 13.60%. Here, we only used 2 elements of 8-node element, and the accuracy of the result was better than that obtained using 32 elements of linear triangular element in Ref. [39].

Table 3.8 Comparison of the frequencies

Mode	Analytical Solution	Ref. [40]	% Difference	Present Computation	% Difference
1	4.9730	6.392	28.53	5.0988	2.53
2	26.3910	32.207	22.04	29.1388	10.41
3	31.9440	32.010	0.21	32.1840	0.21
4	62.0660	74.843	20.59	70.5085	13.60
5	95.8320	96.900	1.11	98.1080	2.37

3.6.3 Analysis of a Tapered Laminate

The tapered structure chosen is 200 mm long, and 10 mm wide. The length is 30 mm between the two tapered ends, the tapered angle is 5.71 degrees. The thick section configuration of the laminate is $[0_4/\pm45_4/\pm45_S/-45_S]_s$, and the thin section configuration of the laminate is $[0_4/\pm45_4]_s$. Each ply is 0.125 mm thick.

The resin pockets of the tapered structure are shown in Figure 3.5. The resins (Epoxy) are present due to the laminate structure tailoring of the Graphite/Epoxy material. The distribution of resin areas are shown in Figure 3.5, and these areas are named separately as Area I, Area II, and Area III. The regions between the resin and ply are crack generating areas when the loading is applied at the thin end of the tapered structure.

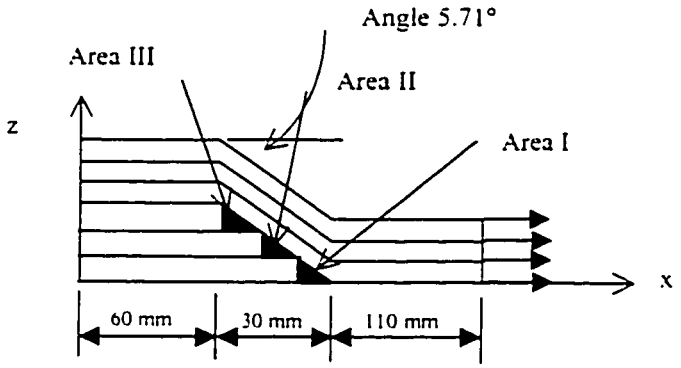

Model A

Figure 3.5 Model A with 5.71° taper

3.6.3.1 Meshing

Considering that the mesh size must be compatible with the generated crack size and that the domain of mesh reflects the behavior of a region with cracks, we only refine those domains included in the resin areas. In order to ensure the precision of the computation, 616 nodes and 189 elements are used for this tapered structure (see Figure 3.6 (a) and (b)). For checking the mesh a small program which can plot each node position (see the Figure 3.6 (a) and (b)) is written. In Figure 3.6, the symbol "o" represents a node and the coordinate unit is mm. Further details about the mesh are given in Appendix IV.

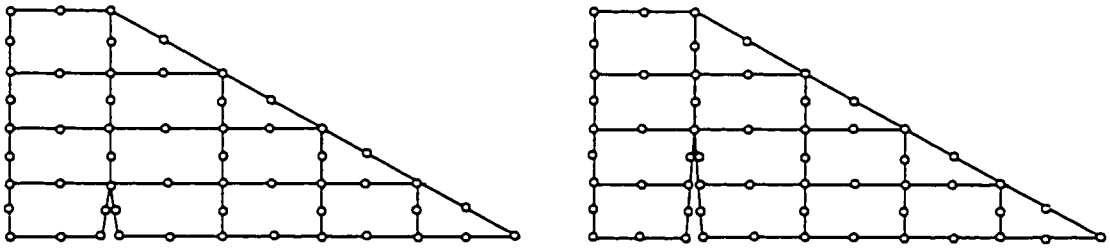

With initial crack

After crack propagation

Figure 3.6 (a) Finite element mesh at crack tip

For comparison purpose, those points that are at the thin end (at x = 200 mm) and that are between ply and resin (between 60-80 mm) are chosen. Those points can be seen in Table 3.9, and these points between 60 and 80 mm can be found from the Figure 3.6 according to the coordinate values.

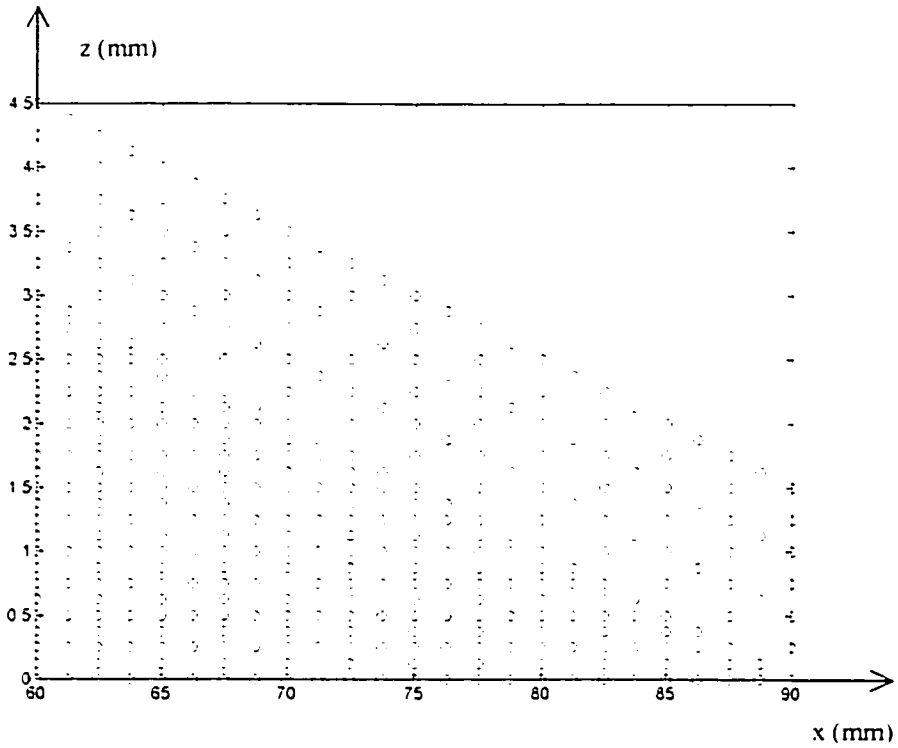

Figure 3.6 (b) A part of the finite element model

Table 3.9 Chosen comparison points

Node no.	At x=200 mm	Node no.	At x=80 mm
1	z= 0.00 mm	122	z= 0.000 mm
2	z= 0.25 mm	126	z= 0.500 mm
3	z= 0.50 mm	130	z= 1.000 mm
4	z= 0.75 mm		
5	z= 1.00 mm		
6	z= 1.25 mm		
7	z= 1.50 mm		
Node no.	At x=70 mm	Node no.	At x=60 mm
242	z=1.000 mm	414	z=2.000 mm
246	z=1.500 mm	418	z=2.500 mm
250	z=2.000 mm	422	z=3.000 mm

The elements for comparison are chosen from the following regions: the regions where the ply elements connect to the resin elements; the central coordinates of the elements are shown in Table 3.10.

Table 3.10 Central coordinates of chosen elements

Thin section end	Near Area I (mm)		Near Area II (mm)		Near Area III (mm)	
x=185mm	x=78.75	x=81.25	x=68.75	x=71.25	x=58.00	x=61.25
z= 0.25mm	z= 0.125	z= 0.125	z= 1.125	z= 1.125	z= 2.125	z= 2.125
z= 0.75mm	z= 0.375	z= 0.375	z=1.375	z=1.375	z= 2.375	z= 2.375
z= 1.25mm	z= 0.625	z= 0.625	z=1.625	z=1.625	z= 2.625	z= 2.625

3.6.3.2 Comparison Between the Displacements

According to the maximum strain theory, failure occurs when at least one of the strain components along the principal material axes exceeds the corresponding ultimate strain in that direction. The ultimate strain of the graphite/epoxy material in its longitudinal tensile direction is about 0.002. When the length of the Model-A is 200 mm, the maximum displacement is limited to 0.4 mm. If the cross-section area of Model A is 15 mm^2, and a uniformly distributed tensile load is chosen as 1800 N (1200×10^5 N/m^2) along the x direction at the thin section end, and the modulus of elasticity E=139 GPa (the tapered structure is considered as a beam), the estimated stress is about 120 MPa, and the estimated displacement is about 0.19 mm at thin section end. The computed displacements are given in Table 3.11. The reference results were obtained from the Ref. [43], and they have been obtained using a 3D modeling and further, those results have in turn been compared with the results obtained using ANSYS software.

Table 3.11 Displacements at the chosen points

Node no.	Present results Displacements(mm)		Corresponding Node no. in Reference	Reference results Displacements(mm)	
	u	v		u	v
1	0.2808	0.0000	22	0.2403	0.0000
2	0.2806	-1.5523e-4	146	0.2489	-4.562e-4
3	0.2803	-3.0824e-4	181	0.2436	-3.874e-4
4	0.2795	-4.6440e-4	216	0.2398	-5.432e-4
5	0.2787	-6.1361e-4	228	0.2508	-3.456e-4
6	0.2780	-7.8973e-4	270	0.2467	-5.076e-4
7	0.2776	-9.6045e-4	282	0.2553	-5.643e-4
122	0.0698	0.0000	11	0.0581	0.0000
126	0.0704	-6.8953e-4	12	0.0581	-1.345e-4
130	0.0728	-1.3168e-3	37	0.0592	-1.456e-4
242	0.0516	-4.2144e-4	81	0.0471	-4.512e-4
246	0.0516	-8.6451e-4	89	0.0472	-1.253e-4
250	0.0512	-1.4303e-3	99	0.0469	-2.354e-4
414	0.0469	-9.2322e-4	97	0.0428	-3.496e-4
418	0.0461	-1.2205e-3	103	0.0426	-4.521e-4
422	0.04676	-1.5625e-3	111	0.04208	-5.213e-4

3.6.3.3 Comparison Between the Stresses

Between resin and ply areas, the displacement can be continuous, but the stresses are not continuous. The chosen areas for comparing stresses are those regions that are between ply and resin. The computed stresses at the chosen points are given in Table 3.12. From these stresses, the area which is the most critical one among the three areas can be determined.

As the tensile loading of the tapered structure is increased, a point is eventually reached at which changes in geometry are no longer entirely reversible. Using the Maximum Distortion Energy Theory (Von Mises Theory, see Ref. 56, pp. 155), it can be shown that failure occurs at a point

when $2\sigma_x^2+2\sigma_z^2 - 2\sigma_x\sigma_z+6\tau_{xz}^2 = 2\sigma_{yp}^2$, where σ_{yp} is the yield stress. When σ is greater than σ_{yp} , where $\sigma^2=((2\sigma_x^2+2\sigma_z^2 - 2\sigma_x\sigma_z+6\tau_{xz}^2)/2)$, the structure will be at failure. This way the load at the first failure in area I can be estimated using the results given in Table 3.12.

Table 3.12 Stresses in the chosen elements

Area I	Present Stresses in the laminate (MPa)		Reference Stresses in the laminate (MPa)	
Central coordinate at x=81.25mm	x direction	z direction	x direction	z direction
z= 0.125mm	31.423	0.8305	29.353	1.321
z= 0.375mm	33.335	0.7999	30.249	1.312
z= 0.625mm	38.419	0.5532	32.789	1.321
	Present stresses in the resin (MPa)		Reference stresses in the resin (MPa)	
Central coordinate at x=78.75mm	x direction	z direction	x direction	z direction
z= 0.125mm	15.365	-2.5432	13.365	-1.375
z= 0.375mm	15.034	-2.5209	12.265	-1.362
z= 0.625mm	14.323	-2.3325	12.189	-1.243

Area II	Present stresses in the laminate (MPa)		Reference stresses in the laminate (MPa)	
Central coordinate at x=71.25mm	x direction	z direction	x direction	z direction
z=1.375mm	28.296	1.1171	25.54	2.13
z=1.625mm	29.074	1.1012	27.89	2.35
	Present stresses in the resin (MPa)		Reference stresses in the resin (MPa)	
Central coordinate at x=68.75mm	x direction	z direction	x direction	z direction
z=1.625mm	8.5742	-1.2242	10.12	-2.16

Area III	Present stresses in the laminate (MPa)		Reference stresses in the laminate (MPa)	
Central coordinate at x=58.00mm	x direction	z direction	x direction	z direction
z= 2.375mm	24.848	0.2026	23.42	0.217
z= 2.625mm	25.022	0.2103	24.56	0.201
	Present stresses in the resin (MPa)		Reference stresses in the resin (MPa)	
Central coordinate at x=61.25mm	x direction	z direction	x direction	z direction
z= 2.625mm	6.4699	-1.7284	7.25	-2.12

3.6.3.4 Comparison Between the Values of Energy Release Rate

The initial crack length is considered as 0.25 mm and the crack width is 0.002 mm. The crack propagates to an incremental distance da=0.25 mm and the crack width is 0.004 mm when the stress intensity factor reaches a critical value. The energy release rate is given in Table 3.13.

Table 3.13 Energy release rate

Model A with Angle 5.71°	Strain-energy (Initial crack width 0.002 mm and initial crack length 0.25 mm)	Strain-energy (after the crack propagation, the crack width and length are 0.004 and 0.50 mm)	Energy-release rate
Present results	0.2515 N.m	0.2516 N.m	38.9520 Pa.m
Reference results	0.2413 N.m	0.2415 N.m	44.0872 Pa.m

3.6.3.5 Comparison of Stress Intensity Factor and J Integral

The stress intensity factor K can be estimated from the energy release rate. As shown in Figure 3.7, for obtaining more accurate estimates of K, singularity elements are used at the crack tip. A high degree of mesh refinement is made for getting a reasonable accuracy. The method detailed in section 3.1.7 has been used. The resin layer near the crack is refined into very small finite elements, such that the side length of the six-node triangle element is 0.001 mm. The plies with same angle are modeled as one ply. The

mesh refinement is mostly enforced in the region surrounding the crack, wherein the maximum interlaminar stresses are present. The results are presented in Table 3.14.

Table 3.14 Stress intensity factor

Model A with Angle 5.71°	Initial crack length a = 0.1 mm	Initial crack length a= 0.05 mm	Initial crack length a = 0.01 mm
Stress intensity factor	6.578×10^{5} Pa $m^{1/2}$	5.604×10^{5} Pa $m^{1/2}$	4.932×10^{5} Pa $m^{1/2}$

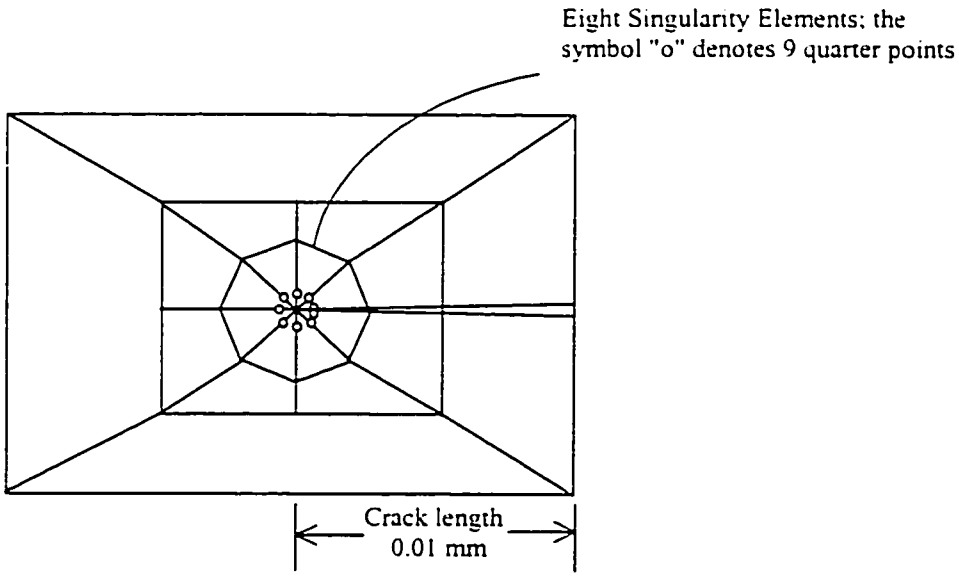

Figure 3.7 Vicinity of the crack

The critical value of the stress intense factor, K_{IC} is a material property that can be found in handbooks. If K_{IC} is less than K, the crack will grow.

Figure 3.8 shows the J contour. The computed values of J integral for different contours are seen to be not constant but the difference in values is only 30 %.

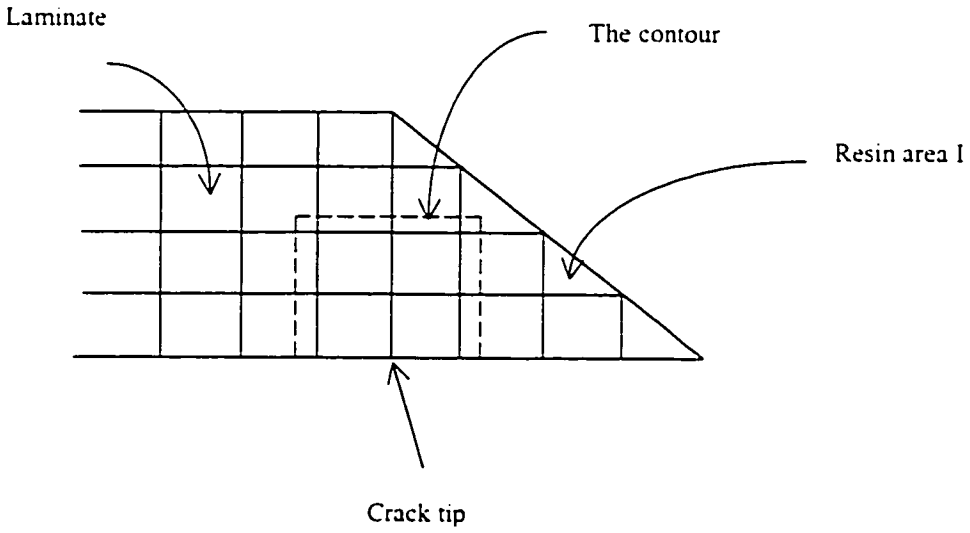

Figure 3.8 A part of the mesh showing J contour

Table 3.15 J integral

Model A with Angle 5.71°	Radial distance r = 2.2916 mm	Radial distance r = 2.7083 mm	Radial distance r = 4.7916 mm
J integral	39.0675 Pa.m	45. 7123 Pa.m	55.3620 Pa.m

3.6.4 Program Construction

In this program, all routines are written in either Fortran or Matlab Language. The finite element program can solve the static problem as well as the dynamic problem. The structure of the program developed is described in detail in Figure 3.9.

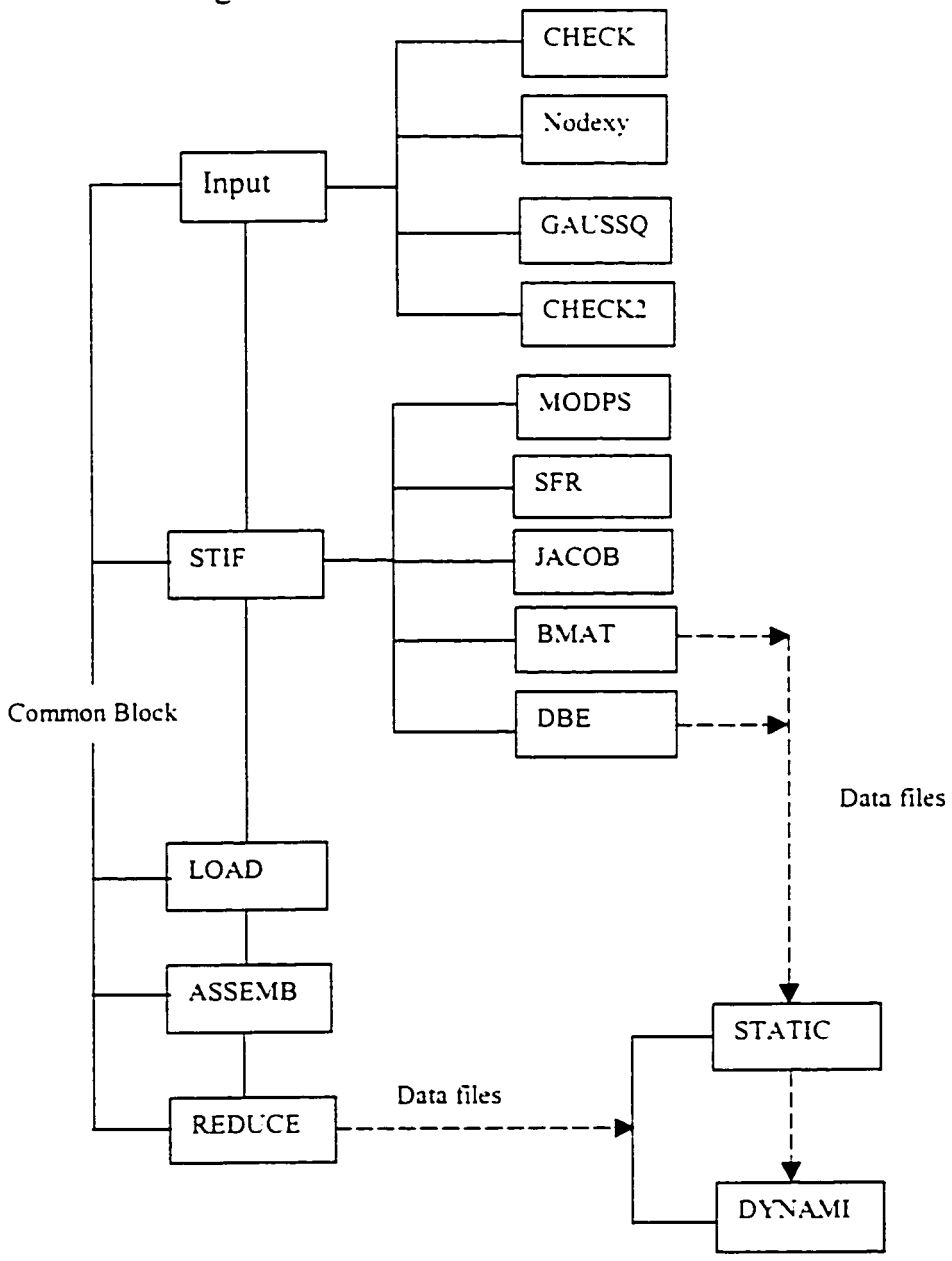

Figure 3.9 Program organization

3.6.4.1 Routines in Fortran Language

INPUT subroutine is subdivided into two functions: one (Input) subroutine inputs a data file and sorts the inputted data according to the data properties, another (Input1) subroutine stores the sorted data and outputs the data (the format of an input data file can be seen in **Appendix III**).

NODEXY generates the coordinates of mid-side nodes that lie on a straight line connecting adjacent corner nodes. In generating singularity element, the NODEXY subroutine will not be used.

GAUSSQ generates the Gauss point positions and weighting factors according to the order of integration rule specified.

CHECK and CHECK2 subroutines scrutinize the inputted data and check any errors that are signaled by diagnostic messages.

MODPS evaluates the elasticity matrix for plane strain problem according to the given material property values.

SFR calculates the shape functions and their derivatives for 2D elements.

JACOB calculates the coordinates of Gauss points, the Jacobian Matrix and its determinant and the inverse for 2D elements.

BMAT calculates the strain matrix for plane strain problem using the Cartesian shape function derivatives; the results will be written in one file.

DBE simply multiplies the elasticity matrix and the strain matrix, the results will be written in one file.

STIFP calculates the element stiffness matrix.

LOAD calculates the loading.

ASSEMB is a subroutine using which the individual element stiffness matrices and load vectors are assembled into the overall structural stiffness matrix and load vector respectively.

REDUCE is a subroutine that can omit the constrained degrees of freedoms, the results will be written in one file.

All these subroutines are provided in the disk attached.

3.6.4.2 Routines in Matlab Language

STATIC calculates the displacements, stresses and strains. These results can be used to calculate the energy release rate (see **Appendix I**).

DYNAMI calculates the eigenvalues, eigenvectors, and the random response (see **Appendix II**).

3.7 Discussion

In this Chapter, the finite element formulations of a two-dimensional plane strain problem have been given. The element stiffness matrix and strain matrix B are calculated based on the quadratic and triangular shape functions. A three-dimensional problem of composite material is transformed into a two-dimensional problem. The singularity elements for obtaining the stress intensity factor are discussed, and it is found that rectangular quarter-point elements are less accurate than triangular quarter-point elements. The virtual crack extension method was introduced. In this method, the energy release rate is related to the change in the potential energy, and further this energy release rate is related to the change in the element stiffness.

The dynamic analysis of any structure starts with the formulation of the equations of motion. The damping is considered to be proportional damping. The frequency response function of coupled system and natural frequencies were considered that will be used to calculate the response of the system and the frequencies of the system.

The mean and standard deviation of the response to random excitation is calculated. A particularly important probability distribution is the Gaussian distribution that is completely defined by its mean and standard deviation. The power spectral density function is an even function that is defined over the range $-\infty \leq \omega \leq +\infty$. When making practical measurements it is more convenient to deal with positive frequencies. In this case, a one-sided spectral density function is introduced.

Comparisons have been made for a two-dimensional model of a cylinder and it has been observed that the results are in excellent agreement. Comparisons between the 6-node and 8-node elements have shown that the 6-node elements do not have any problem. Comparisons between finite element and analytical solution indicate that the accuracy of the result was better in the case of triangular element. Analysis of a tapered laminate has been performed. The analysis results are in excellent agreement with the reference results. Comparison between the values of energy release rate indicates that the computational results of energy release rate are in very good agreement with the reference results. Comparison of stress intensity factor and J integral indicates that the stress intensity factors can be computed easily and that there are very little differences between J integral and energy release rate.

All routines were written in either Fortran or Matlab Language that can solve the static problem as well as the dynamic problem. The Fortran program connects to the Matlab program through the data.

Chapter 4

Parametric Study

4.1 Introduction

In the present work, the laminate deformation is determined based on plane strain theory. The strains can be obtained at any through-the-thickness location of the laminate, where the strains are continuous through the thickness. But the stresses can be discontinuous from one layer to another layer, depending on the material properties and orientation of the layer.

In the failure analysis of a tapered laminate, three different types of failure are involved: initial or first-ply failure, ultimate laminate failure, and inter-laminar failure. In the first case, the laminate is considered to have failed when any one layer fails. In the second case, the laminate is considered to have failed when the maximum load is reached or exceeded. The last failure is a result of separation between individual layers. The first two levels in the failure process, the initial and ultimate, are analogous to the failures at yield and ultimate stresses in materials. The resin can be considered as an isotropic material. The Von Mises yield stress approach can be used with a low safety factor. The crack is initiated when a critical stress level is reached.

The design of the tapered structure considers stiffness, static strength, dynamic stability, and damage tolerance. A major consideration in the tapered structure is the laminate configuration, the ply orientation and taper

angle of the tapered laminate. The laminate configuration involves the stacking sequence and the ply composition. The composite material considered here is selected as a graphite/epoxy material for which the properties are given in Table 4.1. Each ply made of graphite/epoxy material is assumed to be transversely isotropic with principal material axes along and perpendicular to the direction of the fibers. The inter-laminate resin material is epoxy. The resin is considered as an isotropic material, the properties of which are given in Table 4.2.

Table 4.1 Properties of unidirectional graphite/epoxy material

Density(ρ, kg/m^3)	1480
Longitudinal modulus(E_1, GPa)	113.9
Transverse modulus(E_2, GPa)	7.985
E_3 is equal to E_2	
In-plane shear modulus(G_{12}, GPa)	3.137
In-plane shear modulus(G_{21}, GPa)	2.852
G_{21} is equal to G_{31}	
G_{23} is equal to G_{21}	
Poisson's ratio(ν_{12})	0.288
Poisson's ratio(ν_{21})	0.018
Poisson's ratio(ν_{23})	0.4
In-plane shear strength(F_6, MPa)	33.3
Longitudinal tensile strength(F_{1t}, MPa)	1621
Transverse tensile strength(F_{2t}, MPa)	48.28

Table 4.2 Properties of isotropic resin material

Elastic modulus(E,GPa)	3.93
Shear modulus(G,GPa)	1.034
Poisson's ratio(ν)	0.37
Tensile strength(F, MPa)	62.055

Three different types of tapered structures are considered as three models: Model-A, Model-B, and Model-C (see Figure 4.1). All the models of the tapered structure are 200 mm long, and 10 mm wide. All the models of tapered structure are 30 mm long from the right end of the thick section to the left end of the thin section. All the models are symmetric about x-direction. The shaded regions in the three models, shown in Figure 4.1, are resin areas.

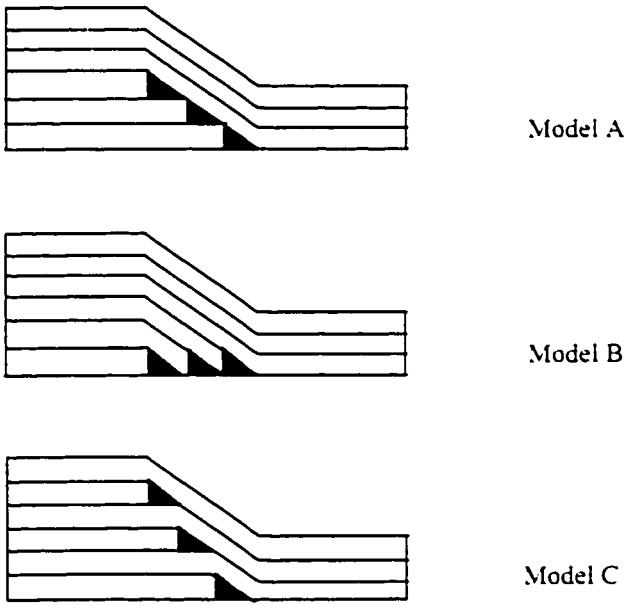

Figure 4.1 Tapered structures

The thick section of the tapered laminate consists of plies that are from 24 to 52 plies and the thin section of the tapered laminate consisted of 12 plies. Each ply is 0.125 mm thick. The taper angles are in the range of 2.86 to 14.04 degrees. The configurations for the thick section of the laminates are given in Table 4.3. The configuration for the thin section is $[0_4/\pm45_4]_s$, and the thickness of sub-laminate is 1.5 mm.

Table 4.3 Configurations for the thick section

Angle	Model A	Model B	Model C
2.86°	$[0_4/\pm45_4/\pm45_4/-45_4]_s$	$[0_4/\pm45_4/\pm45_4/-45_4]_s$	$[0_4/+45_4/-45_4/\pm45_2/+45_4/-45_4]_s$
4.29°	$[0_4/\pm45_4/\pm45_6/-45_6]_s$	$[0_4/\pm45_4/\pm45_6/-45_6]_s$	$[0_4/+45_6/-45_4/\pm45_3/+45_4/-45_6]_s$
5.71°	$[0_4/\pm45_4/\pm45_8/-45_8]_s$	$[0_4/\pm45_4/\pm45_8/-45_8]_s$	$[0_4/+45_8/-45_4/\pm45_4/+45_4/-45_8]_s$
7.13°	$[0_4/\pm45_4/\pm45_{10}/-45_{10}]_s$	$[0_4/\pm45_4/\pm45_{10}/-45_{10}]_s$	$[0_4/+45_{10}/-45_4/\pm45_5/+45_4/-45_{10}]_s$
8.53°	$[0_4/\pm45_4/\pm45_{12}/-45_{12}]_s$	$[0_4/\pm45_4/\pm45_{12}/-45_{12}]_s$	$[0_4/+45_{12}/-45_4/\pm45_6/+45_4/-45_{12}]_s$
9.93°	$[0_4/\pm45_4/\pm45_{14}/-45_{14}]_s$	$[0_4/\pm45_4/\pm45_{14}/-45_{14}]_s$	$[0_4/+45_{14}/-45_4/\pm45_7/+45_4/-45_{14}]_s$
11.31°	$[0_4/\pm45_4/\pm45_{16}/-45_{16}]_s$	$[0_4/\pm45_4/\pm45_{16}/-45_{16}]_s$	$[0_4/+45_{16}/-45_4/\pm45_8/+45_4/-45_{16}]_s$
12.68°	$[0_4/\pm45_4/\pm45_{18}/-45_{18}]_s$	$[0_4/\pm45_4/\pm45_{18}/-45_{18}]_s$	$[0_4/+45_{18}/-45_4/\pm45_9/+45_4/-45_{18}]_s$
14.04°	$[0_4/\pm45_4/\pm45_{20}/-45_{20}]_s$	$[0_4/\pm45_4/\pm45_{20}/-45_{20}]_s$	$[0_4/+45_{20}/-45_4/\pm45_{10}/+45_4/-45_{20}]_s$

The three models have resin pockets at different positions as shown in Figure 4.1. The resin areas are arranged in Model A as shown in Figure 4.2, and these areas are named as area-I, area-II, and area-III as shown in Figure 4.2. The areas between the resin and the sub-laminate cause stress discontinuities when the loading is applied at the thin end of tapered structure.

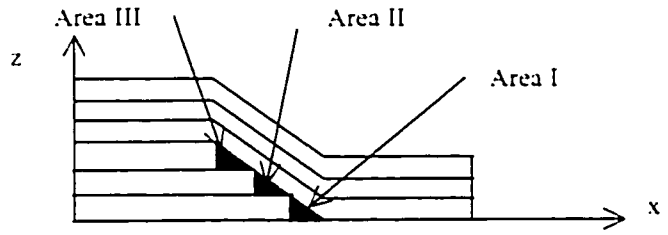

Figure 4.2 Distribution of resin areas

The growths of delaminations are assumed to be along the interfaces a-b, b-c, c-d, d-e, and e-f between shaded resin regions and sub-laminate as shown in Figure 4.3. The initial delamination is assumed to form at point a, and it grows along the line a-b.

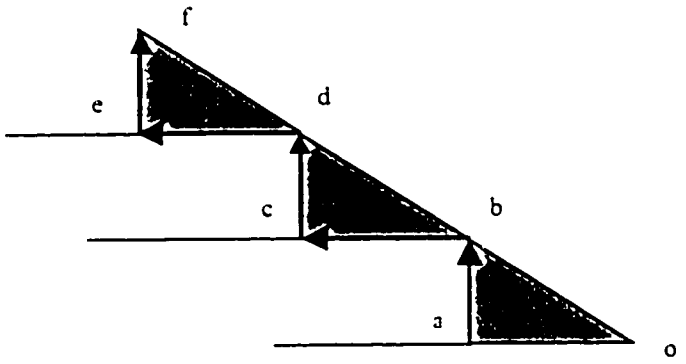

Figure 4.3 Typical delamination

4.2 Finite Element Model

The finite element mesh is determined considering the assumed crack size and the possible regions for crack generation. The cracks are located between sub-laminate and resin where the stress distributions are analyzed.

The finite element meshes are refined in the resin areas and the sub-laminate areas that connect with the resin. In other domains, the meshes of the finite elements are so coarse that the accuracy of computed results is not affected. There are about 616 nodes and 189 elements. The mesh configuration in one resin region is shown in Figure 4.4.

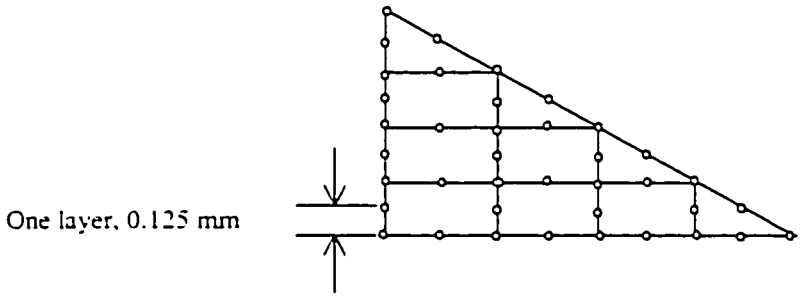

Figure 4.4 Finite element mesh for resin area

For each finite element mesh a small program has been written which can check each node position (see the Figure 3.6). In Figure 3.6, the symbol "o" is used to represent a node.

The side length of the finite element around the crack was considered as matching the crack length. The crack form can be designed as tapered form. When the crack was propagated along the z-direction, the crack form is also presented as tapered form (see the Figure 4.5)

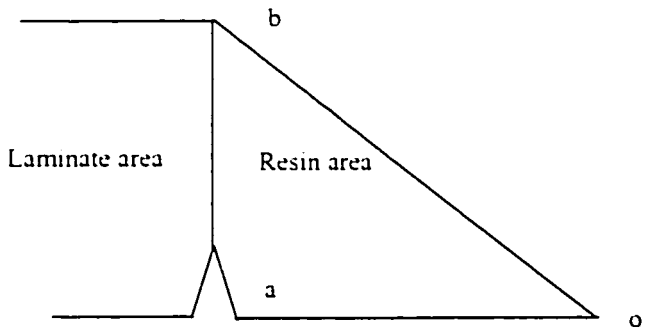

Initial crack

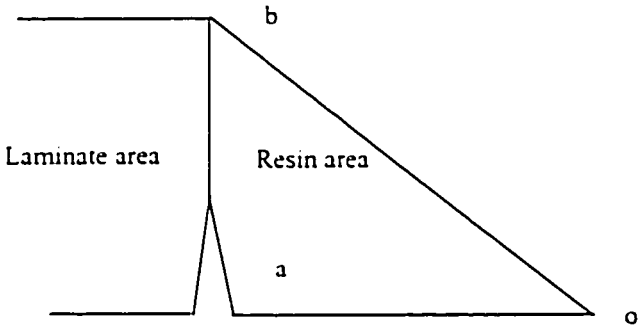

Crack after propagation

Figure 4.5 Crack in the tapered laminate

4.3 Static Load, Constraints, and Displacements

The loads are separated into two cases: the first case, a uniformly distributed load with a magnitude of 1800 N (the distributed loading is 1200×10^5 N/m^2) along the x direction applied at the thin section end (see Figure 4.6). The second case, a concentrated load with a magnitude of 1800 N along the x direction applied at different positions on the thin section end (z=0.00, 0.25, 0.50, 0.75, 1.00, 1.25, 1.50 mm and x =200 mm). In models, the left ends of the thick section are fixed.

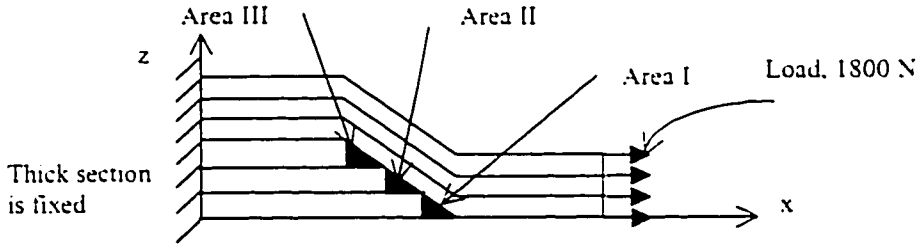

Figure 4.6 Static loading

The computed displacements in Model A with angle 5.71° are shown in Table 3.11 and Figure 4.7. From Figure 4.7, the change in the displacement can be found to be larger near x=80 mm (the same conditions have happened in Model B and Model C, and corresponding to the taper angles from 2.86 to 14.04 degrees). The results indicate that the largest z-direction displacement area is at the area, near x=80 mm.

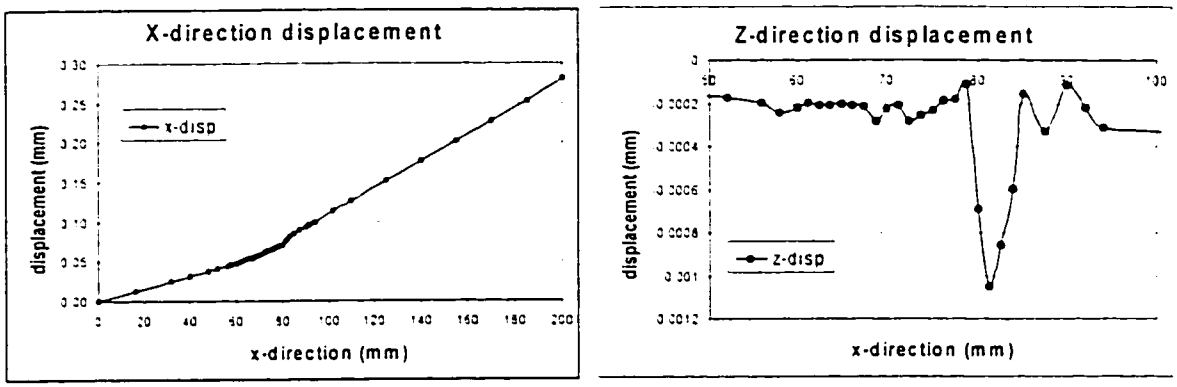

Figure 4.7 Displacements in model A, angle 5.71°

4.4 Interlaminar Stresses

The computed interlaminar stresses between resin and sub-laminate areas are not continuous and are shown in Tables 4.4, 4.5, and 4.6, wherein the values of the stresses at the chosen central points of each element are given. In Tables 4.4, 4.5, and 4.6, σ-stress denotes the Von Mises equivalent stress.

In the Tables 4.4, 4.5, and 4.6, the Von Mises equivalent stresses are different along lines a-b, b-c, and e-f between the sub-laminate and the resin. In the Table 4.4, the tapered angle is 5.71 degrees, the peak value of Von Mises stress in the laminate is observed at z=0.625mm, and the peak value of Von Mises stress in resin is at z=0.125mm (see the left side of Figure 4.8). From Figure 4.8, it can be observed that the largest Von Mises stress occurred at the transition point-a, which is located between the sub-laminate and the resin.

From the computed results given in Tables 4.4, 4.5, and 4.6, it can be seen that the stresses in resin become smaller and the stresses in laminate become higher when the taper angle becomes higher for the same loading. Near point-a, the ratio of laminate and resin Von Mises stresses is 1.848 (31.065/16.805 and at z=0.125) for angle 5.71°, the ratio is 2.252 for angle 4.29°, and the ratio is 2.994 for angle 2.86°. The ratios are higher when the taper angle becomes smaller from angle 14.04 to 2.86 degrees for Model A, Model B, and Model C.

Table 4.4 Stresses in chosen elements (model A, angle=5.71°)

At end	Stresses (MPa)			
x=185mm	x direction	z direction	xz-shear	σ-stress
z= 0.25mm	70.681	-0.5120	0.2791	70.940
z= 0.75mm	69.458	-0.3395	0.9818	69.649
z= 1.25mm	218.22	-0.1032	0.6591	218.27

Area I	Stresses in ply (MPa)			
x=78.75 mm	x direction	z direction	xz- shear	σ-stress
z= 0.125 mm	31.423	0.8305	1.0091	31.065
z= 0.375 mm	33.335	0.7999	3.1124	33.380
z= 0.625 mm	38.419	0.5532	5.3883	39.270
	Stresses in resin (MPa)			
x=81.25 mm	x direction	z direction	xz- shear	σ-stress
z= 0.125 mm	15.365	-2.5432	0.5089	16.805
z= 0.375 mm	15.034	-2.5209	1.5447	16.656
z= 0.625 mm	14.323	-2.3325	2.5689	16.242

Area II	Stresses in ply (MPa)			
x=68.75 mm	x direction	z direction	xz- shear	σ-stress
z= 1.125 mm	33.213	0.3955	-2.3325	33.263
z=1.375 mm	28.296	1.1171	-0.8474	27.793
z=1.625 mm	29.074	1.1012	1.4405	28.648
	Stresses in resin (MPa)			
x=71.25 mm	x direction	z direction	xz- shear	σ-stress
z= 1.125 mm	7.7220	-0.6229	0.0046	8.0515
z=1.375 mm	8.4432	-1.0997	0.3422	9.0628
z=1.625 mm	8.5742	-1.2242	0.9693	9.3985

Area III	Stresses in ply (MPa)			
x=58.00 mm	x direction	z direction	xz- shear	σ-stress
z= 2.125 mm	27.790	-0.2040	-1.8552	28.077
z= 2.375 mm	24.848	0.2026	-1.3673	24.861
z= 2.625 mm	25.022	0.2103	-0.4378	24.929
	Stresses in resin (MPa)			
x=61.25 mm	x direction	z direction	xz- shear	σ-stress
z= 2.125 mm	5.8114	-1.2471	-0.5321	6.5898
z= 2.375 mm	6.3726	-1.6340	-0.2320	7.3385
z= 2.625 mm	6.4699	-1.7284	0.2652	7.4994

Table 4.5 Stresses in chosen elements (model A, angle=4.29°)

Area I	Stresses in ply (MPa)			
x=78.75 mm	x direction	z direction	xz- shear	σ-stress
z=0.09375 mm	33.697	1.4801	0.96254	33.024
z=0.28125 mm	35.570	1.3513	2.8997	35.273
z=0.46875 mm	40.276	0.9456	4.6759	40.627
	Stresses in resin (MPa)			
x=81.25 mm	x direction	z direction	xz- shear	σ-stress
z=0.09375 mm	13.278	-2.4358	0.3902	14.664
z=0.28125 mm	13.001	-2.3613	1.1602	14.469
z=0.46875 mm	12.410	-2.1011	1.8231	13.945

Area II	Stresses in ply (MPa)			
x=68.75 mm	x direction	z direction	xz- shear	σ-stress
z=0.84375 mm	37.173	0.5079	-1.4696	37.009
z=1.03125 mm	32.965	1.1413	-.3765	32.416
z=1.21875 mm	33.606	1.1094	1.3981	33.154
	Stresses in resin (MPa)			
x=71.25 mm	x direction	z direction	xz- shear	σ-stress
z=0.84375 mm	7.5937	-.69792	0.3361	7.9868
z=1.03125 mm	8.1147	-1.0773	0.4552	8.7391
z=1.21875 mm	8.1795	-1.1412	0.9693	8.9113

Area III	Stresses in ply (MPa)			
x=58.00 mm	x direction	z direction	xz- shear	σ-stress
z=1.59375 mm	32.714	-.0649	-1.1850	32.811
z=1.78125 mm	30.378	0.2703	-.9080	30.285
z=1.96875 mm	30.643	0.2644	-0.3057	30.516
	Stresses in resin (MPa)			
x=61.25 mm	x direction	z direction	xz- shear	σ-stress
z=1.59375 mm	6.0266	-1.3082	-.10259	6.7785
z=1.78125 mm	6.4671	-1.6386	.0400	7.4236
z=1.96875 mm	6.5424	-1.6984	.3231	7.5573

Table 4.6 Stresses in chosen elements (Model A, angle=2.86°)

Area I	Stresses in ply (MPa)			
x=78.75 mm	x direction	z direction	xz- shear	σ-stress
z=0.0625 mm	37.594	1.8796	0.7574	36.713
z=0.1875 mm	39.267	1.6923	2.1945	38.636
z=0.3125 mm	43.112	1.2445	3.2496	42.875
	Stresses in resin (MPa)			
x=81.25 mm	x direction	z direction	xz- shear	σ-stress
z=0.0625 mm	11.072	-2.0972	0.2010	12.261
z=0.1875 mm	10.891	-2.0079	0.6030	12.067
z=0.3125 mm	10.513	-1.7475	0.8640	11.584

Area II	Stresses in ply (MPa)			
x=68.75 mm	x direction	z direction	xz- shear	σ-stress
z=0.5625 mm	42.965	0.5931	-.4310	42.678
z=0.6875 mm	39.985	1.0491	0.0972	39.471
z=0.8125 mm	40.414	1.0139	1.0592	39.958
	Stresses in resin (MPa)			
x=71.25 mm	x direction	z direction	xz- shear	σ-stress
z=0.5625 mm	7.5937	-0.6979	0.3361	7.9868
z=0.6875 mm	8.1147	-1.0773	0.4552	8.7391
z=0.8125 mm	8.1795	-1.1412	0.9693	8.9113

Area III	Stresses in ply (MPa)			
x=58.00 mm	x direction	z direction	xz- shear	σ-stress
z=1.0625 mm	40.226	0.06178	-0.4321	40.202
z=1.1875 mm	38.638	0.29359	-0.4268	38.500
z=1.3125 mm	38.828	0.28673	-0.2702	38.689
	Stresses in resin (MPa)			
x=61.25 mm	x direction	z direction	xz- shear	σ-stress
z=1.0625 mm	6.3499	-1.2618	0.2492	7.0790
z=1.1875 mm	6.6299	-1.4925	0.2119	7.4975
z=1.3125 mm	6.6798	-1.5192	0.2368	7.5660

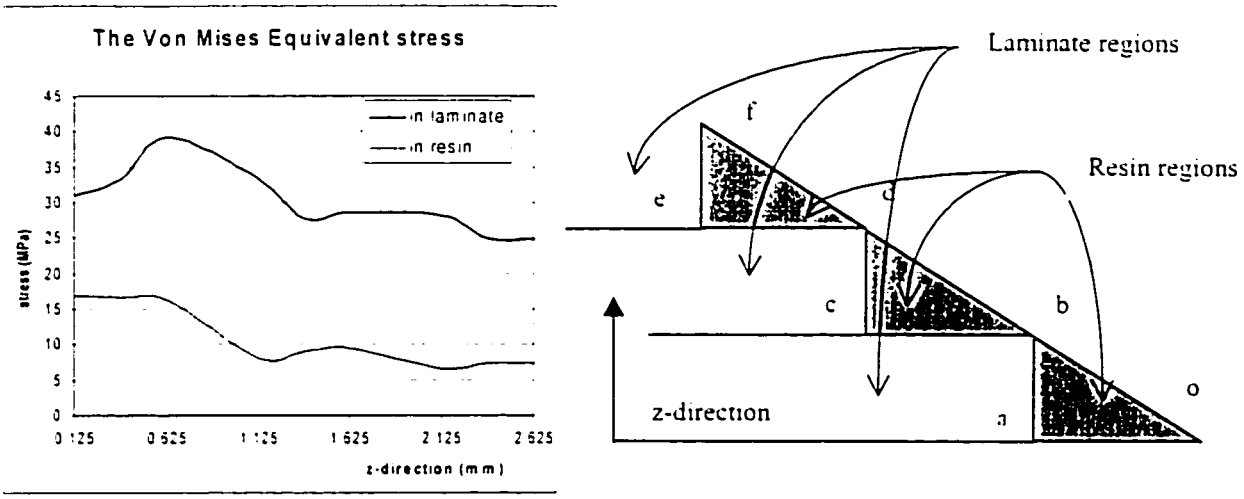

Figure 4.8 Von Mises equivalent stress in z-direction

The Von Mises stresses along the line o-f (see Figure 4.8) were distributed as 7.7332 (point-o), 6.6055, 11.453, 22.384 (point-b), 10.784, 7.4871, 7.0235(point-d), 13.392, 5.9261, 5.0339, 5.2268, 9.4592 (point-f) MPa (see Figure 4.9 for the Von Mises stress along the line o-f). The highest stress (22.384 MPa) is at point-b in resin area I, and the second highest stress (16.805 MPa) is at point-a. From the distribution of the stresses, the initial crack may seem to occur along the line o-b.

Comparison between Figures 4.8 and 4.9 shows that the crack will be initiated in resin area I and near x=80 mm. So the initial crack can be assumed along the line a-b. Two possible conditions of crack propagation can be estimated: one is from point-a to point-b, another from point-b to point-a. Here, the first condition is assumed: the crack propagates from point-a to point-b. The highest stress (22.384 MPa) is at point-b in resin area I, and the second highest stress (16.805 MPa) is at point-a.

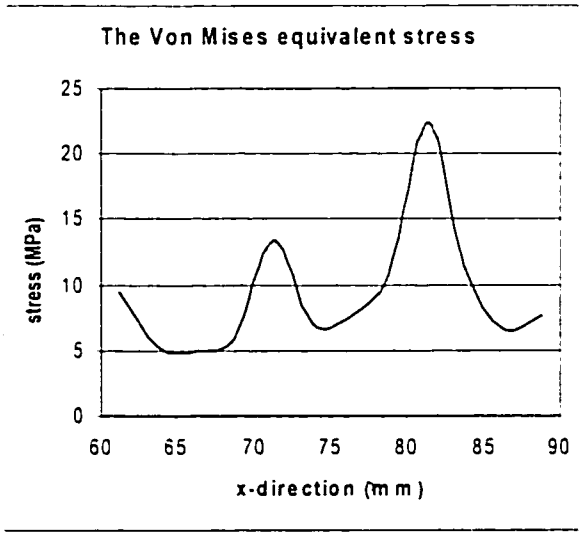

Figure 4.9 Von Mises equivalent stress along the line o-f

In the strain energy release rate study, the crack propagation process is not considered to compute the strain energy release rate. The objective is to obtain the strain energy release rate of initial crack corresponding to the different taper angles of the laminate and to apply a reasonable strain energy release rate criterion for these models.

4.5 Energy Releases Rate

The mode-I and mode-II components of the strain energy release rate under static loading and the total strain energy release rate for fatigue loading can be used to predict delamination growth in a laminated composite structure.

4.5.1 Possible Weak Factor

From the shown stress distribution in resin area, the initial crack may be happened in the resin area-I. It is most possible that the initial crack may be happened along the line a-b. The Von Mises stress at point-b was higher than that at point-a according to the stress values. It is reasonable to assume the initial crack at point-b.

In Figure 4.10, laminates are tailored into a tapered laminate. The processes are assumed as the step-I, step-II, and step-III. The place where the point-a can be assumed is the weakest place. A possible weak factor can be estimated according to the tapered structure tailoring.

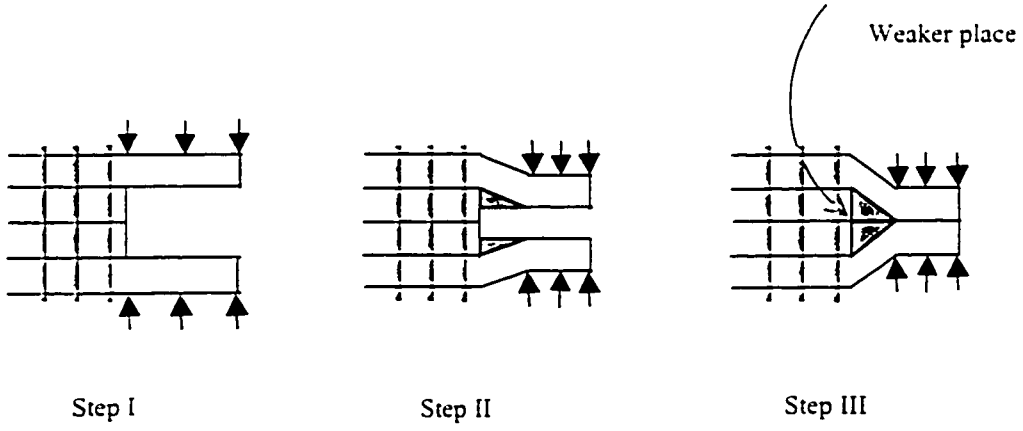

Figure 4.10 Tailoring of the tapered laminate

The possible weak factor has a distribution that is proportional to the stress distribution, the values are assumed as in Figure 4.11. The weak factor is assumed to be 1 for point-b, and it is assumed to be 0.7 for point-a. The resin area-I can be separated into ten sub-areas, and each sub-area will be given a possible weak factor.

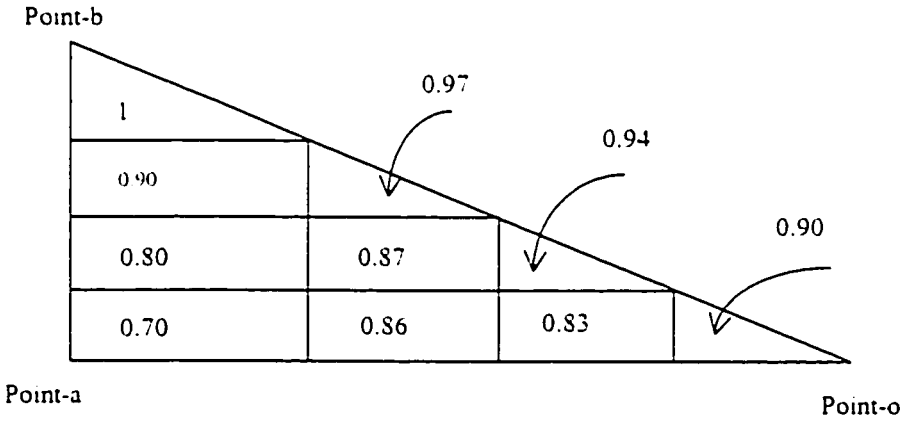

Figure 4.11 Weak factor distribution

In the Table 4.6, the given resin tensile strength is 62.055 MPa, and the computed Von Mises stress is 16.805 MPa at the point-a. In the Table 4.7, considered safety factor is 2.5, and the design tensile strength is 17.375 MPa (62.055 ×0.7÷2.5=17.375). If the safety factor is assumed as 3.3, the design tensile strength is only 13.031 MPa (62.055×0.7÷3.3=13.031). This value is less than the computed stress 16.805 MPa. The cracking may occur at this stress level. The computed Von Mises stress is 22.384 MPa at the point-b. The design tensile strength is 24.8 or 18.626 MPa (62.055×1÷2.5=24.8, 62.055×1÷3.3=18.626). The proportion between strength and stress is 1.080 (17.375/16.805) or 0.775(13.031/16.805) that is lower than the proportion

1.107 (24.822/22.384) or 0.832(18.626/22.384). It is reasonable that the initial cracking may occur at point-a.

Table 4.7 Proportion between the strength and stress

The resin tensile strength is 62.055 MPa, the safety factor is 2.5			
Positions in tapered laminate (weak factor)	Von Mises stress (MPa)	Design tensile strength (MPa)	Proportion between the strength and stress
Point-a (0.7)	16.805	17.375	1.080
Point-b (1.0)	22.384	24.822	1.107
Point-o (0.9)	7.7332	22.340	2.889
The resin tensile strength is 62.055 MPa, the safety factor is 3.3			
Position in tapered laminate (weak factor)	Von Mises stress (MPa)	Design tensile strength (MPa)	Proportion between the strength and stress
Point-a (0.7)	16.805	13.031	0.775
Point-b (1.0)	22.384	18.626	0.832
Point-o (0.9)	7.7332	16.755	2.167

4.5.2 Energy Release Rate for the Three Models

The initial crack length will be considered to be equal to the element side length. In the last section it was mentioned that area-I was the area with the highest stress among the three resin areas, and further point-a had the highest value of Von Mises stress in resin area-I. Therefore, the delamination was assumed to initiate at this point-a. The initial crack length is considered as 0.25 mm, its width is 0.02 mm, and further the crack propagates to an incremental distance da=0.25 mm, and the crack width is 0.004 mm. The

strain energy release rate is given in Tables 4.7, 4.8, and 4.9 for taper angle in the range of 2.86-14.03 degrees.

In Figure 4.12 and Tables 4.7, 4.8, and 4.9, the energy with initial crack or after crack propagation is increasing when the taper angle is decreasing. In Figure 4.13, the energy release rate is increasing when the taper angle is increasing.

Table 4.8 Energy release rate for model A

Taper angle	Energy with initial crack	Energy after crack propagation	Energy release rate
2.86°	0.2669 m.N	0.2670 m.N	6.4280 Pa.m
4.29°	0.2575 m.N	0.2576 m.N	28.8680 Pa.m
5.71°	0.2515 m.N	0.2516 m.N	38.9520 Pa.m
7.13°	0.2475 m.N	0.2477 m.N	93.8560 Pa.m
8.53°	0.2450 m.N	0.2454 m.N	152.0080 Pa.m
9.93°	0.2435 m.N	0.2441 m.N	227.1560 Pa.m
11.31°	0.2426 m.N	0.2435 m.N	322.4880 Pa.m
12.68°	0.2422 m.N	0.2433 m.N	438.6240 Pa.m
14.03°	0.2423 m.N	0.2438 m.N	566.7640 Pa.m

Table 4.9 Energy release rate for model B

Taper angle	Energy with initial crack	Energy after crack propagation	Energy release rate
2.86°	0.2662 m.N	0.2663 m.N	6.9480 Pa.m
4.29°	0.2573 m.N	0.2574 m.N	10.6040 Pa.m
5.71°	0.2516 m.N	0.2517 m.N	28.6360 Pa.m
7.13°	0.2474 m.N	0.2475 m.N	53.4200 Pa.m
8.53°	0.2447 m.N	0.2449 m.N	74.1160 Pa.m
9.93°	0.2432 m.N	0.2434 m.N	101.3440 Pa.m
11.31°	0.2422 m.N	0.2426 m.N	136.9560 Pa.m
12.68°	0.2418 m.N	0.2423 m.N	191.0920 Pa.m
14.03°	0.2418 m.N	0.2424 m.N	239.1640 Pa.m

Table 4.10 Energy release rate for model C

Taper angle	Energy with initial crack	Energy after crack propagation	Energy release rate
2.86°	0.2670 m.N	0.2671 m.N	6.9280 Pa.m
4.29°	0.2575 m.N	0.2576 m.N	22.5560 Pa.m
5.71°	0.2515 m.N	0.2516 m.N	40.1520 Pa.m
7.13°	0.2475 m.N	0.2477 m.N	94.1880 Pa.m
8.53°	0.2449 m.N	0.2453 m.N	150.0200 Pa.m
9.93°	0.2433 m.N	0.2439 m.N	220.8320 Pa.m
11.31°	0.2423 m.N	0.2431 m.N	309.8280 Pa.m
12.68°	0.2419 m.N	0.2430 m.N	418.3800 Pa.m
14.03°	0.2418 m.N	0.2432 m.N	536.3360 Pa.m

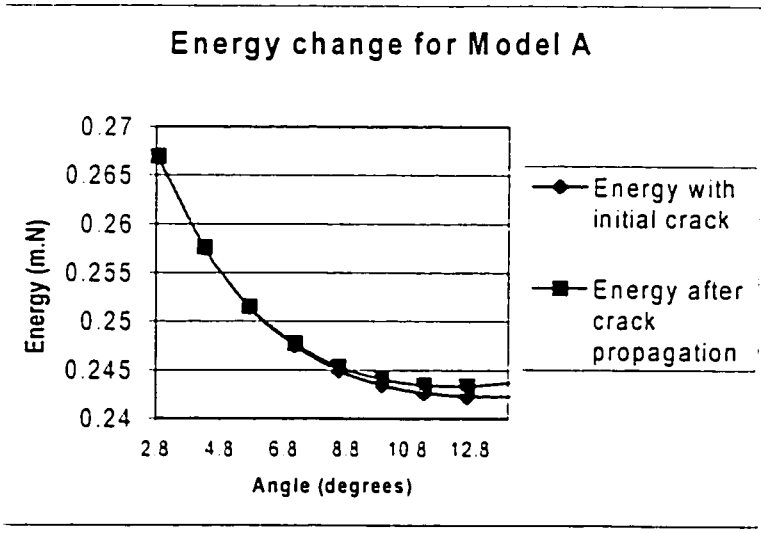

Figure 4.12 Energy change for Model A

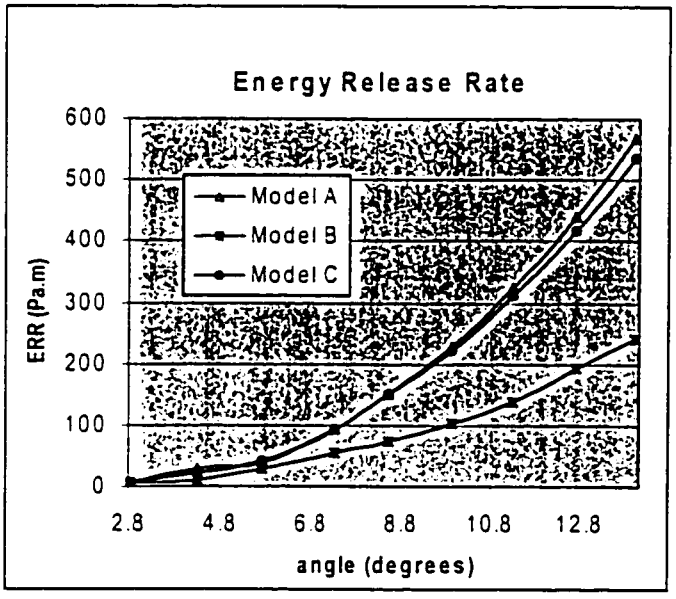

Figure 4.13 Energy Release Rate

4.5.3 Energy Release Rate for Concentrated Loading

When the loading is changed to concentrated loading and applied at different positions, the energy release rates are not changed appreciably (see the Tables 4.11, 4.12, and 4.13).

Table 4.11 Energy release rate for different loading positions (Model A with angle 5.71°)

Loading Position	Energy with initial crack	Energy after crack propagation	Energy release rate
0.00 mm	0.2613 m.N	0.2614 m.N	38.9520 Pa.m
0.25 mm	0.2569 m.N	0.2570 m.N	38.9560 Pa.m
0.50 mm	0.2555 m.N	0.2556 m.N	38.9560 Pa.m
0.75 mm	0.2526 m.N	0.2527 m.N	38.9560 Pa.m
1.00 mm	0.2525 m.N	0.2526 m.N	38.9520 Pa.m
1.25 mm	0.2520 m.N	0.2521 m.N	38.9560 Pa.m
1.50 mm	0.2552 m.N	0.2553 m.N	38.9520 Pa.m

Table 4.12 Energy release rate for different loading positions (Model B with angle 5.71°)

Loading Position	Energy with initial crack	Energy after crack propagation	Energy release rate
0.00 mm	0.2614 m.N	0.2615 m.N	28.6360 Pa.m
0.25 mm	0.2570 m.N	0.2571 m.N	28.6360 Pa.m
0.50 mm	0.2556 m.N	0.2557 m.N	28.6360 Pa.m
0.75 mm	0.2527 m.N	0.2528 m.N	28.6400 Pa.m
1.00 mm	0.2526 m.N	0.2527 m.N	28.6360 Pa.m
1.25 mm	0.2522 m.N	0.2523 m.N	28.6400 Pa.m
1.50 mm	0.2553 m.N	0.2554 m.N	28.6400 Pa.m

Table 4.13 Energy release rate for different loading positions (Model C with angle 5.71°)

Loading Position	Energy with initial crack	Energy after crack propagation	Energy release rate
0.00 mm	0.2614 m.N	0.2615 m.N	40.1520 Pa.m
0.25 mm	0.2569 m.N	0.2570 m.N	40.1520 Pa.m
0.50 mm	0.2555 m.N	0.2556 m.N	40.1520 Pa.m
0.75 mm	0.2527 m.N	0.2528 m.N	40.1520 Pa.m
1.00 mm	0.2526 m.N	0.2527 m.N	40.1520 Pa.m
1.25 mm	0.2521 m.N	0.2522 m.N	40.1520 Pa.m
1.50 mm	0.2553 m.N	0.2554 m.N	40.1520 Pa.m

4.5.4 Stress Intensity Factor

One-ply steps were used to produce the taper, the loading is in the x direction. In this condition, inter-laminar cracking or delamination of the tapered structure can occur under two basic modes: opening (or peel) mode (mode I), forward sliding shear mode (mode II), or under mixed mode. The resistance to delamination growth is expressed in terms of the interlaminar fracture toughness, which has two values corresponding to the two basic delamination modes. The interlaminar fracture toughness is measured in terms of the strain energy release rate, which is the energy dissipated per area of delamination growth.

For a material, the energy release rate is the rate of change in potential energy with crack area, which is also called as the crack extension force or the crack driving force.

The approaches of fracture mechanics can be used through using equation (3.35) if we consider the resin material as isotropic material, for which the elastic modulus E and Poisson's ratio ν are constants. In Tables 4.14, 4.15, and 4.16 the computed results are given.

Table 4.14 Stress intensity factor for model A

Taper angle	Energy release rate	Stress intensity factor ($\times 10^5$ Pa $m^{1/2}$)
2.86°	6.4280 Pa.m	1.711
4.29°	28.8680 Pa.m	3.626
5.71°	38.9520 Pa.m	4.211
7.13°	93.8560 Pa.m	6.537
8.53°	152.0080 Pa.m	8.320
9.93°	227.1560 Pa.m	10.170
11.31°	322.4880 Pa.m	12.118
12.68°	438.6240 Pa.m	14.132
14.03°	566.7640 Pa.m	16.064

Table 4.15 Stress intensity factor for model B

Taper angle	Energy release rate	Stress intensity factor ($\times 10^5$ Pa $m^{1/2}$)
2.86°	6.9480 Pa.m	1.779
4.29°	10.6040 Pa.m	2.197
5.71°	28.6360 Pa.m	3.611
7.13°	53.4200 Pa.m	4.932
8.53°	74.1160 Pa.m	5.809
9.93°	101.3440 Pa.m	6.793
11.31°	136.9560 Pa.m	7.897
12.68°	191.0920 Pa.m	9.328
14.03°	239.1640 Pa.m	10.436

Table 4.16 Stress intensity factor for model C

Taper angle	Energy release rate	Stress intensity factor ($\times 10^5$ Pa $m^{1/2}$)
2.86°	6.9280	1.776
4.29°	22.5560	3.205
5.71°	40.1520	4.276
7.13°	94.1880	6.549
8.53°	150.0200	8.265
9.93°	220.8320	10.028
11.31°	309.8280	11.878
12.68°	418.3800	13.802
14.03°	536.3360	15.627

4.6 Natural Frequencies and Normal Modes

In order to determine the frequencies and modes of free vibration of the tapered structure, it is necessary to solve the linear eigenproblem. The calculated results are given in Table 4.17 for Model-A. The biggest difference between the eigenfrequencies of the laminate with crack and without crack is about 60 Hz in the first five modes. The integral domain can be chosen as 240 Hz for one given eigenfrequency, the integral accuracy can be satisfied when the frequencies of the random excitation have been chosen as the eigenfrequencies.

Table 4.17 Eigen frequencies(Hz)

Taper angle		Mode 1	Mode 2	Mode 3	Mode 4	Mode 5
2.86°	Without crack	1169.480	2650.253	3350.577	4900.201	7564.735
	With crack	1169.004	2639.613	3339.013	4887.133	7548.294
4.29°	Without crack	1159.048	1463.163	2759.098	3470.036	4999.551
	With crack	1159.405	1483.909	2757.282	3462.296	4996.713
5.71°	Without crack	1170.617	2804.155	3592.114	5121.744	8537.601
	With crack	1172.702	2805.245	3598.560	5139.365	8539.808
7.31°	Without crack	1115.797	1229.272	2859.758	3744.275	5376.725
	With crack	1140.212	1283.700	2860.907	3742.565	5376.420
8.53°	Without crack	1155.945	1382.679	2879.551	3916.800	5586.704
	With crack	1155.219	1370.039	2877.144	3913.626	5580.181
9.93°	Without crack	1152.800	1328.966	2900.292	4042.688	5752.104
	With crack	1148.205	1291.638	2897.307	4035.967	5740.878
11.31°	Without crack	1173.281	2907.218	4089.967	5889.148	9411.097
	With crack	1173.448	2903.498	4080.767	5887.541	9359.606
12.68°	Without crack	1162.891	1597.511	2925.983	4213.421	6170.839
	With crack	1162.463	1562.555	2921.632	4200.520	6161.561
14.03°	Without crack	1160.554	1457.295	2935.096	4253.967	6354.460
	With crack	1159.913	1433.772	2929.644	4235.065	6349.116

The first five mode shapes along the x coordinate can be seen in Figure 4.14.

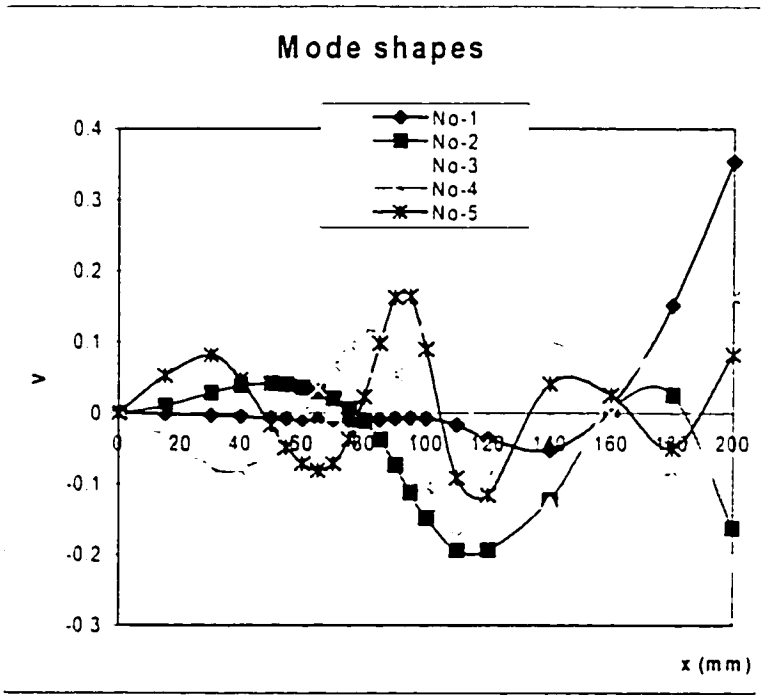

Figure 4.14 The first five mode shapes

In the mode shapes, we should pay particular attention to the peak value area. The five modes of the tapered laminate are same as the modes of a beam with one end fixed.

4.7 Random Excitation

The random excitation is considered by containing some of eigenvalues (frequencies, Hz) in the forcing frequencies, and is constrained by limit time; it is with zero-mean.

$$F_d(t_j) = \sum_{i=1}^{n} F_0 \sin(2\pi f_i t_j) \tag{4.1}$$

where F_0 is a constant (loading with a magnitude of 5 N), f_i is the eigen frequency, and i = 1,2,...,n for n eigen frequencies. Further t_j denotes time, j = 1,2,...,m for the time separating value (here, the m is taken as 10000). When n is taken as 1, the first eigen frequency (1170.617 Hz) is considered for Model-A (angle 5.71°), the excitation is shown in Figure 4.15.

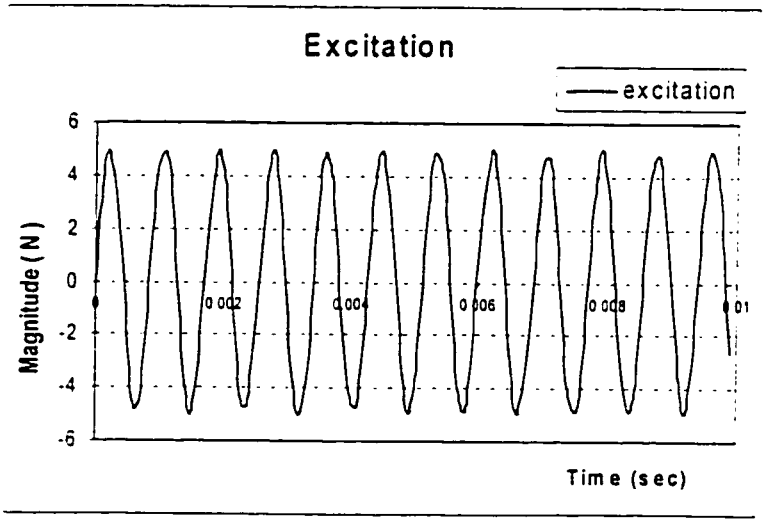

Figure 4.15 The excitation when n = 1

The random excitation can be expressed as

$$F_r(t_j) = F_d(t_j) + R_0 randn(size(t_j)) \tag{4.2}$$

where, R_0 is a constant, 10 N. The function "randn" in Matlab will generate a random number and F will generate a random excitation(see Figure 4.16).

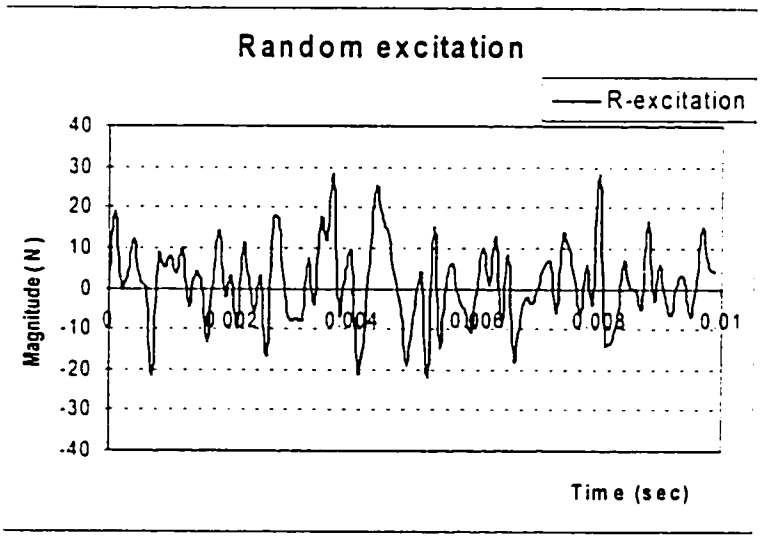

Figure 4.16 A random excitation

4.7.1 Discrete Fourier Transform and Power Spectral Density

When 10000 points are considered to obtain the Fast Fourier Transform, power spectral density is given as below (see Figure 4.17).

$$S_{f_i f_j} = \lim_{T \to \infty} \frac{\pi}{T} \left[\frac{2 \sum_{k=1}^{M} F(t_k) e^{-i\omega_i t_k}}{2\pi} \right] \left[\frac{2 \sum_{k=1}^{M} F(t_k) e^{i\omega_j t_k}}{2\pi} \right] \tag{4.3}$$

In equation (4.3), frequency f_i is equal to f_j and i = j = 1, circular frequency ω_i is equal to ω_j and i = j =1 also. The M was taken as 10000. The power spectral density is a complex conjugate function in general. In the computation for Model A without crack (Taper angle 5.71°), the first eigenfrequency f_1 is 1170.617 Hz. When we take the Fast Fourier Transform of 10000 points, the first peak value of the power spectral density function is reached at 1170.617 Hz; another peak value of the power spectral density is at 8829.383 Hz (10000-1170.617=8829.383).

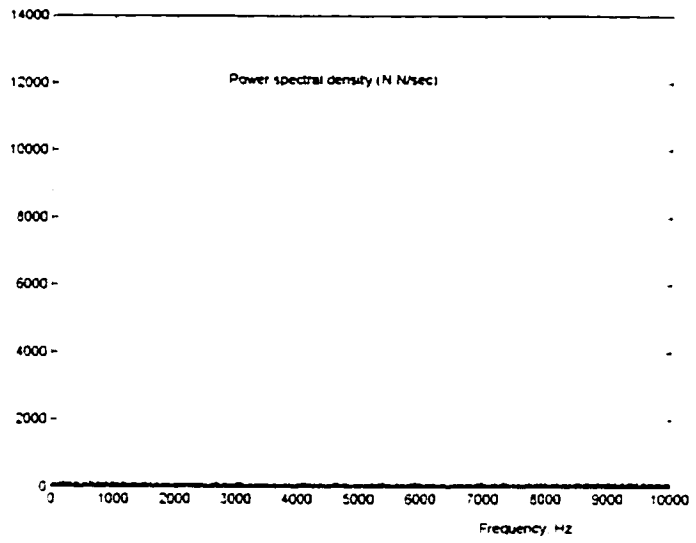

Figure 4.17 Power spectral density function

4.7.2 Mean Square Value and Standard Deviation

The mean square response is given by

$$S_{u_i}(\omega) = |H_{i1}(i\omega)|^2 S_{f_1 f_1}(\omega) + \ldots + |H_{ir}(i\omega)|^2 S_{f_r f_r}(\omega) \tag{4.4}$$

and

$$\sigma_{u_i}^2 = \int_{\omega} S_{u_i}(\omega) d\omega \tag{4.5}$$

The standard deviation values of the response are given by

$$\sigma_{i,u} = \sqrt{\sigma_{i,u}^2} \qquad i = 1,2,3 \tag{4.6}$$

The results of the standard deviations are shown in Tables 4.18 and 4.19 corresponding to node 1 (x = 200 mm and z = 0 mm), and node 2 (x = 80 mm and z = 0 mm).

Table 4.18 Standard deviation of the displacement for Model A

Taper angle	At node 1, (mm)		At node 2, (mm)	
	Without crack	With crack	Without crack	With crack
2.86°	0.2359	0.3560	0.0335	0.2476
4.29°	0.2205	0.3475	0.0262	0.2074
5.71°	0.2124	0.3117	0.0219	0.1812
7.31°	0.1964	0.2859	0.0277	0.1790
8.53°	0.1961	0.2734	0.0261	0.1621
9.93°	0.1848	0.2601	0.0247	0.1560
11.31°	0.1717	0.2519	0.0245	0.1562
12.68°	0.1717	0.2512	0.0239	0.1451
14.03°	0.1690	0.2328	0.0229	0.1381

Table 4.19 Standard deviation of the velocity for Model A

Taper angle	At node 1, (mm/sec)		At node 2, (mm/sec)	
	Without crack	With crack	Without crack	With crack
2.86°	9.3040	14.0405	1.3213	9.7662
4.29°	8.6974	13.7031	1.0347	8.1780
5.71°	8.3786	12.2948	0.8629	7.1448
7.31°	7.7458	11.2738	1.0941	7.0576
8.53°	7.7320	10.7830	1.0306	6.3926
9.93°	7.2877	10.2573	0.9726	6.1513
11.31°	6.7719	9.9342	0.9646	6.1584
12.68°	6.7722	9.9062	0.9435	5.7235
14.03°	6.6656	9.1831	0.9050	5.4448

4.8 Probability of Failure for a Tapered Laminate

The response of a tapered laminate to stationary random excitation was discussed in the previous section for a deterministic structure. The parameters of the tapered structure are taken to be deterministic constants, and the power spectral density was calculated as a function of the structural parameters and the external excitation. The computed response has been the displacement at any given point in the tapered laminate.

A stationary Gaussian excitation process with zero mean represents the excitation that is commonly encountered by tapered structure. This case, which results in a stationary Gaussian response process, can be solved thereby leading to closed form expressions for response statistics.

4.8.1 A Stationary Gaussian Process

A certain tapered structure response S(t) (which is a displacement or velocity) can be described by a stationary Gaussian process with zero mean and a power spectral density function in the positive frequency domain, $0 \leq \omega \leq \infty$. The absolute maximum value of this process during a period, τ, is defined by a variable S_τ:

$$S_\tau = \max_\tau |S(t)| \tag{4.7}$$

S(t) can be a function of {u}, a vector of structure random variables. Assume that s is a threshold value that may be a random variable, so that when the response is higher than s, the tapered structure will be at failure. In Ref. [44], the equation for the conditional probability of failure has been determined:

$$P_f(u) \approx 1-[1-P_{f0}(u)]e^{-\frac{\upsilon(u)\tau}{1-P_{f0}(u)}} \tag{4.8}$$

In the above, P_{f0} is the conditional probability that, at time t = 0, S(t) is higher than s. Given the value of {u}, υ(u) is the rate of the response process crossing the value s upward. It was also shown in Ref. [44] that

$$P_{f0} = e^{-\frac{s^2}{2\sigma_0^2}} \tag{4.9}$$

$$\upsilon(u) = \frac{1}{2\pi}\sqrt{\frac{\sigma_2}{\sigma_0}} \cdot e^{-\frac{s^2}{2\sigma_0^2}} \tag{4.10}$$

where σ_0 and σ_2 are defined in equation (3.97). The above equation describes the conditional probability for the event that process S(t) has a value higher than a prescribed value s, which is defined as a failure.

The spectral moments are functions of the power spectral density of the response which is a stationary Gaussian process, which also is a function of the power spectral density of the excitation and other structural parameters. Because the spectral moments are functions of the components of the random vector {u} of the tapered structure, including the random excitation, the above equations yield

$$P_f(u) = 1 - F_{s\tau} = 1 - \left[1 - \exp\left(-\frac{s^2}{2\sigma_0}\right)\right] \times \exp\left[-\frac{\sqrt{\sigma_2/\sigma_0}\,\tau \exp\left(-s^2/2\sigma_0\right)}{2\pi\left(1-\exp\left(-s^2/2\sigma_0\right)\right)}\right] \tag{4.11}$$

where $F_{s\tau}$ is the conditional probability of failure of the maximum value S_τ. For model-A with taper angle 5.71° and without crack, the spectral moments corresponding to displacements at point-a are (x = 80 mm, z = 0 mm, see Tables 4.13 and 4.14)

σ_0=0.021878 mm

σ_2=0.862862 mm/sec

In static analysis, the computed result for Von Mises equivalent stress was 16.805 MPa at the point-a for model-A with angle 5.71°. Considered safety factor is 2.5 and the corresponding design tensile strength is 17.375 MPa. If the safety factor is assumed as 3.3, the design tensile strength is only 13.031

MPa. So the threshold value s can be taken to be in the range 13.031~17.375 MPa.

4.8.2 Discussion of the Conditional Probability

From equation (4.11) and Figure 4.18, it can be shown that: the maximum value of the conditional probability is 1 for the curve of the 1000 sec at the threshold value 0.0701 mm (at this displacement level, the stress is calculated as 16.87 MPa at point-a). The conditional probability is 0.019 for the curve of the 1000 sec at the threshold value 0.1101 mm (at this displacement level, the stress is calculated as 26.49 MPa at point-a). The maximum value of the conditional probability is 1 for the curve of the 10000 sec at the threshold value 0.0851 mm (at this displacement level, the stress is calculated as 20.47 MPa at point-a). The maximum value of the conditional probability is 1 for the curve of the 10000 sec at the threshold value 0.1101 mm (at this displacement level, the stress is calculated as 26.49 MPa at point-a).

Because the maximum value of the conditional probability is 1 for the curve of the 10000 sec at the threshold value 0.0851 mm (at this displacement level, the stress is calculated as 20.47 MPa at point-a), and the stress 20.47 MPa is higher than 17.375 MPa, the failure will happen absolutely after 10000 sec. The maximum value of the conditional probability is 1 for the curve of the 1000 sec at the threshold value 0.0701 mm (at this displacement level, the stress is calculated as 16.87 MPa at point-a). The stress 16.87 MPa is between 13.031 and 17.375 MPa, so the failure may happen. The maximum value of the conditional probability is

0.961 for the curve of the 1000 sec at the threshold value 0.0851 mm (at this displacement level, the stress is calculated as 20.47 MPa at point-a). The stress 20.47 MPa is higher than 17.375 MPa, so the failure will happen with the conditional probability of 96.1%.

It is evident from Figure 4.18 that the conditional probability for a short duration, which is higher than a relatively low threshold, is a small value. This conditional probability of failure increases as the process continues in time. The variations of conditional probability values with the threshold value, s, are plotted in Figure 4.18.

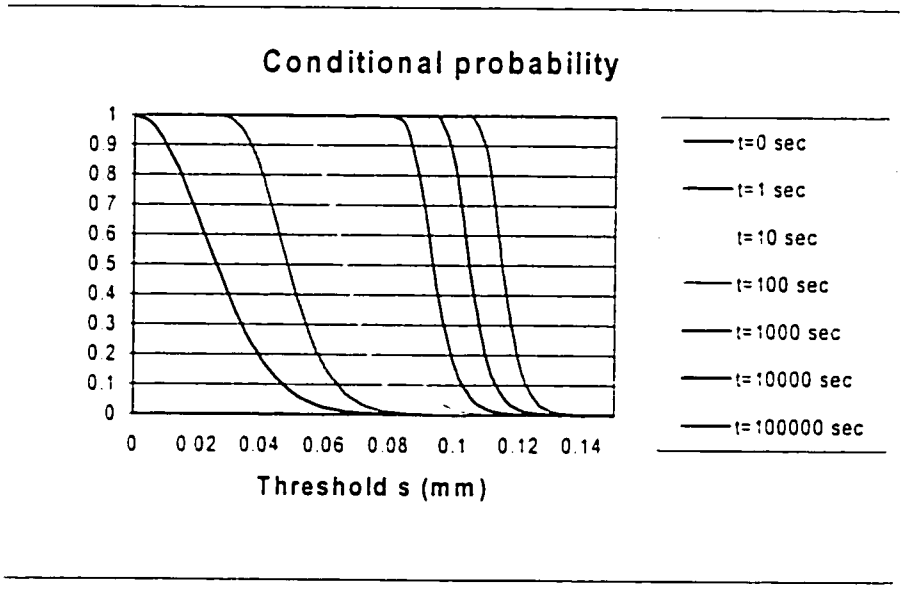

Figure 4.18 Conditional probability

In Figure 4.19, the CDFs of the maximum values of S, are shown for different periods. As time increases, the probability that the maximum value of the process is lower than a certain threshold value increases.

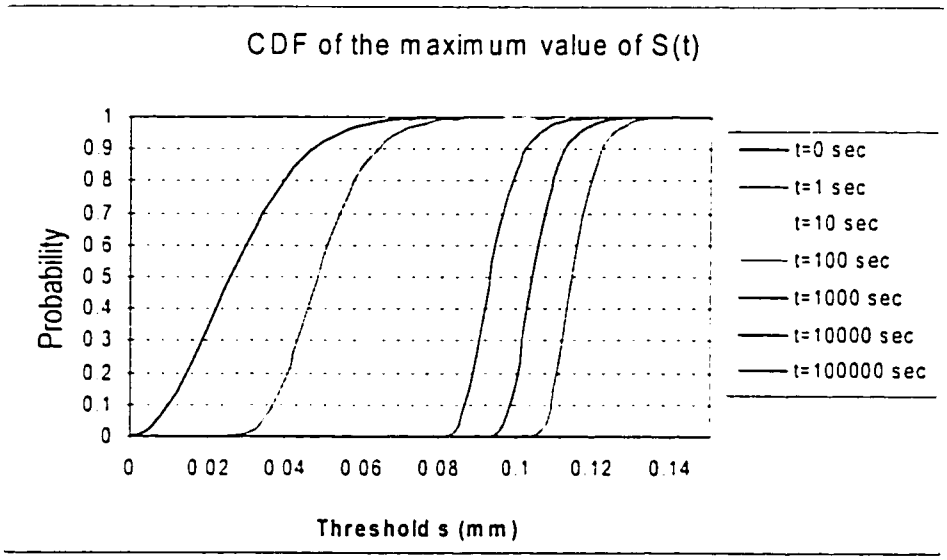

Figure 4.19 CDF of the maximum values of S(t)

In the calculation process for the probability of failure of a tapered laminate, failure is defined as the case when a certain response (displacement or velocity) is higher than a given threshold. The probability of failure is calculated by using equation (4.11), and the spectral moments are calculated by using equation (3.97) and the results are shown in Tables 4.13 and 4.14. The analysis of the random process is limited to this case in which the mode shapes are deterministic.

4.9 Discussion

In this Chapter, the composite material considered is a graphite/epoxy material and the resin material is selected as epoxy. Each ply made of graphite/epoxy material is assumed to be transversely isotropic. The resin is considered as an isotropic material.

Three different types of tapered structures were considered as three models: Model-A, Model-B, and Model-C. All the models of the tapered structure were 200 mm long, and 10 mm wide. All the models of tapered structure were 30 mm long from the right end of the thick section to the left end of the thin section. All the models are symmetric about x-direction. The thick section of the tapered laminate consists of plies that are from 24 to 52 plies and the thin section of the tapered laminate consisted of 12 plies. Each ply is 0.125 mm thick. The taper angles are in the range of 2.86 to 14.04 degrees.

The finite element meshes are refined in the resin areas and the sub-laminate areas that connect with the resin. In other domains, the meshes of the finite elements are so coarse that the accuracy of computed results is not affected. There are about 616 nodes and 189 elements for each finite element model.

The loads are separated into two cases: a uniformly distributed load with a magnitude of 1800 N (the distributed loading is 1200×10^5 N/m^2) along the x direction applied at the thin section end. The second case, a concentrated

load with a magnitude of 1800 N along the x direction applied at different positions on the thin section end.

Near the point located at x = 80 mm and z = 0 mm, the ratio of laminate and resin Von Mises stresses was higher when the taper angle becomes larger for Model A, Model B, and Model C.

The largest Von Mises stress 22.384 MPa in the resin area I occurred near the transition point x = 80 mm and z = 1 mm. The second largest Von Mises stress 16.805 MPa in the resin area I occurred near the transition point x = 80 mm and z = 0 mm.

The initial crack may seem to occur along the line from the point x = 80 mm and z = 1 mm to the point x = 80 mm and z = 0 mm or along the line from the point x = 80 mm and z = 0 mm to the point x = 80 mm and z = 1 mm.

The random values of the possible weak factor had been assumed to be 1, near point x = 80 and z = 1 mm, and assumed to be 0.7 near point x = 80 mm and z = 0.

The given resin tensile strength is 62.055 MPa. The computed Von Mises stress is 16.805 MPa at the point x = 80 mm and z = 0 mm. The considered safety factor is 2.5, and the design tensile strength is 17.375 MPa. If the safety factor is assumed as 3.3, the design tensile strength is 13.031 MPa. This value is less than the computed stress 16.805 MPa. The cracking may occur at this stress level. The computed Von Mises stress is 22.384 MPa at

the point x = 80 mm and z = 1 mm. The design tensile strength is 24.8 or 18.626 MPa. The proportion between the design tensile strength and stress was 1.080 or 0.775 for point x = 80 mm and z = 0 mm that was lower than the proportion 1.107 or 0.832 for point x = 80 mm and z = 1 mm. It was reasonable that the initial cracking may occur from point x = 80 mm and z = 0 mm to point x = 80 mm and z = 1 mm.

The initial crack length was considered as 0.25 mm, its width was 0.02 mm, and further the crack propagates to an incremental distance da=0.25 mm, and the crack width was 0.004 mm. The energy with initial crack or after crack propagation was increasing when the taper angle was decreasing. The energy release rate was increasing when the taper angle was increasing. The energy release rates were calculated for Model A, Model B and Model C.

When the loading was changed to concentrated loading and applied at different positions, the energy release rates were not changed appreciably.

The resin material was considered as isotropic material, for which the elastic modulus E and Poisson's ratio ν were constants. The computed results of the stress intensity factor were given for Model A, Model B and Model C.

The random excitation was considered by containing some of eigenvalues in the forcing frequencies, and was constrained by limit time and with zero-mean. When 10000 points were considered to obtain the Fast Fourier Transform, power spectral density was given. The mean square response and the standard deviation values of the response were given.

The parameters of the tapered structure were taken to be deterministic constants, and the power spectral density was calculated as a function of the structural parameters and the external excitation. The computed response had been the displacement at any given point in the tapered laminate. A stationary Gaussian excitation process with zero mean has been used to represent the excitation, thereby leading to closed form expressions for response statistics.

A threshold value was assumed that may be a random variable, so that when the response was higher than s, the tapered structure will be at failure. The conditional probability of failure has been determined.

The conditional probability was 1 at the threshold value 0.0851 mm at point x = 80 mm and z = 0 mm for the curve of the 10000 sec. At this displacement level, the stress was calculated as 20.47 MPa at this point. The stress 20.47 MPa was higher than the design tensile strength 19.85 MPa, so the failure will be happened absolutely after 10000 sec. The conditional probability is 1 at the threshold value 0.0701 mm at point x = 80 mm and z = 0 mm for the curve of the 1000 sec. At this displacement level, the stress was calculated as 16.87 MPa at this point. The stress 16.87 MPa is between the design tensile strengths 13.031MPa and 17.375 MPa, so the failure may occur.

Chapter 5

Conclusion and Recommendation

A tapered composite laminate subjected to tension load was analyzed using the finite element method. The different stacking sequences of the laminate were considered. The groups of tapered laminates, with the tapered angles of 2.86° to 14.03°, were analyzed. A two-dimensional plane strain analysis was performed to determine the Von Mises stress distributions in these tapered laminates without a delamination. The interlaminar Von Mises stress distributions along the tapered interface were computed. The initial crack was assumed at the point-a that is near the intersection of the tapered interface and the thin region of the tapered laminate. Delamination growth in the finite element model was assumed along the z-direction. The total strain-energy-release-rates were computed at the delamination tip using the virtual crack closure technique.

1. Interlaminar Von Mises stresses existing at the points of material and geometric discontinuities were calculated. The highest level of interlaminar Von Mises stress appears to occur at the intersection of tapered interface and thin region of the laminate.

2. A possible weak factor distribution has been considered and the safety factor has then been determined. The site where a delamination would initiate is determined.

3. The strain energy release rates were computed for a delamination initiating at point-a, located at the intersection of the taper and the thin laminate.

4. The strain energy release rates for tapered laminates with taper angles between 2.86° to 14.04° were computed. The strain energy release rates increase when the tapered angles were increased.

The response of a deterministic structure to stationary random excitation has been computed for tapered laminates (Model-A, angles 2.86° to 14.03°). It has been assumed that parameters of the structure are known constants, and power spectral density is calculated as a function of the external excitation. The response of the linear tapered structural system to stationary random excitation is determined based on the differential equations of the tapered structure. For lightly damped systems, $|H(\omega)|$ is a function whose value is very small over most of the frequency axis, with large values only in the vicinity of the resonance frequency. In solving the tapered structure problem, our main interest is on the mean square value and the standard deviation of the response at each nodal point. From the computed standard deviation value, we can determine where the initial crack will occur.

1. The mean square of the response is obtained by integrating the response power spectrum over the frequency range; here excitation frequency is same as the first order eigen-frequency.

2. When the excitation has zero mean, the calculated mean square values and the standard deviations of response can indicate where the initial delamination will occur.

A calculation process for the probability of failure of a vibrating tapered structure is introduced. Failure is defined as the case where a certain response, displacement or stress, is higher than a certain given threshold.

1. Expressions for this probability of failure were given for a stationary Gaussian response process with zero mean, which is a common and

useful case in structural dynamics. The analysis of tapered laminate (Model-A, angle 5.71°) has been conducted for which the mode shapes are deterministic.

2. The spectral moments are defined and computed, these moments are functions of the natural frequencies.

3. By adding an extra standard Gaussian variable, a failure function was built. The conditional probability of having a response, which is higher than a prescribed threshold, has been calculated. This information can be used to predict when the delamination of tapered laminate will occur.

The present work can be extended so as to include the nonlinear behavior of the resin rich regions and the interleaving plies. Also, the stochastic nature of laminate material properties and strength parameters has to be included in the analysis, so that the reliability-based design of tapered laminates can be achieved.

References

1 Adams, D.F., Ramkumar, R.L., and Walrath, D.E., "Analysis of porous laminates in the presence of ply drop-offs and fastener holes", Northrop Technical Report NOR 84-113, Northrop Corporation, Hawthorne, CA 90250, and the University of Wyoming, Laramie, Wyoming 820271, May 1984.

2 Curry, J.M., Johnson, E.R., and Starnes Jr, J.H., "Effect of dropped plies on the strength of graphite-epoxy laminates", AIAA Journal, Vol. 30, No. 2, pp. 449-456, February 1992.

3 Fish, J.C. and Lee, S.W., "Delamination of tapered composite structures", Engineering Fracture Mechanics, Vol. 34, No. 1, pp. 43-54, 1989.

4 Kemp B.L., and Johnson, E.R., "Response and failure analysis of graphite-epoxy laminate containing terminating internal plies", Proceedings of the AIAA/ASME/ASCE/AHS 26th Structures, Structural Dynamics, and Materials Conference, Pt. 1, AIAA, New York, pp. 13-24, April 1985; AIAA Paper 85-0608.

5 Mukherjee, A. and Varughese, B., "A ply drop-off element for inclusion of drop-off in the global analysis of layered composite structures", Computers & Structures, Vol. 54, No. 5, pp. 865-870, 1995.

6 Murri G.B., O'Brien, T.K., and Rousseau, C.Q., "Fatigue life methodology for tapered composite flexbeam laminates", Journal of the American Helicopter Society, Vol. 43, No. 2, pp. 146-155, April 1998.

7 Ochoa, O.O. and Chan, W.S., "Tapered laminates: A study on delamination characterization", Proceedings of the America Society for Composites Third Technical Conference, Technomic, Lancaster, PA, pp. 633-641, September 1988.

8 Poon, C.Y., Ruiz, C., and Allen, C.B., "Finite element analysis of a tapered composite", Composite Science and Technology, Vol. 51,n3, pp. 429-440, 1994.

9 Harrison, P.N. and Johnson, E.R., "A mixed variational formulation for interlaminar stresses in thickness-tapered composite laminates", Int. J. of Solids and Structures, Vol. 33, No. 16, pp. 2377-2399, 1996.

10 Vizzini, A.J., "Shear-lag analysis about an internally-dropped ply", Journal of Reinforced Plastics and Composites, Vol. 16, No. 1, pp. 73-85, 1997.

11 Rhim J. and Vizzini, A.J., "Analysis of interlaminar stresses in an internally-dropped ply region", Proceedings of the 11th international Conference on Composite Materials, Queensland, Australia, July 1997.

12 Salpekar, S.I., Raju, I.S., and O'Brian, T.K., "Strain-energy-release rate analysis of delamination in a tapered laminate subjected to tension load", J. of Composite Materials, Vol. 25, pp. 118-141, February 1991.

13 Vizzini, A.J., and Lee, S.W., "Damage analysis of composite tapered beams", J. of The American Helicopter Society, Vol. 40, No. 2, pp.43-50, April 1995.

14 Wisnom, M.R., Jones, M.I., and Cui, W., "Failure of tapered composites under static and fatigue tension loading", AIAA Journal, Vol. 33, No. 5, pp. 911-918, May 1995.

15 Botting, A.D, Vizzini, A.J., and Lee, S.W., "Effect of ply-drop configuration on delamination strength of tapered composite structures", AIAA J., Vol. 34, No.8, pp. 1650-1656, August 1996.

16 Cairns, D.S., Mandell, J.F., Scott, M.E., and Maccagnano, J.Z., "Design and manufacturing considerations for ply drops in composite structures", Proceedings of the 11th International Conference on Composite Materials, Queensland, Australia, 1997. Composites Part B: Engineering, Vol. 30, n5, pp. 523-354, 1999.

17 Cui, W., Wisnom, M.R., and Jones, M., "Effect of step spacing on delamination of tapered laminates", Composites Science and Technology, Vol 52, pp. 39-46, 1994.

18 Fish, J.C. and Vizzini, A.J., "Delamination of ply-drop configurations", Composite Materials: Testing and Design, ASTM STP 1206. E.T. Camponeschi, Jr., Ed.,

American Society for Testing and Materials, Philadelphia, Vol. 11, pp. 323-332, 1993.

19 Llanos, A.S., Lee, S.W., and Vizzini, A.J., "Delamination prevention in tapered composite structures under uniaxial tensile loads", 31st AIAA/ASME/ASCE/AHS/ASC Structures, Structural Dynamics and Materials Conference, Long Beach, CA, Apr. 2-4, 1990, Technical Papers, Part 2 (A90-29283 11-39), Washington, DC, AIAA, pp. 1242-1252, 1990.

20 Daoust, J. and Hoa, S.V., "Parameters affecting interlaminar stresses in tapered laminates under static loading conditions", Polymer Composites, Vol. 10, No. 5, pp. 374-383, October 1989.

21 Hoa, S.V., Du, B.L., and Vu-Khanh, T., "Interlaminatar stresses in tapered laminates", Polymer Composites, Vol. No. 5, pp. 337-344, October 1988.

22 Miravete, A., "Strain and stress anlysis of tapered laminated composite structures", Composite Structures, Vol. 16, pp. 64-84, 1990.

23 Wu, C.M.L. and Webber, J.P.H., "Analysis of tapered (in steps) laminated plates under uniform in plane load", Composite Structures, Vol. 5, pp. 87-100, 1986.

24 Hofman, B.B. and Ochoa, O.O., "Shear deformable user finite element for MARC to model composite with taper", Proceedings of the 12th American Society for Composites, Dearborn, Michigan, 1997.

25 Cui, W., Wisnom, M. R. and Jones, M., "Effect of step spacing on delamination of tapered laminates", Composites Science and Technology, Vol. 52, pp. 39-46, 1994.

26 Clough, R. W., "The finite element method in plane stress analysis," Journal of Structures Division, ASCE, Proceedings of 2nd Conference on Electronic Computation, pp. 345-378, 1960.

27 Lekhnitskii, S.G., Theory of Elasticity of an Anisotropic Body, MIR Publishers, Moscow (1981). English translation of the revised 1977 Russian edition.

28 Williams, M.L., " On the stress distribution at the base of a stationary crack", Journal of Applied Mechanics, Vol. 24, pp. 109-114, 1957.

29 Lapidus, L. and Pinder, G.F., Numerical Solution of Partial Differential Equations in Science and Engineering, John Wiley and Sons, New York, 1982.

30 Zienkiewicz, O.C. and Taylor, R.L., The Finite Element Method, (Fourth Edition) McGraw-Hill, New York, 1989.

31 Anderson, T.L., Fracture Mechanics, Second Edition, CRC Press, New York, 1995.

32 Parks, D.M., "A stiffness derivative finite element technique for determination of crack tip stress intensity factors", International Journal of Fracture, Vol. 10, pp. 487-502, 1974.

33 Hellen, T.K., "On the method of Virtual Crack Extension", International Journal for Numerical Methods in Engineering, Vol. 9, pp. 187-207, 1975.

34 Parks, D.M., "The Virtual Crack Extension method for nonlinear material behavior", Computer Methods in Applied mechanics and Engineering, Vol. 12, pp. 353-364, 1977.

35 DeLorenzi, H.G., "On the Energy Release Rate and the J-Integral of 3-D crack configurations", International Journal of Fracture, Vol. 19, pp. 183-193, 1982.

36 DeLorenzi, H.G., "Energy Release Rate calculations by the finite element method", Engineering Fracture Mechanics, Vol. 21, pp. 129-143, 1985.

37 Shih, C.F., Moran, B., and Nakamura, T., "Energy Release Rate along a three-dimensional crack front in a thermally stressed body", International Journal of Fracture, Vol. 30, pp. 79-102, 1986.

38 Moran, B. and Shih, C.F., " A general treatment of crack tip contour integrals", International Journal of Fracture, Vol. 35, pp. 295-310, 1987.

39 Tong, Pin and Rossettos, J. N., Finite-Element Method, Cambridge, Mass., 1977.

40 Owen, D. R. J. and Fawkes, A. J., Engineering Fracture Mechanics, Swansea, U.K. Pineridge Press Ltd., 1983.

41 Dimarogonas, Andrew, Vibration for Engineers, Second Edition, Enhlewood Cliffs, N.J, Prentice Hall, 1996.

42 Hinton, E. and Owen, D.R.J., Finite Element Programming, United States Edition published by ACADEMIC PRESS INC., 1977.

43 Li, KePing, M.A.Sc. Thesis to be submitted, Concordia University, 2002.

44 Maymon, Giora, Some Engineering Applications in Random Vibrations and Random Structures, Published by Reston, Va.: American Institute of Aeronautics and Astronautics, Series: Progress in Astronautics and Aeronautics, Vol. 178, 1998.

Appendix I (Static Analysis Routine)

STATIC

%%% Matlab routine for static

```
NFREE=1128;NZERO=104;nelem1=177;Nodele1=8;nelem2=12;Nodele2=6;
cMK1=0.001;cMK2=0.0002;RF1=300;RF0=0.01000*RF1;
f13=fopen('output.txt','w');

% open the file tem08 and read the K, M, P, N matries
f01 = fopen('c:/Chen-Hai/theses/fatigue1/tem08','r');
  K = fscanf(f01,'%g',[NFREE NFREE]);M = fscanf(f01,'%g',[NFREE NFREE]);
  P = fscanf(f01,'%g',[1  NFREE]);   N = fscanf(f01,'%d',[1  NFREE]);
  fclose(f01);

% Solve the problem for static problem
Pload=zeros(NFREE,1);Disp0=zeros(NFREE,1);Disp00=zeros(NZERO,1);
for iP=1:5;Pload(iP*2)=RF1;end;Pload(1)=RF1/2;Pload(12)=RF1/2;
Disp=inv(K)*Pload;
Dispa=[Disp0;Disp00];
for inu=1:NFREE; Dispa(N(inu))=Disp(inu);end
fprintf(f13,'Disp      u             v\n');
 for iDisp=1:2:1232;
    iDis=iDisp-(iDisp-1)/2;
  fprintf(f13,'%4g %12.6e %12.6e\n',iDis,Dispa(iDisp),Dispa(iDisp+1));
end;
xn1=[590   572   543   525   496  478   449  431   402   384];
xd1=[0     16    32    40    48   52    56   58    60    61.25];
xn2=[357   340   315   299   276  261   240  226   207   194];
xd2=[62.5  63.75 65    66.25 67.5 68.75 70   71.25 72.5  73.75];
xn3=[177   165   150   139   126  116   105  96    87    71];
xd3=[75    76.25 77.5  78.75 80   81.25 82.5 83.75 85    87.5];
xn4=[58    53    47    42   36    31   25    20   14   9   3];
xd4=[90    92    94    102  110   125  140   155  170  185 200];
xn=[xn1 xn2 xn3 xn4];
xd=[xd1 xd2 xd3 xd4];
for iyd=1:41
   yd(iyd)=Dispa(xn(iyd)*2-1);
end
plot(xd,yd,'-*');

% The local cartesian stresses
f11=fopen('c:/Chen-Hai/theses/fatigue1/tem51','r');frewind(f11);
f12=fopen('c:/Chen-Hai/theses/fatigue1/tem52','r');frewind(f12);

% Stress for each element of the element
syp=62.055e9;
 F1t=1280.0e6;%F2t=49.0e6;F6=69.0e6;F1c=-690.0e6;F2c=-158.0e6;
 ff1=1/F1t-1/F1c ;ff2=1/F2t-1/F2c;
 ff11=1/(F1t*F1c);ff22=1/(F2t*F2c);
 ff12=-sqrt(ff11*ff22)/2;ff66=1/F6^2;

% QUAD element
for ielem=1:nelem1;
  ENOQ=fscanf(f12,'%g\n',[10]);Dispst=zeros(16,1);
  Nu11=(ENOQ(3)-1)*2+1 ;Nu12=ENOQ(3)*2;
  Nu21=(ENOQ(4)-1)*2+1 ;Nu22=ENOQ(4)*2;
  Nu31=(ENOQ(5)-1)*2+1 ;Nu32=ENOQ(5)*2;
  Nu41=(ENOQ(6)-1)*2+1 ;Nu42=ENOQ(6)*2;
  Nu51=(ENOQ(7)-1)*2+1 ;Nu52=ENOQ(7)*2;
  Nu61=(ENOQ(8)-1)*2+1 ;Nu62=ENOQ(8)*2;
  Nu71=(ENOQ(9)-1)*2+1 ;Nu72=ENOQ(9)*2;
  Nu81=(ENOQ(10)-1)*2+1;Nu82=ENOQ(10)*2;
  Disp1=Dispa(Nu11:Nu12);Disp2=Dispa(Nu21:Nu22);
  Disp3=Dispa(Nu31:Nu32);Disp4=Dispa(Nu41:Nu42);
  Disp5=Dispa(Nu51:Nu52);Disp6=Dispa(Nu61:Nu62);
```

```
  Disp7=Dispa(Nu71:Nu72);Disp8=Dispa(Nu81:Nu82);
  Dispst=[Disp1; Disp2; Disp3; Disp4; Disp5; Disp6; Disp7; Disp8];
  fprintf(f13,'QUAD element %4g\n',ielem);
fprintf(f13,'stresses     x-dir        z-dir        xz-dir    yp-stress\n',ielem);
  for iBmat=1:Nodele1+1
    Sbmat=fscanf(f11,'%g %g %g\n',[16,3]);
    str1=Sbmat'*Dispst;
    stryp=sqrt((str1(1)^2+str1(2)^2+(str1(2)-str1(1))^2+6*str1(3)^2)/2);
    fprintf(f13,'node%4g %12.4e %12.4e %12.4e %12.4e\n',iBmat,str1,stryp);
    if stryp >= syp
       fprintf(f13,'** F1 ** %12.4e\n',stryp);
    end
  end
end

% TRIA element
for ielem=1+nelem1:nelem1+nelem2;
  ENOQ=fscanf(f12,'%g\n',[8]);Dispst=zeros(12,1);
  Nu11=(ENOQ(3)-1)*2+1 ;Nu12=ENOQ(3)*2;
  Nu21=(ENOQ(4)-1)*2+1 ;Nu22=ENOQ(4)*2;
  Nu31=(ENOQ(5)-1)*2+1 ;Nu32=ENOQ(5)*2;
  Nu41=(ENOQ(6)-1)*2+1 ;Nu42=ENOQ(6)*2;
  Nu51=(ENOQ(7)-1)*2+1 ;Nu52=ENOQ(7)*2;
  Nu61=(ENOQ(8)-1)*2+1 ;Nu62=ENOQ(8)*2;
  Disp1=Dispa(Nu11:Nu12);Disp2=Dispa(Nu21:Nu22);
  Disp3=Dispa(Nu31:Nu32);Disp4=Dispa(Nu41:Nu42);
  Disp5=Dispa(Nu51:Nu52);Disp6=Dispa(Nu61:Nu62);
  Dispst=[Disp1; Disp2; Disp3; Disp4; Disp5; Disp6];
  fprintf(f13,'TRIA element %4g\n',ielem);
fprintf(f13,'stresses     x-dir        z-dir        xz-dir    yp-stress\n',ielem);
  for iBmat=1:Nodele2+1
    Sbmat=fscanf(f11,'%g %g %g\n',[12,3]);
    str1=Sbmat'*Dispst;
    stryp=sqrt((str1(1)^2+str1(2)^2+(str1(2)-str1(1))^2+6*str1(3)^2)/2);
    fprintf(f13,'node%4g %12.4e %12.4e %12.4e %12.4e\n',iBmat,str1,stryp);
    if stryp >= syp
       fprintf(f13,'** F1 ** %12.4e\n',stryp);
    end
  end
end

% close all files
fclose(f11);fclose(f12);fclose(f13);
```

Appendix II (Dynamic Analysis Routine)

DYNAMI

```
%%% Matlab routine for dynamic

% open file and parameters are given
NFREE=30;NZERO=6
NFREE=1170;NZERO=62;nelem1=177;Nodele1=8;nelem2=12;Nodele2=6;
cMK1=0.001;cMK2=0.0002;RF1=1800;RF0=0.01000*RF1;
f13=fopen('output.txt','w');

% open the file tem08 and read the K, M, P, N matries
f01 = fopen('c:/Chen-Hai/theses/fatigue1/tem08','r');
  K = fscanf(f01,'%g',[NFREE NFREE]);M = fscanf(f01,'%g',[NFREE NFREE]);
  P = fscanf(f01,'%g',[1  NFREE]);  N = fscanf(f01,'%d',[1  NFREE]);
  fclose(f01);
  nnub=1;
    reg=[29    7.045000e+002];
 % reg=[29    200]

% Form a load containing 270.85-5406.19 Hz (<1000) and corrupt it
% with some zero-mean random
t=0:0.001:1.0;load=0;
for iload=1:nnub
    load =load+RF0*(sin(2*pi*reg(iload,2)*t))/(nnub);
end
plot(load(1:1000));
Dload2 = load+RF0*randn(size(t));
plot(Dload2(1:100));

% The discrete Fourier transform of the load Dload2 is found by taking
% the 1000 time (to frequency) points fast Fourier transform FFT
F = fft(Dload2,10000);

% The power spectral density, a measurement of the energy at
% various frequencies
Time=10000;
PYY = F.*conj(F)/(pi*Time);
f = 1000*(0:9999)/10000;
plot(f,PYY(1:10000));
fsma=10000./10000;

% The ith point (frequency ,fama, Hz) of the system is
Sinput=zeros(NFREE,NFREE);Souts0=zeros(NFREE,1);
Souts1=zeros(NFREE,1) ;Sinps2=zeros(NFREE,1);
CC=cMK1*M+cMK2*K;
for ith=1:nnub
   for jth1=0:30
      fsma1=reg(ith,2)-15+jth1*1;
      integ=uint32(fsma1*10);
      PYY(integ);
      Hfreq=inv(-(2*pi*fsma1)^2*M+2*pi*fsma1*CC*sqrt(-1)+K);
     for jth2=1:NFREE
        %       Souts0(jth2)=conj(Hfreq(jth2,2))*Hfreq(jth2,2)*PYY(integ);
   Souts0(jth2)=conj(Hfreq(jth2,2))*Hfreq(jth2,2)*PYY(integ);
     end
     % The mean square E(x) of the response at point.
     Souts1=Souts1+Souts0*2*pi*fsma1;
  end
     for jth1=0:30
      fsma1=1000.-reg(ith,2)-15+jth1*1;
      integ=uint32(fsma1*10);
      PYY(integ);
      Hfreq=inv(-(2*pi*fsma1)^2*M+2*pi*fsma1*CC*sqrt(-1)+K);
     for jth2=1:NFREE
```

```
        %       Souts0(jth2)=conj(Hfreq(jth2,2))*Hfreq(jth2,2)*PYY(integ);
    Souts0(jth2)=conj(Hfreq(jth2,2))*Hfreq(jth2,2)*PYY(integ);
      end
      % The mean square E(x) of the response at point.
      Souts1=Souts1+Souts0*2*pi*fsmal;
    end
end

% The standart deviation of the response
Souts2=sqrt(Souts1);Disp0=zeros(NZERO,1);
Dispas=[Souts2;Disp0];
fprintf(f13,'Deviation  u            v\n');
for iDisp=1:2:NFREE;
    iDis=iDisp-(iDisp-1)/2;
  fprintf(f13,'%4g %12.6e %12.6e\n',iDis,Dispas(iDisp),Dispas(iDisp+1));
end;

fclose(f13);
```

Appendix III (Data file)

1) Data File Names

A2801.txt	A2802.txt	A2803.txt
A4201.txt	A4202.txt	A4203.txt
A5701.txt	A5702.txt	A5703.txt
A7301.txt	A7302.txt	A7303.txt
A8501.txt	A8502.txt	A8503.txt
A9901.txt	A9902.txt	A9903.txt
A11301.txt	A11302.txt	A11303.txt
A12601.txt	A12602.txt	A12603.txt
A14001.txt	A14002.txt	A14003.txt
B2801.txt	B2802.txt	B2803.txt
B4201.txt	B4202.txt	B4203.txt
B5701.txt	B5702.txt	B5703.txt
B7301.txt	B7302.txt	B7303.txt
B8501.txt	B8502.txt	B8503.txt
B9901.txt	B9902.txt	B9903.txt
B11301.txt	B11302.txt	B11303.txt
B12601.txt	B12602.txt	B12603.txt
B14001.txt	B14002.txt	B14003.txt
C2801.txt	C2802.txt	C2803.txt
C4201.txt	C4202.txt	C4203.txt
C5701.txt	C5702.txt	C5703.txt
C7301.txt	C7302.txt	C7303.txt
C8501.txt	C8502.txt	C8503.txt
C9901.txt	C9902.txt	C9903.txt
C11301.txt	C11302.txt	C11303.txt
C12601.txt	C12602.txt	C12603.txt
C14001.txt	C14002.txt	C14003.txt

2) The Format of a Data File

```
$PARA1 TITLE
$   6 >> 84
$
PARA1 This is a real tapered structure   No. A5701
$
$ except the NPOINT, the parameters only for quad element
$
$     NPOIN NELEM NVFIX NCASE NTYPE NNODE NDOFN NMATS NPROP NGAUS NDIME NSTRE NEVAB
$   6    6    6    6    6    6    6    6    6    6    6    6    6    6
$
PARA2   616  177   31    1    3    8    2    4    8    3    2    3   16
$
$LOAD1 IPLOD IGRAV IEDGE ITEMP ICASE NEDGE
$   6    6    6    6    6          6    6
LOAD1     0    0    1    0    1    1
$
$LOAD2    6    6    6    6
$LOAD3      8         8         8         8     8     8
$
LOAD2     1   12    8    1
LOAD3     10.0       10.0       10.0       0.0        0.0        0.0
$
$   the element nodal, connections, and the property numbers
$ 4    6    6    6    6    6    6    6    6    6    6
$
QUAD    1    4   12    8    1    2    3    9   14   13
QUAD    2    3   14    9    3    4    5   10   16   15
QUAD    3    1   16   10    5    6    7   11   18   17
QUAD    4    4   23   19   12   13   14   20   25   24
```

```
QUAD   5   3  25  20  14  15  16  21  27  26
QUAD   6   1  27  21  16  17  18  22  29  28
QUAD   7   4  34  30  23  24  25  31  36  35
QUAD   8   3  36  31  25  26  27  32  38  37
QUAD   9   1  38  32  27  28  29  33  40  39
QUAD  10   4  45  41  34  35  36  42  47  46
QUAD  11   3  47  42  36  37  38  43  49  48
QUAD  12   1  49  43  38  39  40  44  51  50
QUAD  13   4  56  52  45  46  47  53  58  57
QUAD  14   3  58  53  47  48  49  54  60  59
QUAD  15   1  60  54  49  50  51  55  62  61
QUAD  16   4  70  64  56  57  58  65  72  71
QUAD  17   3  72  65  58  59  60  66  74  73
QUAD  18   1  74  66  60  61  62  67  76  75
QUAD  19   2  83  77  68  69  70  78  85  84
QUAD  20   4  86  79  70  71  72  80  88  87
QUAD  21   3  88  80  72  73  74  81  90  89
QUAD  22   1  90  81  74  75  76  82  92  91
QUAD  23   2 101  94  83  84  85  95 103 102
QUAD  24   2 103  95  85  86  87  96 105 104
QUAD  25   4 107  97  87  88  89  98 109 108
QUAD  26   3 109  98  89  90  91  99 111 110
QUAD  27   1 111  99  91  92  93 100 113 112
QUAD  28   2 122 114 101 102 103 115 124 123
QUAD  29   2 124 115 103 104 105 116 126 125
QUAD  30   2 126 116 105 106 107 117 128 127
QUAD  31   4 130 118 107 108 109 119 132 131
QUAD  32   3 132 119 109 110 111 120 134 133
QUAD  33   1 134 120 111 112 113 121 136 135
QUAD  34   3 146 137 122 123 124 138 148 147
QUAD  35   3 148 138 124 125 126 139 150 149
QUAD  36   3 150 139 126 127 128 140 152 151
QUAD  37   3 152 140 128 129 130 141 154 153
QUAD  38   4 156 142 130 131 132 143 158 157
QUAD  39   3 158 143 132 133 134 144 160 159
QUAD  40   1 160 144 134 135 136 145 162 161
QUAD  41   3 173 163 146 147 148 164 175 174
QUAD  42   3 175 164 148 149 150 165 177 176
QUAD  43   3 177 165 150 151 152 166 179 178
QUAD  44   3 179 166 152 153 154 167 181 180
QUAD  45   2 181 167 154 155 156 168 183 182
QUAD  46   4 185 169 156 157 158 170 187 186
QUAD  47   3 187 170 158 159 160 171 189 188
QUAD  48   1 189 171 160 161 162 172 191 190
QUAD  49   3 203 192 173 174 175 193 205 204
QUAD  50   3 205 193 175 176 177 194 207 206
QUAD  51   3 207 194 177 178 179 195 209 208
QUAD  52   3 209 195 179 180 181 196 211 210
QUAD  53   2 211 196 181 182 183 197 213 212
QUAD  54   2 213 197 183 184 185 198 215 214
QUAD  55   4 217 199 185 186 187 200 219 218
QUAD  56   3 219 200 187 188 189 201 221 220
QUAD  57   1 221 201 189 190 191 202 223 222
QUAD  58   3 236 224 203 204 205 225 238 237
QUAD  59   3 238 225 205 206 207 226 240 239
QUAD  60   3 240 226 207 208 209 227 242 241
QUAD  61   3 242 227 209 210 211 228 244 243
QUAD  62   2 244 228 211 212 213 229 246 245
QUAD  63   2 246 229 213 214 215 230 248 247
QUAD  64   2 248 230 215 216 217 231 250 249
QUAD  65   4 252 232 217 218 219 233 254 253
QUAD  66   3 254 233 219 220 221 234 256 255
QUAD  67   1 256 234 221 222 223 235 258 257
QUAD  68   3 272 259 236 237 238 260 274 273
QUAD  69   3 274 260 238 239 240 261 276 275
QUAD  70   3 276 261 240 241 242 262 278 277
QUAD  71   3 278 262 242 243 244 263 280 279
QUAD  72   4 280 263 244 245 246 264 282 281
QUAD  73   4 282 264 246 247 248 265 284 283
QUAD  74   4 284 265 248 249 250 266 286 285
```

QUAD	75	4	286	266	250	251	252	267	288	287
QUAD	76	4	290	268	252	253	254	269	292	291
QUAD	77	3	292	269	254	255	256	270	294	293
QUAD	78	1	294	270	256	257	258	271	296	295
QUAD	79	3	311	297	272	273	274	298	313	312
QUAD	80	3	313	298	274	275	276	299	315	314
QUAD	81	3	315	299	276	277	278	300	317	316
QUAD	82	3	317	300	278	279	280	301	319	318
QUAD	83	4	319	301	280	281	282	302	321	320
QUAD	84	4	321	302	282	283	284	303	323	322
QUAD	85	4	323	303	284	285	286	304	325	324
QUAD	86	4	325	304	286	287	288	305	327	326
QUAD	87	2	327	305	288	289	290	306	329	328
QUAD	88	4	331	307	290	291	292	308	333	332
QUAD	89	3	333	308	292	293	294	309	335	334
QUAD	90	1	335	309	294	295	296	310	337	336
QUAD	91	3	353	338	311	312	313	339	355	354
QUAD	92	3	355	339	313	314	315	340	357	356
QUAD	93	3	357	340	315	316	317	341	359	358
QUAD	94	3	359	341	317	318	319	342	361	360
QUAD	95	4	361	342	319	320	321	343	363	362
QUAD	96	4	363	343	321	322	323	344	365	364
QUAD	97	4	365	344	323	324	325	345	367	366
QUAD	98	4	367	345	325	326	327	346	369	368
QUAD	99	2	369	346	327	328	329	347	371	370
QUAD	100	2	371	347	329	330	331	348	373	372
QUAD	101	4	375	349	331	332	333	350	377	376
QUAD	102	3	377	350	333	334	335	351	379	378
QUAD	103	1	379	351	335	336	337	352	381	380
QUAD	104	3	398	382	353	354	355	383	400	399
QUAD	105	3	400	383	355	356	357	384	402	401
QUAD	106	3	402	384	357	358	359	385	404	403
QUAD	107	3	404	385	359	360	361	386	406	405
QUAD	108	4	406	386	361	362	363	387	408	407
QUAD	109	4	408	387	363	364	365	388	410	409
QUAD	110	4	410	388	365	366	367	389	412	411
QUAD	111	4	412	389	367	368	369	390	414	413
QUAD	112	2	414	390	369	370	371	391	416	415
QUAD	113	2	416	391	371	372	373	392	418	417
QUAD	114	2	418	392	373	374	375	393	420	419
QUAD	115	4	422	394	375	376	377	395	424	423
QUAD	116	3	424	395	377	378	379	396	426	425
QUAD	117	1	426	396	379	380	381	397	428	427
QUAD	118	3	445	429	398	399	400	430	447	446
QUAD	119	3	447	430	400	401	402	431	449	448
QUAD	120	3	449	431	402	403	404	432	451	450
QUAD	121	3	451	432	404	405	406	433	453	452
QUAD	122	4	453	433	406	407	408	434	455	454
QUAD	123	4	455	434	408	409	410	435	457	456
QUAD	124	4	457	435	410	411	412	436	459	458
QUAD	125	4	459	436	412	413	414	437	461	460
QUAD	126	3	461	437	414	415	416	438	463	462
QUAD	127	3	463	438	416	417	418	439	465	464
QUAD	128	3	465	439	418	419	420	440	467	466
QUAD	129	3	467	440	420	421	422	441	469	468
QUAD	130	4	469	441	422	423	424	442	471	470
QUAD	131	3	471	442	424	425	426	443	473	472
QUAD	132	1	473	443	426	427	428	444	475	474
QUAD	133	3	492	476	445	446	447	477	494	493
QUAD	134	3	494	477	447	448	449	478	496	495
QUAD	135	3	496	478	449	450	451	479	498	497
QUAD	136	3	498	479	451	452	453	480	500	499
QUAD	137	4	500	480	453	454	455	481	502	501
QUAD	138	4	502	481	455	456	457	482	504	503
QUAD	139	4	504	482	457	458	459	483	506	505
QUAD	140	4	506	483	459	460	461	484	508	507
QUAD	141	3	508	484	461	462	463	485	510	509
QUAD	142	3	510	485	463	464	465	486	512	511
QUAD	143	3	512	486	465	466	467	487	514	513
QUAD	144	3	514	487	467	468	469	488	516	515

```
QUAD  145   4  516  488  469  470  471  489  518  517
QUAD  146   3  518  489  471  472  473  490  520  519
QUAD  147   1  520  490  473  474  475  491  522  521
QUAD  148   3  539  523  492  493  494  524  541  540
QUAD  149   3  541  524  494  495  496  525  543  542
QUAD  150   3  543  525  496  497  498  526  545  544
QUAD  151   3  545  526  498  499  500  527  547  546
QUAD  152   4  547  527  500  501  502  528  549  548
QUAD  153   4  549  528  502  503  504  529  551  550
QUAD  154   4  551  529  504  505  506  530  553  552
QUAD  155   4  553  530  506  507  508  531  555  554
QUAD  156   3  555  531  508  509  510  532  557  556
QUAD  157   3  557  532  510  511  512  533  559  558
QUAD  158   3  559  533  512  513  514  534  561  560
QUAD  159   3  561  534  514  515  516  535  563  562
QUAD  160   4  563  535  516  517  518  536  565  564
QUAD  161   3  565  536  518  519  520  537  567  566
QUAD  162   1  567  537  520  521  522  538  569  568
QUAD  163   3  586  570  539  540  541  571  588  587
QUAD  164   3  588  571  541  542  543  572  590  589
QUAD  165   3  590  572  543  544  545  573  592  591
QUAD  166   3  592  573  545  546  547  574  594  593
QUAD  167   4  594  574  547  548  549  575  596  595
QUAD  168   4  596  575  549  550  551  576  598  597
QUAD  169   4  598  576  551  552  553  577  600  599
QUAD  170   4  600  577  553  554  555  578  602  601
QUAD  171   3  602  578  555  556  557  579  604  603
QUAD  172   3  604  579  557  558  559  580  606  605
QUAD  173   3  606  580  559  560  561  581  608  607
QUAD  174   3  608  581  561  562  563  582  610  609
QUAD  175   4  610  582  563  564  565  583  612  611
QUAD  176   3  612  583  565  566  567  584  614  613
QUAD  177   1  614  584  567  568  569  585  616  615
$
TRIA  178   2   68   63   56   64   70   69
TRIA  179   2   85   78   70   79   87   86
TRIA  180   2  105   96   87   97  107  106
TRIA  181   2  128  117  107  118  130  129
TRIA  182   2  154  141  130  142  156  155
TRIA  183   2  183  168  156  169  185  184
TRIA  184   2  215  198  185  199  217  216
TRIA  185   2  250  231  217  232  252  251
$
TRIA  186   2  288  267  252  268  290  289
TRIA  187   2  329  306  290  307  331  330
TRIA  188   2  373  348  331  349  375  374
TRIA  189   2  420  393  375  394  422  421
$
$ gnd and tne nodal coordinates
$ 4   6       12       12
$
GRID    1 0.20000000 0.00000000
GRID    2 0.20000000 0.00025000
GRID    3 0.20000000 0.00050000
GRID    4 0.20000000 0.00075000
GRID    5 0.20000000 0.00100000
GRID    6 0.20000000 0.00125000
GRID    7 0.20000000 0.00150000
GRID    8 0.18500000 0.00000000
GRID    9 0.18500000 0.00050000
GRID   10 0.18500000 0.00100000
GRID   11 0.18500000 0.00150000
GRID   12 0.17000000 0.00000000
GRID   13 0.17000000 0.00025000
GRID   14 0.17000000 0.00050000
GRID   15 0.17000000 0.00075000
GRID   16 0.17000000 0.00100000
GRID   17 0.17000000 0.00125000
GRID   18 0.17000000 0.00150000
GRID   19 0.15500000 0.00000000
```

```
GRID   20 0.15500000 0.00050000
GRID   21 0.15500000 0.00100000
GRID   22 0.15500000 0.00150000
GRID   23 0.14000000 0.00000000
GRID   24 0.14000000 0.00025000
GRID   25 0.14000000 0.00050000
GRID   26 0.14000000 0.00075000
GRID   27 0.14000000 0.00100000
GRID   28 0.14000000 0.00125000
GRID   29 0.14000000 0.00150000
GRID   30 0.12500000 0.00000000
GRID   31 0.12500000 0.00050000
GRID   32 0.12500000 0.00100000
GRID   33 0.12500000 0.00150000
GRID   34 0.11000000 0.00000000
GRID   35 0.11000000 0.00025000
GRID   36 0.11000000 0.00050000
GRID   37 0.11000000 0.00075000
GRID   38 0.11000000 0.00100000
GRID   39 0.11000000 0.00125000
GRID   40 0.11000000 0.00150000
GRID   41 0.10200000 0.00000000
GRID   42 0.10200000 0.00050000
GRID   43 0.10200000 0.00100000
GRID   44 0.10200000 0.00150000
GRID   45 0.09400000 0.00000000
GRID   46 0.09400000 0.00025000
GRID   47 0.09400000 0.00050000
GRID   48 0.09400000 0.00075000
GRID   49 0.09400000 0.00100000
GRID   50 0.09400000 0.00125000
GRID   51 0.09400000 0.00150000
GRID   52 0.09200000 0.00000000
GRID   53 0.09200000 0.00050000
GRID   54 0.09200000 0.00100000
GRID   55 0.09200000 0.00150000
GRID   56 0.09000000 0.00000000
GRID   57 0.09000000 0.00025000
GRID   58 0.09000000 0.00050000
GRID   59 0.09000000 0.00075000
GRID   60 0.09000000 0.00100000
GRID   61 0.09000000 0.00125000
GRID   62 0.09000000 0.00150000
GRID   63 0.08875000 0.00000000
GRID   64 0.08875000 0.00012500
GRID   65 0.08875000 0.00062500
GRID   66 0.08875000 0.00112500
GRID   67 0.08875000 0.00162500
GRID   68 0.08750000 0.00000000
GRID   69 0.08750000 0.00012500
GRID   70 0.08750000 0.00025000
GRID   71 0.08750000 0.00050000
GRID   72 0.08750000 0.00075000
GRID   73 0.08750000 0.00100000
GRID   74 0.08750000 0.00125000
GRID   75 0.08750000 0.00150000
GRID   76 0.08750000 0.00175000
GRID   77 0.08625000 0.00000000
GRID   78 0.08625000 0.00025000
GRID   79 0.08625000 0.00037500
GRID   80 0.08625000 0.00087500
GRID   81 0.08625000 0.00137500
GRID   82 0.08625000 0.00187500
GRID   83 0.08500000 0.00000000
GRID   84 0.08500000 0.00012500
GRID   85 0.08500000 0.00025000
GRID   86 0.08500000 0.00037500
GRID   87 0.08500000 0.00050000
GRID   88 0.08500000 0.00075000
GRID   89 0.08500000 0.00100000
```

```
GRID    90 0.08500000 0.00125000
GRID    91 0.08500000 0.00150000
GRID    92 0.08500000 0.00175000
GRID    93 0.08500000 0.00200000
GRID    94 0.08375000 0.00000000
GRID    95 0.08375000 0.00025000
GRID    96 0.08375000 0.00050000
GRID    97 0.08375000 0.00062500
GRID    98 0.08375000 0.00112500
GRID    99 0.08375000 0.00162500
GRID   100 0.08375000 0.00212500
GRID   101 0.08250000 0.00000000
GRID   102 0.08250000 0.00012500
GRID   103 0.08250000 0.00025000
GRID   104 0.08250000 0.00037500
GRID   105 0.08250000 0.00050000
GRID   106 0.08250000 0.00062500
GRID   107 0.08250000 0.00075000
GRID   108 0.08250000 0.00100000
GRID   109 0.08250000 0.00125000
GRID   110 0.08250000 0.00150000
GRID   111 0.08250000 0.00175000
GRID   112 0.08250000 0.00200000
GRID   113 0.08250000 0.00225000
GRID   114 0.08125000 0.00000000
GRID   115 0.08125000 0.00025000
GRID   116 0.08125000 0.00050000
GRID   117 0.08125000 0.00075000
GRID   118 0.08125000 0.00087500
GRID   119 0.08125000 0.00137500
GRID   120 0.08125000 0.00187500
GRID   121 0.08125000 0.00237500
GRID   122 0.08000000 0.00000000
GRID   123 0.08000000 0.00012500
GRID   124 0.08000000 0.00025000
GRID   125 0.08000000 0.00037500
GRID   126 0.08000000 0.00050000
GRID   127 0.08000000 0.00062500
GRID   128 0.08000000 0.00075000
GRID   129 0.08000000 0.00087500
GRID   130 0.08000000 0.00100000
GRID   131 0.08000000 0.00125000
GRID   132 0.08000000 0.00150000
GRID   133 0.08000000 0.00175000
GRID   134 0.08000000 0.00200000
GRID   135 0.08000000 0.00225000
GRID   136 0.08000000 0.00250000
GRID   137 0.07875000 0.00000000
GRID   138 0.07875000 0.00025000
GRID   139 0.07875000 0.00050000
GRID   140 0.07875000 0.00075000
GRID   141 0.07875000 0.00100000
GRID   142 0.07875000 0.00112500
GRID   143 0.07875000 0.00162500
GRID   144 0.07875000 0.00212500
GRID   145 0.07875000 0.00262500
GRID   146 0.07750000 0.00000000
GRID   147 0.07750000 0.00012500
GRID   148 0.07750000 0.00025000
GRID   149 0.07750000 0.00037500
GRID   150 0.07750000 0.00050000
GRID   151 0.07750000 0.00062500
GRID   152 0.07750000 0.00075000
GRID   153 0.07750000 0.00087500
GRID   154 0.07750000 0.00100000
GRID   155 0.07750000 0.00112500
GRID   156 0.07750000 0.00125000
GRID   157 0.07750000 0.00150000
GRID   158 0.07750000 0.00175000
GRID   159 0.07750000 0.00200000
```

```
GRID  160 0.07750000 0.00225000
GRID  161 0.07750000 0.00250000
GRID  162 0.07750000 0.00275000
GRID  163 0.07625000 0.00000000
GRID  164 0.07625000 0.00025000
GRID  165 0.07625000 0.00050000
GRID  166 0.07625000 0.00075000
GRID  167 0.07625000 0.00100000
GRID  168 0.07625000 0.00125000
GRID  169 0.07625000 0.00137500
GRID  170 0.07625000 0.00187500
GRID  171 0.07625000 0.00237500
GRID  172 0.07625000 0.00287500
GRID  173 0.07500000 0.00000000
GRID  174 0.07500000 0.00012500
GRID  175 0.07500000 0.00025000
GRID  176 0.07500000 0.00037500
GRID  177 0.07500000 0.00050000
GRID  178 0.07500000 0.00062500
GRID  179 0.07500000 0.00075000
GRID  180 0.07500000 0.00087500
GRID  181 0.07500000 0.00100000
GRID  182 0.07500000 0.00112500
GRID  183 0.07500000 0.00125000
GRID  184 0.07500000 0.00137500
GRID  185 0.07500000 0.00150000
GRID  186 0.07500000 0.00175000
GRID  187 0.07500000 0.00200000
GRID  188 0.07500000 0.00225000
GRID  189 0.07500000 0.00250000
GRID  190 0.07500000 0.00275000
GRID  191 0.07500000 0.00300000
GRID  192 0.07375000 0.00000000
GRID  193 0.07375000 0.00025000
GRID  194 0.07375000 0.00050000
GRID  195 0.07375000 0.00075000
GRID  196 0.07375000 0.00100000
GRID  197 0.07375000 0.00125000
GRID  198 0.07375000 0.00150000
GRID  199 0.07375000 0.00162500
GRID  200 0.07375000 0.00212500
GRID  201 0.07375000 0.00262500
GRID  202 0.07375000 0.00312500
GRID  203 0.07250000 0.00000000
GRID  204 0.07250000 0.00012500
GRID  205 0.07250000 0.00025000
GRID  206 0.07250000 0.00037500
GRID  207 0.07250000 0.00050000
GRID  208 0.07250000 0.00062500
GRID  209 0.07250000 0.00075000
GRID  210 0.07250000 0.00087500
GRID  211 0.07250000 0.00100000
GRID  212 0.07250000 0.00112500
GRID  213 0.07250000 0.00125000
GRID  214 0.07250000 0.00137500
GRID  215 0.07250000 0.00150000
GRID  216 0.07250000 0.00162500
GRID  217 0.07250000 0.00175000
GRID  218 0.07250000 0.00200000
GRID  219 0.07250000 0.00225000
GRID  220 0.07250000 0.00250000
GRID  221 0.07250000 0.00275000
GRID  222 0.07250000 0.00300000
GRID  223 0.07250000 0.00325000
GRID  224 0.07125000 0.00000000
GRID  225 0.07125000 0.00025000
GRID  226 0.07125000 0.00050000
GRID  227 0.07125000 0.00075000
GRID  228 0.07125000 0.00100000
GRID  229 0.07125000 0.00125000
```

```
GRID  230 0.07125000 0.00150000
GRID  231 0.07125000 0.00175000
GRID  232 0.07125000 0.00187500
GRID  233 0.07125000 0.00237500
GRID  234 0.07125000 0.00287500
GRID  235 0.07125000 0.00337500
GRID  236 0.07000000 0.00000000
GRID  237 0.07000000 0.00012500
GRID  238 0.07000000 0.00025000
GRID  239 0.07000000 0.00037500
GRID  240 0.07000000 0.00050000
GRID  241 0.07000000 0.00062500
GRID  242 0.07000000 0.00075000
GRID  243 0.07000000 0.00087500
GRID  244 0.07000000 0.00100000
GRID  245 0.07000000 0.00112500
GRID  246 0.07000000 0.00125000
GRID  247 0.07000000 0.00137500
GRID  248 0.07000000 0.00150000
GRID  249 0.07000000 0.00162500
GRID  250 0.07000000 0.00175000
GRID  251 0.07000000 0.00187500
GRID  252 0.07000000 0.00200000
GRID  253 0.07000000 0.00225000
GRID  254 0.07000000 0.00250000
GRID  255 0.07000000 0.00275000
GRID  256 0.07000000 0.00300000
GRID  257 0.07000000 0.00325000
GRID  258 0.07000000 0.00350000
GRID  259 0.06875000 0.00000000
GRID  260 0.06875000 0.00025000
GRID  261 0.06875000 0.00050000
GRID  262 0.06875000 0.00075000
GRID  263 0.06875000 0.00100000
GRID  264 0.06875000 0.00125000
GRID  265 0.06875000 0.00150000
GRID  266 0.06875000 0.00175000
GRID  267 0.06875000 0.00200000
GRID  268 0.06875000 0.00212500
GRID  269 0.06875000 0.00262500
GRID  270 0.06875000 0.00312500
GRID  271 0.06875000 0.00362500
GRID  272 0.06750000 0.00000000
GRID  273 0.06750000 0.00012500
GRID  274 0.06750000 0.00025000
GRID  275 0.06750000 0.00037500
GRID  276 0.06750000 0.00050000
GRID  277 0.06750000 0.00062500
GRID  278 0.06750000 0.00075000
GRID  279 0.06750000 0.00087500
GRID  280 0.06750000 0.00100000
GRID  281 0.06750000 0.00112500
GRID  282 0.06750000 0.00125000
GRID  283 0.06750000 0.00137500
GRID  284 0.06750000 0.00150000
GRID  285 0.06750000 0.00162500
GRID  286 0.06750000 0.00175000
GRID  287 0.06750000 0.00187500
GRID  288 0.06750000 0.00200000
GRID  289 0.06750000 0.00212500
GRID  290 0.06750000 0.00225000
GRID  291 0.06750000 0.00250000
GRID  292 0.06750000 0.00275000
GRID  293 0.06750000 0.00300000
GRID  294 0.06750000 0.00325000
GRID  295 0.06750000 0.00350000
GRID  296 0.06750000 0.00375000
GRID  297 0.06625000 0.00000000
GRID  298 0.06625000 0.00025000
GRID  299 0.06625000 0.00050000
```

```
GRID  300 0.06625000 0.00075000
GRID  301 0.06625000 0.00100000
GRID  302 0.06625000 0.00125000
GRID  303 0.06625000 0.00150000
GRID  304 0.06625000 0.00175000
GRID  305 0.06625000 0.00200000
GRID  306 0.06625000 0.00225000
GRID  307 0.06625000 0.00237500
GRID  308 0.06625000 0.00287500
GRID  309 0.06625000 0.00337500
GRID  310 0.06625000 0.00387500
GRID  311 0.06500000 0.00000000
GRID  312 0.06500000 0.00012500
GRID  313 0.06500000 0.00025000
GRID  314 0.06500000 0.00037500
GRID  315 0.06500000 0.00050000
GRID  316 0.06500000 0.00062500
GRID  317 0.06500000 0.00075000
GRID  318 0.06500000 0.00087500
GRID  319 0.06500000 0.00100000
GRID  320 0.06500000 0.00112500
GRID  321 0.06500000 0.00125000
GRID  322 0.06500000 0.00137500
GRID  323 0.06500000 0.00150000
GRID  324 0.06500000 0.00162500
GRID  325 0.06500000 0.00175000
GRID  326 0.06500000 0.00187500
GRID  327 0.06500000 0.00200000
GRID  328 0.06500000 0.00212500
GRID  329 0.06500000 0.00225000
GRID  330 0.06500000 0.00237500
GRID  331 0.06500000 0.00250000
GRID  332 0.06500000 0.00275000
GRID  333 0.06500000 0.00300000
GRID  334 0.06500000 0.00325000
GRID  335 0.06500000 0.00350000
GRID  336 0.06500000 0.00375000
GRID  337 0.06500000 0.00400000
GRID  338 0.06375000 0.00000000
GRID  339 0.06375000 0.00025000
GRID  340 0.06375000 0.00050000
GRID  341 0.06375000 0.00075000
GRID  342 0.06375000 0.00100000
GRID  343 0.06375000 0.00125000
GRID  344 0.06375000 0.00150000
GRID  345 0.06375000 0.00175000
GRID  346 0.06375000 0.00200000
GRID  347 0.06375000 0.00225000
GRID  348 0.06375000 0.00250000
GRID  349 0.06375000 0.00262500
GRID  350 0.06375000 0.00312500
GRID  351 0.06375000 0.00362500
GRID  352 0.06375000 0.00412500
GRID  353 0.06250000 0.00000000
GRID  354 0.06250000 0.00012500
GRID  355 0.06250000 0.00025000
GRID  356 0.06250000 0.00037500
GRID  357 0.06250000 0.00050000
GRID  358 0.06250000 0.00062500
GRID  359 0.06250000 0.00075000
GRID  360 0.06250000 0.00087500
GRID  361 0.06250000 0.00100000
GRID  362 0.06250000 0.00112500
GRID  363 0.06250000 0.00125000
GRID  364 0.06250000 0.00137500
GRID  365 0.06250000 0.00150000
GRID  366 0.06250000 0.00162500
GRID  367 0.06250000 0.00175000
GRID  368 0.06250000 0.00187500
GRID  369 0.06250000 0.00200000
```

```
GRID  370 0.06250000 0.00212500
GRID  371 0.06250000 0.00225000
GRID  372 0.06250000 0.00237500
GRID  373 0.06250000 0.00250000
GRID  374 0.06250000 0.00262500
GRID  375 0.06250000 0.00275000
GRID  376 0.06250000 0.00300000
GRID  377 0.06250000 0.00325000
GRID  378 0.06250000 0.00350000
GRID  379 0.06250000 0.00375000
GRID  380 0.06250000 0.00400000
GRID  381 0.06250000 0.00425000
GRID  382 0.06125000 0.00000000
GRID  383 0.06125000 0.00025000
GRID  384 0.06125000 0.00050000
GRID  385 0.06125000 0.00075000
GRID  386 0.06125000 0.00100000
GRID  387 0.06125000 0.00125000
GRID  388 0.06125000 0.00150000
GRID  389 0.06125000 0.00175000
GRID  390 0.06125000 0.00200000
GRID  391 0.06125000 0.00225000
GRID  392 0.06125000 0.00250000
GRID  393 0.06125000 0.00275000
GRID  394 0.06125000 0.00287500
GRID  395 0.06125000 0.00337500
GRID  396 0.06125000 0.00387500
GRID  397 0.06125000 0.00437500
GRID  398 0.06000000 0.00000000
GRID  399 0.06000000 0.00012500
GRID  400 0.06000000 0.00025000
GRID  401 0.06000000 0.00037500
GRID  402 0.06000000 0.00050000
GRID  403 0.06000000 0.00062500
GRID  404 0.06000000 0.00075000
GRID  405 0.06000000 0.00087500
GRID  406 0.06000000 0.00100000
GRID  407 0.06000000 0.00112500
GRID  408 0.06000000 0.00125000
GRID  409 0.06000000 0.00137500
GRID  410 0.06000000 0.00150000
GRID  411 0.06000000 0.00162500
GRID  412 0.06000000 0.00175000
GRID  413 0.06000000 0.00187500
GRID  414 0.06000000 0.00200000
GRID  415 0.06000000 0.00212500
GRID  416 0.06000000 0.00225000
GRID  417 0.06000000 0.00237500
GRID  418 0.06000000 0.00250000
GRID  419 0.06000000 0.00262500
GRID  420 0.06000000 0.00275000
GRID  421 0.06000000 0.00287500
GRID  422 0.06000000 0.00300000
GRID  423 0.06000000 0.00325000
GRID  424 0.06000000 0.00350000
GRID  425 0.06000000 0.00375000
GRID  426 0.06000000 0.00400000
GRID  427 0.06000000 0.00425000
GRID  428 0.06000000 0.00450000
GRID  429 0.05800000 0.00000000
GRID  430 0.05800000 0.00025000
GRID  431 0.05800000 0.00050000
GRID  432 0.05800000 0.00075000
GRID  433 0.05800000 0.00100000
GRID  434 0.05800000 0.00125000
GRID  435 0.05800000 0.00150000
GRID  436 0.05800000 0.00175000
GRID  437 0.05800000 0.00200000
GRID  438 0.05800000 0.00225000
GRID  439 0.05800000 0.00250000
```

```
GRID  440 0.05800000 0.00275000
GRID  441 0.05800000 0.00300000
GRID  442 0.05800000 0.00350000
GRID  443 0.05800000 0.00400000
GRID  444 0.05800000 0.00450000
GRID  445 0.05600000 0.00000000
GRID  446 0.05600000 0.00012500
GRID  447 0.05600000 0.00025000
GRID  448 0.05600000 0.00037500
GRID  449 0.05600000 0.00050000
GRID  450 0.05600000 0.00062500
GRID  451 0.05600000 0.00075000
GRID  452 0.05600000 0.00087500
GRID  453 0.05600000 0.00100000
GRID  454 0.05600000 0.00112500
GRID  455 0.05600000 0.00125000
GRID  456 0.05600000 0.00137500
GRID  457 0.05600000 0.00150000
GRID  458 0.05600000 0.00162500
GRID  459 0.05600000 0.00175000
GRID  460 0.05600000 0.00187500
GRID  461 0.05600000 0.00200000
GRID  462 0.05600000 0.00212500
GRID  463 0.05600000 0.00225000
GRID  464 0.05600000 0.00237500
GRID  465 0.05600000 0.00250000
GRID  466 0.05600000 0.00262500
GRID  467 0.05600000 0.00275000
GRID  468 0.05600000 0.00287500
GRID  469 0.05600000 0.00300000
GRID  470 0.05600000 0.00325000
GRID  471 0.05600000 0.00350000
GRID  472 0.05600000 0.00375000
GRID  473 0.05600000 0.00400000
GRID  474 0.05600000 0.00425000
GRID  475 0.05600000 0.00450000
GRID  476 0.05200000 0.00000000
GRID  477 0.05200000 0.00025000
GRID  478 0.05200000 0.00050000
GRID  479 0.05200000 0.00075000
GRID  480 0.05200000 0.00100000
GRID  481 0.05200000 0.00125000
GRID  482 0.05200000 0.00150000
GRID  483 0.05200000 0.00175000
GRID  484 0.05200000 0.00200000
GRID  485 0.05200000 0.00225000
GRID  486 0.05200000 0.00250000
GRID  487 0.05200000 0.00275000
GRID  488 0.05200000 0.00300000
GRID  489 0.05200000 0.00350000
GRID  490 0.05200000 0.00400000
GRID  491 0.05200000 0.00450000
GRID  492 0.04800000 0.00000000
GRID  493 0.04800000 0.00012500
GRID  494 0.04800000 0.00025000
GRID  495 0.04800000 0.00037500
GRID  496 0.04800000 0.00050000
GRID  497 0.04800000 0.00062500
GRID  498 0.04800000 0.00075000
GRID  499 0.04800000 0.00087500
GRID  500 0.04800000 0.00100000
GRID  501 0.04800000 0.00112500
GRID  502 0.04800000 0.00125000
GRID  503 0.04800000 0.00137500
GRID  504 0.04800000 0.00150000
GRID  505 0.04800000 0.00162500
GRID  506 0.04800000 0.00175000
GRID  507 0.04800000 0.00187500
GRID  508 0.04800000 0.00200000
GRID  509 0.04800000 0.00212500
```

```
GRID  510 0.04800000 0.00225000
GRID  511 0.04800000 0.00237500
GRID  512 0.04800000 0.00250000
GRID  513 0.04800000 0.00262500
GRID  514 0.04800000 0.00275000
GRID  515 0.04800000 0.00287500
GRID  516 0.04800000 0.00300000
GRID  517 0.04800000 0.00325000
GRID  518 0.04800000 0.00350000
GRID  519 0.04800000 0.00375000
GRID  520 0.04800000 0.00400000
GRID  521 0.04800000 0.00425000
GRID  522 0.04800000 0.00450000
GRID  523 0.04000000 0.00000000
GRID  524 0.04000000 0.00025000
GRID  525 0.04000000 0.00050000
GRID  526 0.04000000 0.00075000
GRID  527 0.04000000 0.00100000
GRID  528 0.04000000 0.00125000
GRID  529 0.04000000 0.00150000
GRID  530 0.04000000 0.00175000
GRID  531 0.04000000 0.00200000
GRID  532 0.04000000 0.00225000
GRID  533 0.04000000 0.00250000
GRID  534 0.04000000 0.00275000
GRID  535 0.04000000 0.00300000
GRID  536 0.04000000 0.00350000
GRID  537 0.04000000 0.00400000
GRID  538 0.04000000 0.00450000
GRID  539 0.03200000 0.00000000
GRID  540 0.03200000 0.00012500
GRID  541 0.03200000 0.00025000
GRID  542 0.03200000 0.00037500
GRID  543 0.03200000 0.00050000
GRID  544 0.03200000 0.00062500
GRID  545 0.03200000 0.00075000
GRID  546 0.03200000 0.00087500
GRID  547 0.03200000 0.00100000
GRID  548 0.03200000 0.00112500
GRID  549 0.03200000 0.00125000
GRID  550 0.03200000 0.00137500
GRID  551 0.03200000 0.00150000
GRID  552 0.03200000 0.00162500
GRID  553 0.03200000 0.00175000
GRID  554 0.03200000 0.00187500
GRID  555 0.03200000 0.00200000
GRID  556 0.03200000 0.00212500
GRID  557 0.03200000 0.00225000
GRID  558 0.03200000 0.00237500
GRID  559 0.03200000 0.00250000
GRID  560 0.03200000 0.00262500
GRID  561 0.03200000 0.00275000
GRID  562 0.03200000 0.00287500
GRID  563 0.03200000 0.00300000
GRID  564 0.03200000 0.00325000
GRID  565 0.03200000 0.00350000
GRID  566 0.03200000 0.00375000
GRID  567 0.03200000 0.00400000
GRID  568 0.03200000 0.00425000
GRID  569 0.03200000 0.00450000
GRID  570 0.01600000 0.00000000
GRID  571 0.01600000 0.00025000
GRID  572 0.01600000 0.00050000
GRID  573 0.01600000 0.00075000
GRID  574 0.01600000 0.00100000
GRID  575 0.01600000 0.00125000
GRID  576 0.01600000 0.00150000
GRID  577 0.01600000 0.00175000
GRID  578 0.01600000 0.00200000
GRID  579 0.01600000 0.00225000
```

```
GRID   580 0.01600000 0.00250000
GRID   581 0.01600000 0.00275000
GRID   582 0.01600000 0.00300000
GRID   583 0.01600000 0.00350000
GRID   584 0.01600000 0.00400000
GRID   585 0.01600000 0.00450000
GRID   586 0.00000000 0.00000000
GRID   587 0.00000000 0.00012500
GRID   588 0.00000000 0.00025000
GRID   589 0.00000000 0.00037500
GRID   590 0.00000000 0.00050000
GRID   591 0.00000000 0.00062500
GRID   592 0.00000000 0.00075000
GRID   593 0.00000000 0.00087500
GRID   594 0.00000000 0.00100000
GRID   595 0.00000000 0.00112500
GRID   596 0.00000000 0.00125000
GRID   597 0.00000000 0.00137500
GRID   598 0.00000000 0.00150000
GRID   599 0.00000000 0.00162500
GRID   600 0.00000000 0.00175000
GRID   601 0.00000000 0.00187500
GRID   602 0.00000000 0.00200000
GRID   603 0.00000000 0.00212500
GRID   604 0.00000000 0.00225000
GRID   605 0.00000000 0.00237500
GRID   606 0.00000000 0.00250000
GRID   607 0.00000000 0.00262500
GRID   608 0.00000000 0.00275000
GRID   609 0.00000000 0.00287500
GRID   610 0.00000000 0.00300000
GRID   611 0.00000000 0.00325000
GRID   612 0.00000000 0.00350000
GRID   613 0.00000000 0.00375000
GRID   614 0.00000000 0.00400000
GRID   615 0.00000000 0.00425000
GRID   616 0.00000000 0.00450000
$
$ the fixed values
$ 4    6    6    6    6    6
$
$SPC1    1    0    1  0.0  0.0
$SPC1    8    0    1  0.0  0.0
$SPC1   12    0    1  0.0  0.0
$SPC1   19    0    1  0.0  0.0
$SPC1   23    0    1  0.0  0.0
$SPC1   30    0    1  0.0  0.0
$SPC1   34    0    1  0.0  0.0
$SPC1   41    0    1  0.0  0.0
$SPC1   45    0    1  0.0  0.0
$SPC1   52    0    1  0.0  0.0
$SPC1   56    0    1  0.0  0.0
$SPC1   63    0    1  0.0  0.0
$SPC1   68    0    1  0.0  0.0
$SPC1   77    0    1  0.0  0.0
$SPC1   83    0    1  0.0  0.0
$SPC1   94    0    1  0.0  0.0
$SPC1  101    0    1  0.0  0.0
$SPC1  114    0    1  0.0  0.0
$SPC1  122    0    1  0.0  0.0
$SPC1  137    0    1  0.0  0.0
$SPC1  146    0    1  0.0  0.0
$SPC1  163    0    1  0.0  0.0
$SPC1  173    0    1  0.0  0.0
$SPC1  192    0    1  0.0  0.0
$SPC1  203    0    1  0.0  0.0
$SPC1  224    0    1  0.0  0.0
$SPC1  236    0    1  0.0  0.0
$SPC1  259    0    1  0.0  0.0
$SPC1  272    0    1  0.0  0.0
```

```
$SPC1  297   0   1  0.0  0.0
$SPC1  311   0   1  0.0  0.0
$SPC1  338   0   1  0.0  0.0
$SPC1  353   0   1  0.0  0.0
$SPC1  382   0   1  0.0  0.0
$SPC1  398   0   1  0.0  0.0
$SPC1  429   0   1  0.0  0.0
$SPC1  445   0   1  0.0  0.0
$SPC1  476   0   1  0.0  0.0
$SPC1  492   0   1  0.0  0.0
$SPC1  523   0   1  0.0  0.0
$SPC1  539   0   1  0.0  0.0
$SPC1  570   0   1  0.0  0.0
$
SPC1  586   1   1  0.0  0.0
SPC1  587   1   1  0.0  0.0
SPC1  588   1   1  0.0  0.0
SPC1  589   1   1  0.0  0.0
SPC1  590   1   1  0.0  0.0
SPC1  591   1   1  0.0  0.0
SPC1  592   1   1  0.0  0.0
SPC1  593   1   1  0.0  0.0
SPC1  594   1   1  0.0  0.0
SPC1  595   1   1  0.0  0.0
SPC1  596   1   1  0.0  0.0
SPC1  597   1   1  0.0  0.0
SPC1  598   1   1  0.0  0.0
SPC1  599   1   1  0.0  0.0
SPC1  600   1   1  0.0  0.0
SPC1  601   1   1  0.0  0.0
SPC1  602   1   1  0.0  0.0
SPC1  603   1   1  0.0  0.0
SPC1  604   1   1  0.0  0.0
SPC1  605   1   1  0.0  0.0
SPC1  606   1   1  0.0  0.0
SPC1  607   1   1  0.0  0.0
SPC1  608   1   1  0.0  0.0
SPC1  609   1   1  0.0  0.0
SPC1  610   1   1  0.0  0.0
SPC1  611   1   1  0.0  0.0
SPC1  612   1   1  0.0  0.0
SPC1  613   1   1  0.0  0.0
SPC1  614   1   1  0.0  0.0
SPC1  615   1   1  0.0  0.0
SPC1  616   1   1  0.0  0.0
$
$ material card
$       elastic-m  poisson1 thickness shear-mod m-density elastic-m  poisson2  ang
$ 4   6      10       10       10       10       10       10       10
$ Graphite/epoxy  E1      v12      TH      G12      De       E2      V21     m-ang
MAT1     1 129.43E+9   0.3322    0.01  4.28E+9  1.48E+3  7.99E+9  0.0205     0.0
MAT1     2  3.93E+9   0.30      0.01  4.28E+9  1.48E+3  7.99E+9  0.0205     0.0
MAT1     3 129.43E+9   0.3322    0.01  4.28E+9  1.48E+3  7.99E+9  0.0205   -45.0
MAT1     4 129.43E+9   0.3322    0.01  4.28E+9  1.48E+3  7.99E+9  0.0205    45.0
```

Appendix IV (For Problem in Figure 3.6 (a))

The detailed mesh can not be shown in one figure, so meshes that correspond to different parts of the laminate shown in Figure 3.6 (a) are given in Figure 2, Figure 3, Figure 4, Figure 5, and Figure 6.

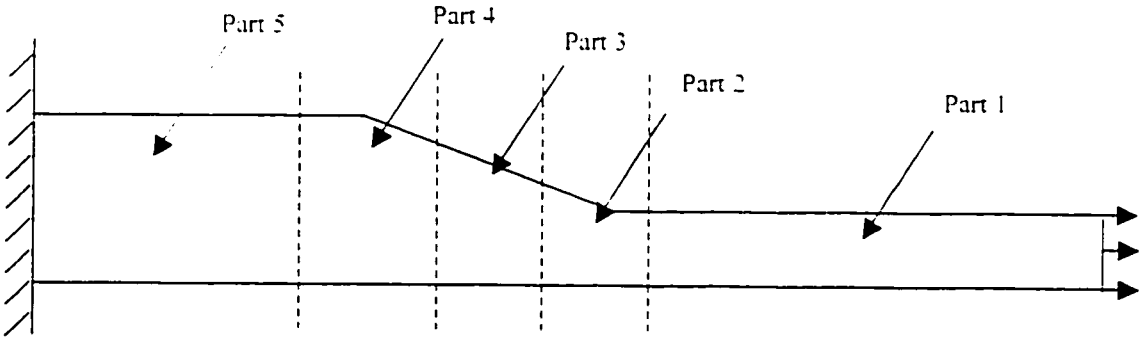

Figure 1 Parts 1-5 of the laminate

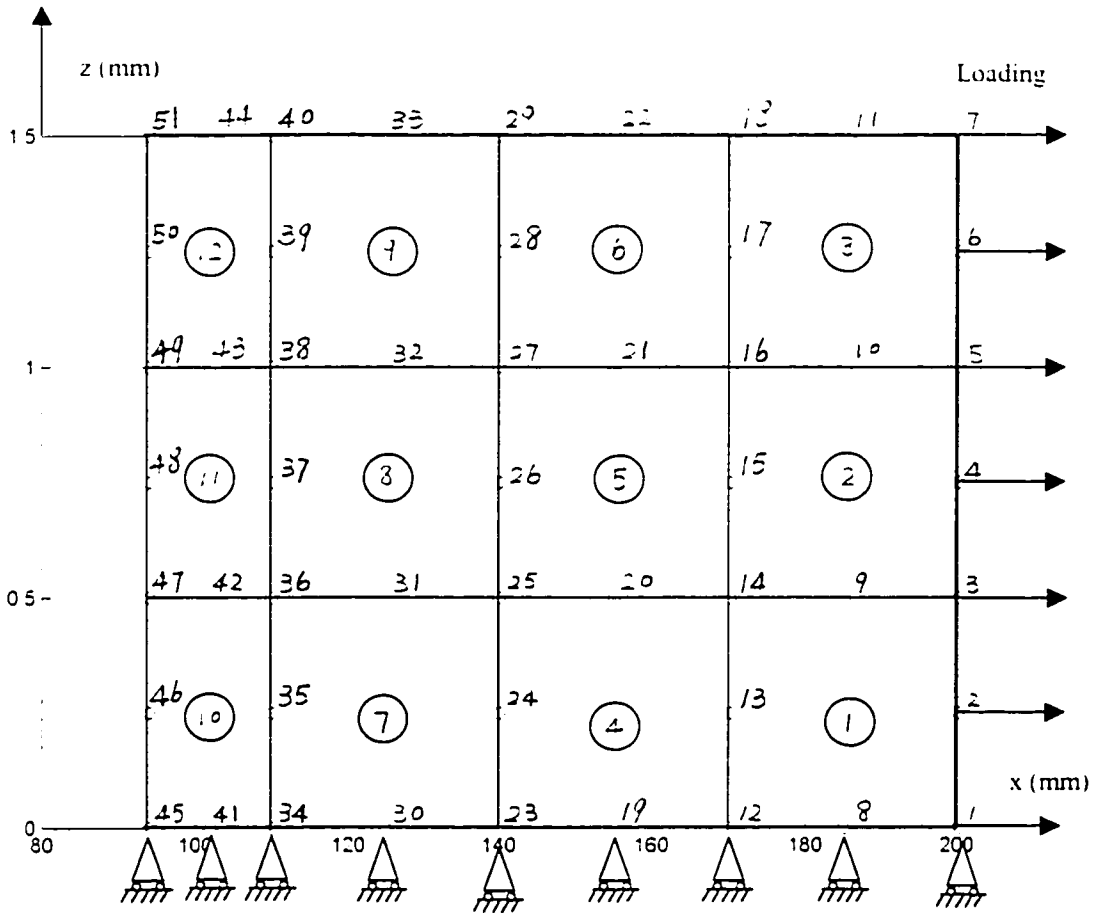

Figure 2 Mesh in Part 1

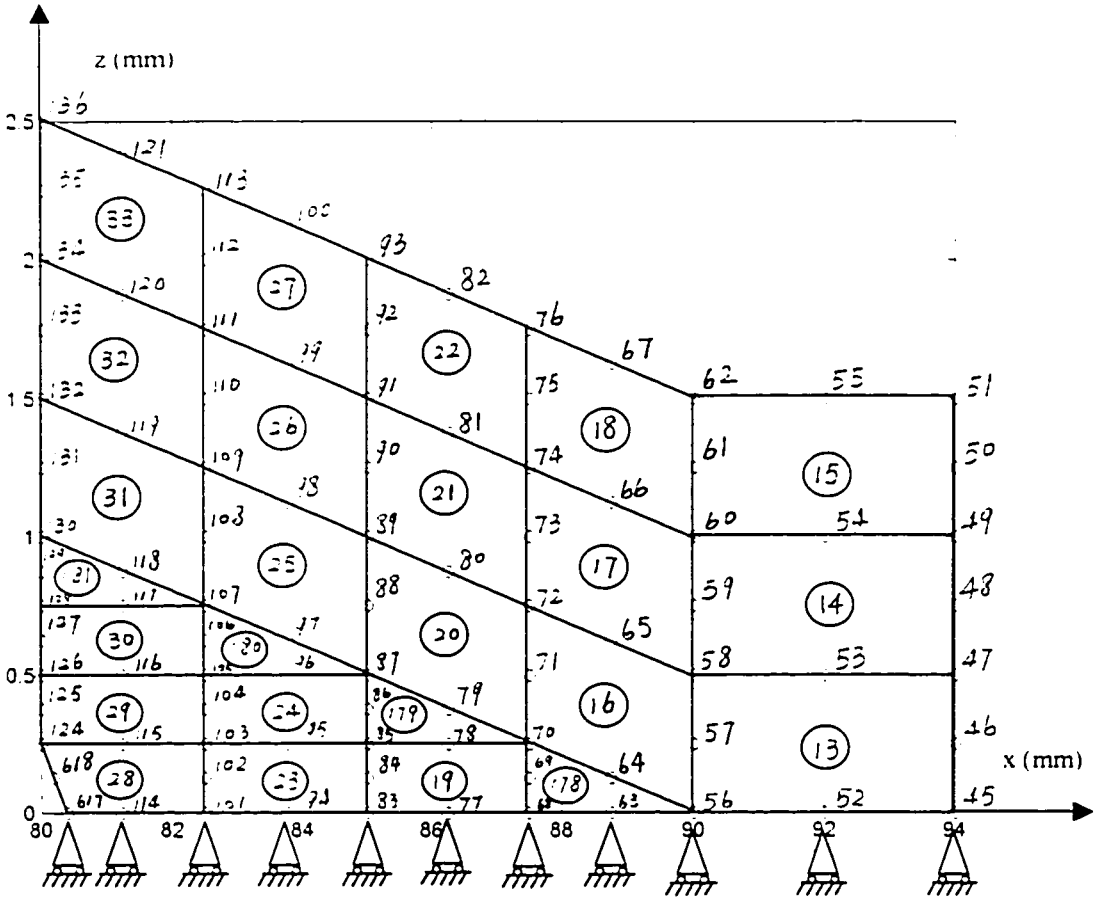

Figure 3 Mesh in Part 2

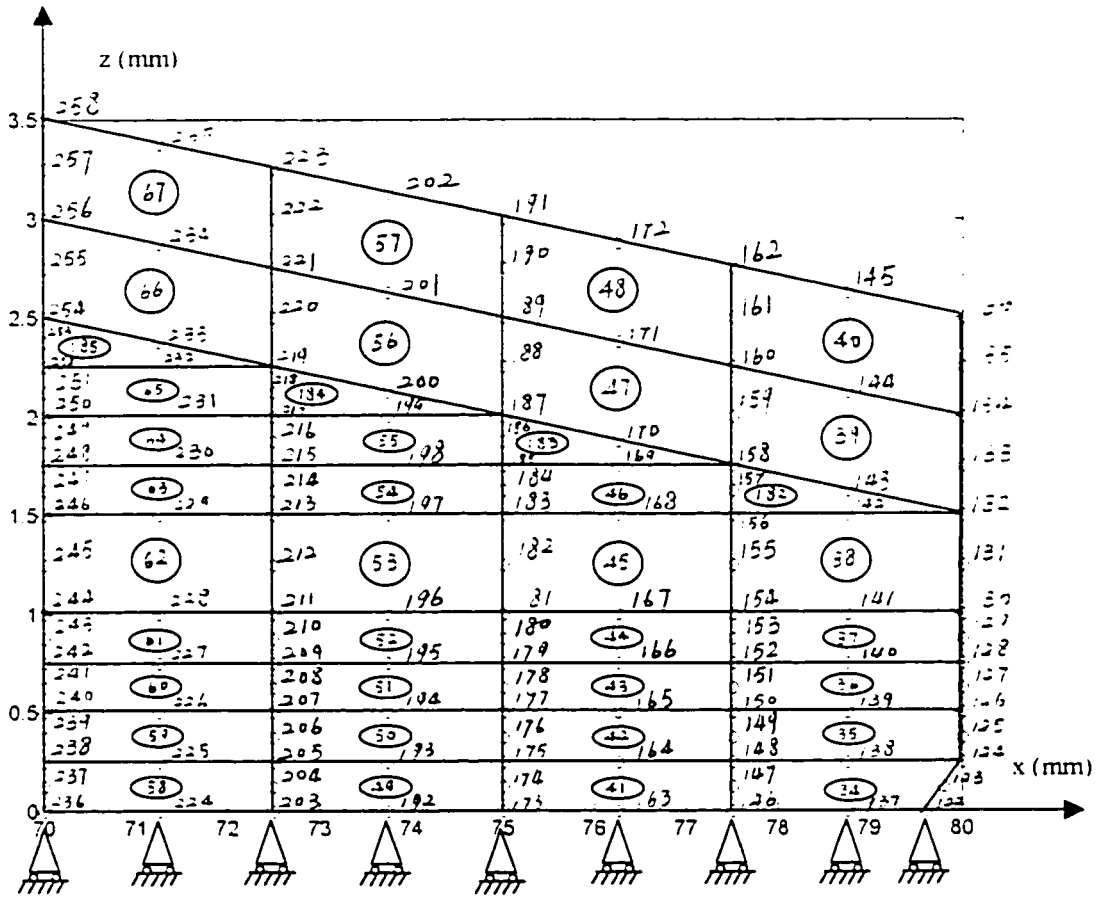

Figure 4 Mesh in Part 3

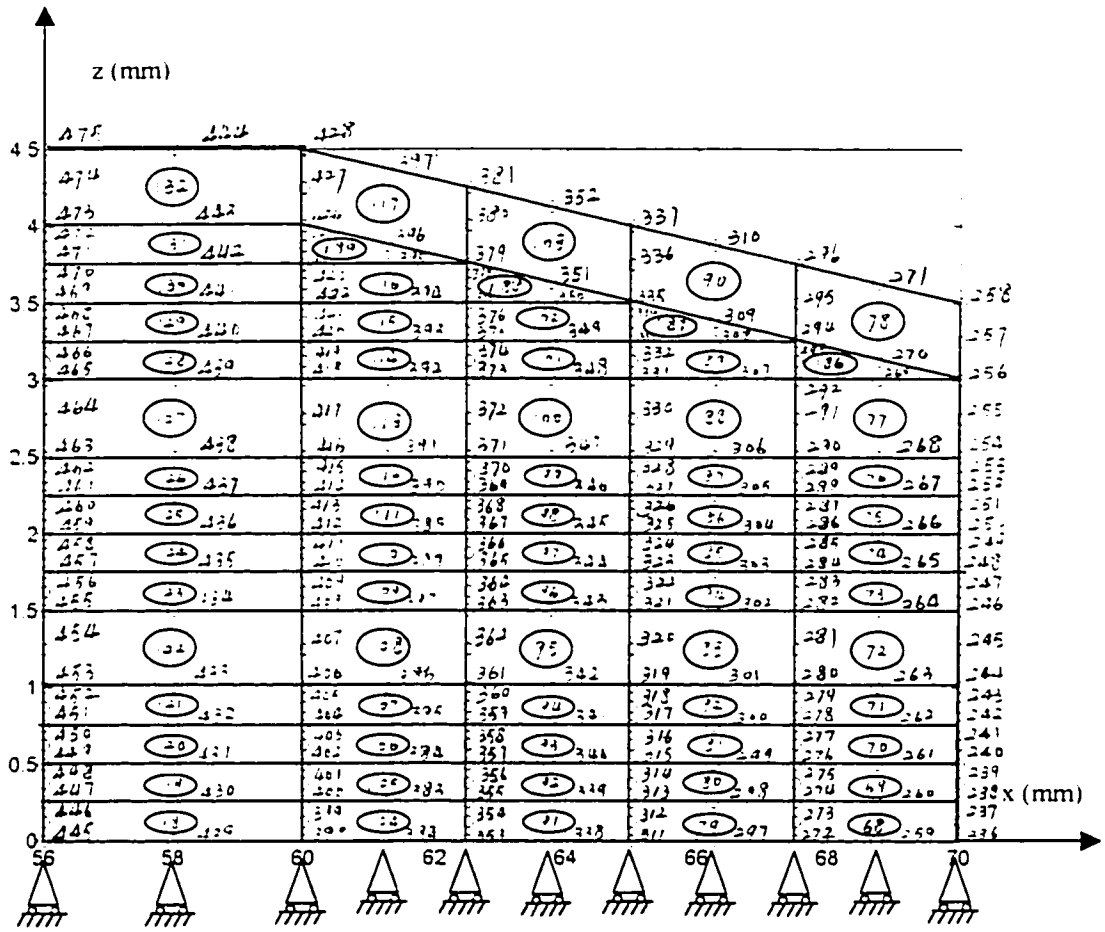

Figure 5 Mesh in Part 4

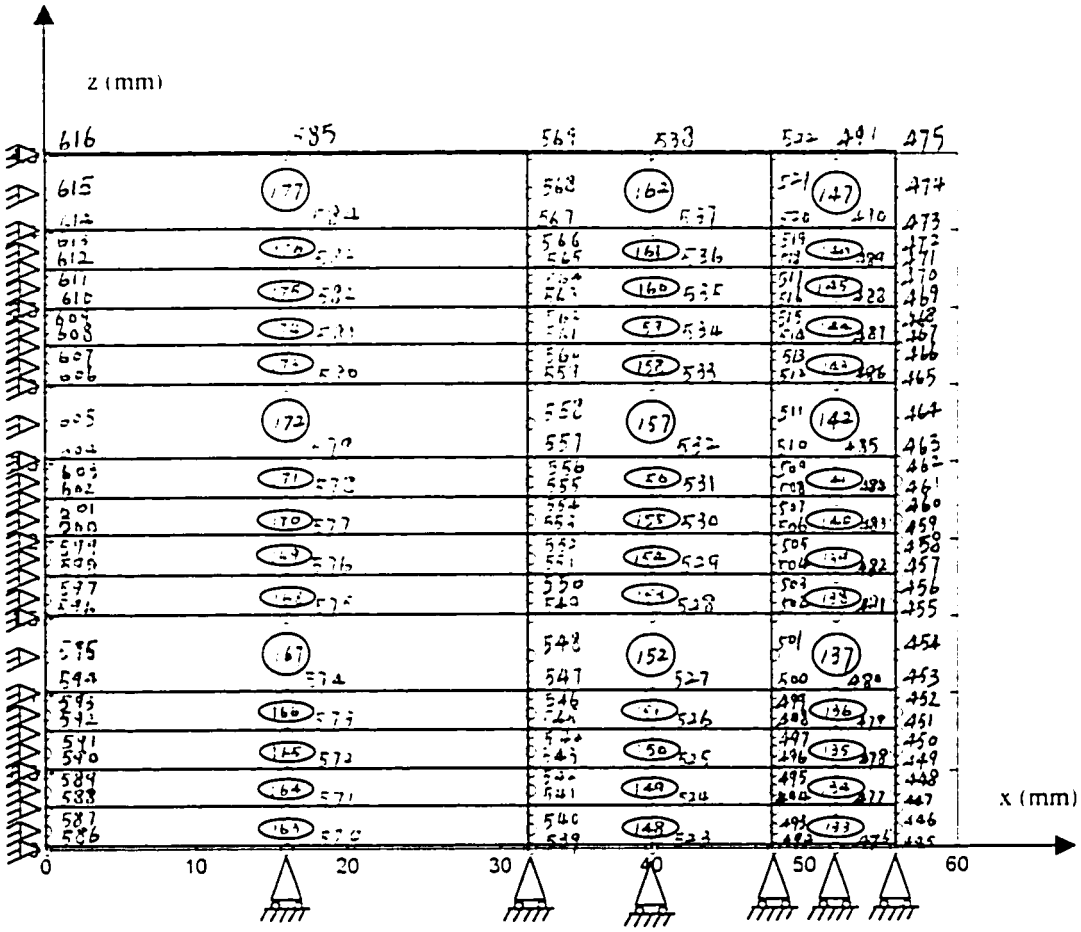

Figure 6 Mesh in Part 5